SPATIAL ANALYSIS OF SEA LEVEL RISE ASSOCIATED WITH CLIMATE CHANGE

A Dissertation
Presented to
The Academic Faculty

by

Biao Chang

In Partial Fulfillment
of the Requirements for the Degree
Doctor of Philosophy in the
School of Civil and Environmental Engineering

Georgia Institute of Technology
August 2013

SPATIAL ANALYSIS OF SEA LEVEL RISE ASSOCIATED WITH CLIMATE CHANGE

Approved by:

Dr. Mustafa M. Aral, Advisor
School of Civil and Environmental Engineering
Georgia Institute of Technology

Dr. Marc Stieglitz
School of Civil and Environmental Engineering
Georgia Institute of Technology

Dr. Jiabao Guan
School of Civil and Environmental Engineering
Georgia Institute of Technology

Dr. Turgay Uzer
School of Physics
Georgia Institute of Technology

Dr. Philip J. Roberts
School of Civil and Environmental Engineering
Georgia Institute of Technology

Date Approved: June 5, 2013

This dissertation is dedicated to my parents, Jinling Chang and Liying Liu, and to my brothers Jian and Xiao. Thank you for your unconditional love and support.

ACKNOWLEDGEMENTS

This dissertation has been made possible by a large number of colleagues, collaborators, friends, and family. I would first like to thank my Ph.D. Advisory Committee members: Dr. Jiabao Guan, Dr. Marc Stieglitz, Dr. Philip Roberts, and Dr. Turgay Uzer. Their insightful and challenging questions have been extremely helpful for my Ph.D. study, and their guidance and encouragement have made this experience even more enjoyable.

My gratitude also goes to the past and current members of our research group MESL: Dr. Wonyong Jang, Dr. Recep Kaya Goktas, Dr. Ilker Tonguc Telci, Mr. Andi Zhang, Mr. William Morgan for their support and friendship. Their discussions during MESL seminars have been an asset to me, and the chatting and joking during lunch breaks with them will always be a pleasant memory of mine.

I would like to express my appreciations to my friends Zhicheng Wei, Dongxu Zhou, Jiali Li, and Qingduo Yin. They became close friends of mine since high school or college, and have been a strong support since. They have always believed in me, and they are there when I need them. I would not have been able to apply for graduate study in the U.S. without their helps in college, and it would have been impossible for me to successfully complete my Ph.D. study without their continued support during the six years after college.

My sincere thanks also go to my girlfriend Chenwei Deng, and parents of hers and mine back in China. My words fall short of expressing my deepest gratitude to you. I feel truly blessed to have all of you in my life.

Lastly and most importantly, I want to thank my faculty advisor Dr. Mustafa M. Aral. As a mentor and a role model, Dr. Aral has taught me to be open-minded to research ideas, to work hard to reach goals, and not to be afraid of mistakes. Through the four years of collaborative work between us, Dr. Aral has showed me the combination of enthusiasm, innovativeness, and attention to details. When I struggle in research, work, and life, he is the one who has stronger confidence in me than myself. I will never forget that the door of his office is always open and he will always put his work aside to discuss with me whenever I show up.

TABLE OF CONTENTS

LIST OF TABLES

LIST OF FIGURES

SUMMARY

Sea level rise (SLR) is one of the most damaging impacts associated with climate change. An important aspect of SLR analysis is to characterize its spatial variability, so that potential threats of SLR to local regions of interest can be assessed more accurately. Despite various studies on geographical pattern identification of sea level change, the related physical, empirical, and stochastic models are still in a fairly preliminary stage. The objective of this study is to develop a comprehensive framework to identify the spatial patterns of sea level in the historical records, project regional mean sea levels in the future, and assess the corresponding impacts on the coastal communities.

In the first part of the study, a spatial pattern recognition methodology is developed to characterize the spatial variations of sea level and to investigate the sea level footprints of climatic signals. Utilizing clustering algorithms, this methodology is capable of grouping sea level data with changing magnitude of spatial variations over time into separate regions, and it also has the functionality to assess the relative strengths of different climate phenomena's sea level footprints. When applied to a spatial sea level dataset for the period of 1950 to 2001, the pattern recognition methodology identified spatial patterns in the data that are potentially associated with climate phenomena such as El Nino-Southern Oscillation (ENSO), Pacific Decadal Oscillation (PDO), and North Atlantic Oscillation (NAO). ENSO was evaluated as the strongest spatial signal in the data, which supports related findings of previous studies. A technique based on artificial neural network is subsequently proposed to reconstruct average sea levels for the characteristic regions identified. Utilizing the correlative relationship between sea level and sea surface temperature (SST), the neural network takes regional average SST's and global average sea level as input variables, and it generates regional average sea levels as

outputs. By applying this neural network approach, regional average sea levels were reconstructed for the characteristic regions identified by the pattern recognition technique, as well as regions based on major ocean basins.

In the second part of the study, a spatial dynamic system model (DSM) is developed to simulate and project the changes in regional sea levels and sea surface temperatures (SST) under different development scenarios of the world. Among the four marker scenarios and two illustrative scenarios proposed by the Intergovernmental Panel on Climate Change (IPCC), the highest and the lowest projected SST's occur under scenarios A1FI and B1, respectively, responding to the highest and the lowest predicted global mean CO_2 concentrations. The highest sea levels are predicted under the scenario A1FI, ranging from 71 cm to 86 cm (relative to 1990 global mean sea level); the lowest predicted sea levels are under the scenario B1, ranging from 51 cm to 64 cm (relative to 1990 global mean sea level). Predicted sea levels and SST's of the Indian Ocean are significantly lower than those of the Pacific and the Atlantic Ocean under all six scenarios. Sea levels projected by the spatial DSM models are generally lower than those by previous semi-empirical sea level models, which reflect the importance of feedback mechanisms to the dynamic system of sea level and SST.

The third part of this dissertation assesses the inundation impacts of projected regional SLR on three representative coastal U.S. states through a geographic information system (GIS) analysis, namely Florida, Georgia and New Jersey. Remarkably different magnitudes of land inundation were projected for these three study regions, which reflect the variations among their land topography. The projected total area of land inundation from 2010 to 2100 is about 3,000 square miles for Florida under all six IPCC SRES scenarios, making it the most severely affected region among the three. The corresponding value for Georgia ranges from 201 to 376 square miles, while that range

for the state of New Jersey is from 142 to 202 square miles. These projections correspond to about 5.4%, 0.3% - 0.6%, and 1.9% - 2.7% of the current total land area of Florida, Georgia, and New Jersey. The importance of consistent elevation datum referencing and data accuracy was demonstrated through the example of Florida, suggesting the necessity of examining the reference datum issue and establishing high accuracy elevation data for future research.

CHAPTER 1

INTRODUCTION

1.1 Background

Sea level rise (SLR) is becoming one of the most concerning environmental issues faced by the human society. According to the Intergovernmental Panel on Climate Change (Meehl et al., 2007), the average rate of global mean SLR over the 20th century is 1.5-2.0 mm/yr, the average value for the period 1961-2003 is about 1.8 mm/yr, and that for 1993-2003 is about 3.1 mm/yr. Since 160 million people currently live in coastal regions that are less than 1 meter above sea level (Allison et al., 2009), even relatively small magnitude of sea level rise can pose significant threats to human populations and properties close to the coast.

Different processes in the Earth system with potentially non-linear interactions can contribute to sea level change. On decadal and larger time scales, global mean sea level rise is mainly caused by four mechanisms: (i) thermal expansion of sea water; (ii) melting of mountain glaciers and polar ice sheets; (iii) human interventions in the hydrologic cycle (dam building, extraction of groundwater, etc.); and, (iv) vertical land movement associated with glacial isostatic adjustment (GIA) (Cazenave et al., 2008) and other geological phenomena. Note that mechanisms such as (iii) and (iv) are not directly related to climate change at relevant time scales. Accordingly, these mechanisms should be excluded from the quantification of sea level rise associated with climate change.

To quantitatively investigate the phenomenon of sea level change, researchers have long been devoted to building mathematical models. Previous models adopted to study the

phenomenon of SLR can be generally divided into two categories: (i) those that are based on physical processes, and (ii) those that are based on the statistical/empirical relationship between sea level and other variables of the climate system (i.e., global surface temperature).

Models based on physical processes conceptually divide the total global mean change into contributions by thermal expansion of the ocean, mountain glaciers and ice caps, and ice sheets. The spatial pattern of sea level (dynamic topography) is affected by the ocean's density structure and dynamics, which are further maintained by air-sea fluxes of heat, freshwater and momentum. These physical models then calculate the contribution to sea level change by each component separately using different formulations of the physical processes under consideration. The second model category is frequently referred to as the "semi-empirical" models. They utilize numerical and statistical techniques to characterize the link between global sea level and global temperature based on historical observations, which will then be used to project the future. The term "semi-empirical" comes from the fact that the model formulation originates from basic physical considerations but parameters of the model needs to be determined empirically from data (Rahmstorf et al., 2012). The rationale behind empirical modeling is that all major contributors to sea level rise will respond to temperature change (Grinsted et al., 2010). Accordingly, by quantifying the correlation between sea level rise and temperature, all known and unknown mechanisms of sea level rise could be incorporated into the analysis (Rahmstorf, 2007).

To incorporate the potential interactions between sea level and temperature and the possible feedbacks, the semi-empirical approach has been extended to the dynamic system model (DSM) by recent studies (Aral et al., 2012; Schmith et al., 2012). Like previous semi-empirical models, the DSM models also determine their parameters

empirically from historical data. However, unlike previous semi-empirical models, the the DSM models take into account the possible interactions and feedbacks between sea level and temperature, thus treating the two as interactive dynamic systems (Aral et al., 2012; Schmith et al., 2012).

The potential threats of the projected sea level rise need to be quantitatively assessed to assist managerial decision makers. Previous studies have analyzed the inundation impacts of potential SLR at global, regional, and local scales. At global scale, inundation impact assessments were conducted using geographic information system (GIS) methods under hypothetical SLR on the order of magnitude of meters (Gornitz et al., 2002; Li et al., 2009; Lichter and Felsenstein, 2012; Dasgupta et al., 2009).

1.2 Motivation and objective

As mentioned in the previous section, climate models based on physical mechanisms have been extensively adopted to simulate sea level change (Meehl et al., 2007). However, these process-based climate models, such as the state-of-the-art coupled atmosphere-ocean general circulation models (AOGCMs), by far are still struggling to characterize all the relevant processes adequately (e.g., ice loss of mountain glaciers, ice sheet melting, etc.). Further, predictions of sea level by the process-based models do not satisfactorily match observational records (Jevrejeva et al., 2012).

In contrast, the semi-empirical models all reproduce the historical sea levels well. However, their decadal projections of global mean sea level are generally higher than those obtained by physical climate models. Questions have been raised about the semi-empirical models regarding their physical basis, as well as the statistical methodologies

involved (Holgate et al., 2007; Schmith et al., 2007; Taboada and Anadon, 2010; von Storch et al., 2008).

A common issue faced by both process-based and semi-empirical models is the spatial variability of sea level. Process-based models generally have the functionality to simulate the spatial patterns of sea level change. However, these models differ significantly with each other with respect to the simulated spatial patterns (Meehl et al., 2007). In addition, process-based models like AOGCMs are often restrained by their computational costs, which limit their ability to quantify the uncertainties in spatial analysis. The previous semi-empirical models mainly target global average sea level change, and are not able to quantitatively assess the spatial variations in sea level (Grinsted et al., 2010; Horton et al., 2008; Jevrejeva et al., 2009; Jevrejeva et al., 2012; Rahmstorf, 2007; Rahmstorf et al., 2012; Vermeer and Rahmstorf, 2009).

As historical records exhibit significant spatial variations in sea level change (Church et al., 2004) and local/regional sea level rise threats are particularly relevant to coastal communities, the development of models targeting sea level's spatial variability is critical. Motivated by this challenge, the central objective of this study is to develop a spatial dynamic system model (DSM) to simulate and project regional sea levels.

Despite numerous studies on spatial variations of sea level in the literature (Cabanes et al., 2006; Mitrovica et al., 2001; Mitrovica et al., 2009; Pardaens et al., 2011; Wunsch et al., 2007), few studies developed methodologies to identify spatial patterns automatically from spatial sea level data. This study develops a spatial pattern recognition technique based on clustering algorithms to characterize spatial variations of the sea level signal.

Time series of regional average sea level for these regions have particular characteristics related to corresponding climate phenomena. Temporal patterns contained in long time series of mean sea level for these regions may provide support for related climate studies. Unfortunately, spatial sea level data is scarce and time span of spatial data sets generally are also relatively short (Chambers et al., 2002; Hamlington et al., 2012; Meyssignac et al., 2012; Smith, 2000). To address this issue, a neural network approach is proposed to reconstruct regional mean sea level from global mean sea level and spatial temperature data.

Despite the large number of previous studies on inundation impact assessment of potential SLR, issues still exist in the related methodologies. A critical issue in previous inundation impact studies is consistent datum referencing for sea level data and land elevation data. The accuracy of elevation data also plays an important role in the inundation mapping process. This study applies a GIS method to analyze the inundation impacts by projected SLR on several coastal regions of the United States, and the important issues are investigated through practical examples.

1.3 Thesis organization

A literature review of research topics on sea level rise modeling is presented in Chapter 2. This chapter analyzes the strengths and limitations of both process-based and empirical/semi-empirical models. Based on the analysis, areas in need of further investigations are identified, and suggestions for future research are propose subsequently.

Chapter 3 is focused on addressing the need of sea level spatial pattern characterization and regional sea level reconstruction. A pattern recognition technique based on clustering algorithms is developed to characterize the spatial variations of sea level. A neural

network approach is then described to reconstruct regional mean sea levels from time series of global mean sea level records and spatial temperature records.

In Chapter 4, a spatial form of the dynamic system model (DSM) is proposed to analyze spatial variations in sea level and temperature change. Using spatial sea surface temperature (SST) and reconstructed spatial sea level and, the spatial DSM model was calibrated for two different configurations: (i) external forcing function embedded in the system matrix; and, (ii) external forcing function treated explicitly. The dynamic system matrices identified are analyzed to describe the characteristics of the system, and regional sea levels and SST's are subsequently for the 21st century

Inundation impacts of the spatial DSM model's projected sea levels are quantitatively assessed for three representative states along the east coast of the United States, namely Florida, Georgia and New Jersey, in Chapter 5. The critical issues of elevation datum and data accuracy are also discussed in this chapter.

As the last chapter, Chapter 6 summarizes the major findings and conclusions of this study, and it also provides suggestions for future research.

CHAPTER 2

LITERATURE REVIEW

2.1 Introduction

Different processes in the Earth system with potentially nonlinear interactions can contribute to sea level change. On decadal and larger time scales, global mean sea level rise is mainly caused by four mechanisms: (i) thermal expansion of sea water; (ii) melting of mountain glaciers and polar ice sheets; (iii) human interventions in the hydrologic cycle (dam building, extraction of groundwater, etc.); and, (iv) vertical land movement associated with glacial isostatic adjustment (GIA) (Cazenave et al., 2008) and other geological phenomena. Note that mechanisms such as (iii) and (iv) are not directly related to climate change at relevant time scales. Accordingly, these mechanisms should be excluded from the quantification of sea level rise associated with climate change.

To quantitatively investigate the phenomenon of sea level change, researchers have long been devoted to building mathematical models. Climate models based on physical mechanisms described in the previous paragraph have been extensively adopted to simulate sea level change (Meehl et al., 2007). However, these process-based climate models, such as the state-of-the-art coupled atmosphere-ocean general circulation models (AOGCMs), by far are still struggling to characterize all the relevant processes adequately (e.g., ice loss of mountain glaciers, ice sheet melting, etc.). Further, predictions of sea level by the process-based models do not satisfactorily match observational records (Jevrejeva et al., 2012).

The issues of process-based models, as reflected in the latest assessment report by the Intergovernmental Panel on Climate Change (IPCC) (Meehl et al., 2007), led to the relatively recent development of the alternative sea level change modeling approach, generally classified as empirical or semi-empirical modeling (Grinsted et al., 2010; Horton et al., 2008; Jevrejeva et al., 2009; Jevrejeva et al., 2012; Rahmstorf, 2007; Rahmstorf et al., 2012; Vermeer and Rahmstorf, 2009). The semi-empirical models all reproduce the historical sea levels well, but their decadal projections of global mean sea level are generally higher than those obtained by physical climate models that are used in the IPCC assessment report (Meehl et al., 2007). Thus, questions have been raised about the semi-empirical models regarding their physical basis or lack there-of, as well as the use of the statistical methodologies involved (Holgate et al., 2007; Schmith et al., 2007; Taboada and Anadon, 2010; von Storch et al., 2008).

A common issue faced by both process-based and semi-empirical models is the spatial variability of sea level. Process-based models generally have the functionality to simulate the spatial patterns of sea level change. However, these models differ significantly with each other with respect to the simulated spatial patterns (Meehl et al., 2007), putting their validity in doubt. In addition, process-based models like AOGCMs are often restrained by their computational costs, which limit their ability to quantify the uncertainties in spatial analysis. The previous semi-empirical models mainly target global average sea level change, and are not able to quantitatively assess the spatial variations in sea level (Grinsted et al., 2010; Horton et al., 2008; Jevrejeva et al., 2009; Jevrejeva et al., 2012; Rahmstorf, 2007; Rahmstorf et al., 2012; Vermeer and Rahmstorf, 2009). As records show significant spatial variations in sea level change (Church et al., 2004) and local sea level rise is particularly relevant to coastal communities. Thus the development of models targeting sea level's spatial variability is critical.

In this chapter, the literature review is presented on sea level rise modeling. The focus of this chapter is to analyze the strengths and limitations of both process-based and empirical/semi-empirical models. Based on the analysis, areas in need of further investigations are identified, and suggestions for future research are provided.

2.2 Models based on physical processes

2.2.1 Review of process-based models

Since the change of sea level associated with anthropogenic climate change is mainly concerned about, models targeting other types of sea level change (e.g., change associated with Earth's Milankovitch cycles) are not considered here. Among the relevant climate models, the most comprehensive ones are the coupled atmosphere-ocean general circulation models (AOGCMs). AOGCMs include three-dimensional representation of the major components of the climate system, namely, atmosphere, ocean, cryosphere, and land surface (Randall et al., 2007). These models also characterize the interactions among different components of the climate system through related physical mechanisms to the best of our knowledge.

With respect to the simulation of sea level change, models based on physical processes (e.g., those adopted by the IPCC) conceptually divide the total global mean change into contributions by thermal expansion of the ocean, mountain glaciers and ice caps, and ice sheets. The spatial pattern of sea level (dynamic topography) is affected by the ocean's density structure and dynamics, which are further maintained by air-sea fluxes of heat, freshwater and momentum (Meehl et al., 2007). These physical models then calculate the contribution to sea level change by each component separately using different formulations of the physical processes under consideration. For the models cited in the

IPCC's most recent assessment report (Meehl et al., 2007), approaches that characterize each component are described below.

The global average sea level rise due to thermal expansion is calculated from change of density of sea-water due to temperature changes, with the assumptions that ocean mass is conserved and that density change due to salinity change is negligible (Gregory et al., 2001). The mathematical model applied (Gregory et al., 2001) is

$$\Delta h = -\frac{1}{S}\int_{S}\int_{-H}^{0}\frac{\Delta\rho}{\rho}\mathrm{d}z\mathrm{d}S \tag{2.1}$$

where Δh is the global mean sea level rise, ρ is the density of sea water ($\Delta\rho$ is its change caused by thermal expansion), z is the vertical elevation relative to sea level (positive upwards), H is the depth of sea water as a function of location, and S is the surface area of the ocean.

For the contribution to sea level change by glaciers and ice caps, models adopted by the IPCC (2007) were developed from the central concept in form of

$$\frac{dh}{dt} = -\frac{1}{A_0}\sum_i b_i A_i \Delta T_i \tag{2.2}$$

where dh/dt is the global mean sea level rise caused by ablation glaciers and ice caps, A_0 is the total surface area of the ocean, i denotes the region of a certain glacier or ice cap, A_i the area of the glacier or ice cap in the region, ΔT_i is the temperature change in the region, b_i is the sensitivity of glacier and ice cap mass balance to temperature change (Gregory et al., 2006). In Equation (2.2) b_i can be estimated by energy balance modeling (Zuo and Oerlemans, 1997) or degree-day model (Braithwaite and Zhang, 1999). The global average sensitivity can be further calculated as the area-weighted average of local

sensitivities in different regions. Later studies considered the feedback of glaciers' mass balance, recognizing that mass loss will reduce the area of glaciers and hence decrease the rate of ice ablation (Meehl et al., 2007). The feedback is modeled by linking the surface area of a glacier A_i to its volume V through a power law, such as $V = cA_i^n$ (Van de Wal and Wild, 2001), where c is a constant and n is an empirical constant. In a well-known study (Bahr et al., 1997), n is configured as 1.375 for valley glaciers and 1.25 for ice caps.

Ice sheets on Greenland and Antarctica can contribute to sea level change through two mechanisms: (i) surface mass balance (SMB); and, (ii) flux of ice crossing the grounding line (Meehl et al., 2007). For surface mass balance, general circulation models (GCMs) are utilized. These GCMs have higher spatial resolutions than those of the AOGCMs chosen by the IPCC for climate simulation (van Lipzig et al., 2002; Wild et al., 2003). This finer resolution is intended to better characterize the features of the ice sheets such as the steep slope near the edge of an ice sheet. In the projection of sea level for the 21st century, IPCC (Meehl et al., 2007) applied a second-order fitting to the SMB change of ice sheet versus global average temperature change. This fitting is based on the results of a related study using AOGCM simulations and scaling methods (Gregory and Huybrechts, 2006). Modeling for ice flux is even more challenging. Understanding of some major physical mechanisms related to ice sheet dynamics is still lacking, such as the impacts of ice shelf on the inland ice flow. Because of this lack of knowledge, the IPCC's Fourth Assessment Report (Meehl et al., 2007) resorted to simplistic approximation for calculation of sea level change caused by the dynamics of ice sheet. Part of the contribution by ice sheet dynamics is accounted for by modifying the contribution of SMB change by –5%± 5% for Antarctica, and 0% ± 10% for Greenland.

As another component of the ice sheet dynamics' impact on sea level change, the contribution from scaled-up ice sheet discharge is estimated according to the equation

$$\frac{dh}{dt} = a\frac{T}{T_0} \tag{2.3}$$

where $\frac{dh}{dt}$ is the equivalent rate of sea level rise, $a = 0.32mm/yr$ (contribution during 1993 to 2003 due to recent acceleration), $T_0 = 0.63^{\circ}C$, and T is the global mean temperature relative to the 1865 to 1894 average.

In this approach, by adding the contributions of different components together, the total sea level change is quantified. Models adopted by the IPCC actually used this summation approach to project global mean sea level rise in the 21st century. Table 2.1 below shows the projections of global mean sea level rise from the average level of 1980-1999 to the average level of 2090-2099 (Meehl et al., 2007), which can be viewed approximately as the rise from 1990 to 2095. Since the lowest value among the lower bound values under different scenarios is 18 cm, and the highest value among the upper bound values is 59 cm, related studies have frequently quoted the range of IPCC's prediction of sea level rise by 2100 as 18-59 cm (Allison et al., 2009; Grinsted et al., 2010).

Table 2.1 Global mean sea level rise projection by the IPCC

Scenario	90% Confidence interval of sea level rise (cm)	
	Lower bound	Upper bound
B1	18	38
B2	20	43
A1B	21	48
A1T	20	45
A2	23	51
A1FI	26	59

2.2.2 Strengths of process-based models

The major strength of the "component-by-component" sea level rise models described above is that they are closely linked to physical mechanisms. As the U.S. Climate Change Science Program (2008) stated, "to the extent that the simulation is successful and convincing, the model can be analyzed and manipulated to uncover the detailed physical mechanisms." The fact that model fundamentals are based on established physical laws, such as conservation of mass, energy, and momentum, makes these models powerful in investigating the mechanisms behind or associated with sea level rise.

This strength is specifically reflected in modeling the sea level change contributed by thermal expansion. Processes affecting thermal expansion of the ocean, such as global average surface air temperature change, ocean heat uptake, change of sea water physical properties, are all well studied. Mathematical representation of these processes gives accurate characterization of the physical system and consequently convincing simulation results.

The development of our understanding of physical mechanisms, combined with the increase of our computational power, can significantly improve the performance of the physical models of sea level rise. The improvements will make them more realistic representations of the physical system and more powerful tools to probe characteristics of the climate system. For instance, the recent development of full-stress ice sheet models (Larour et al., 2012; Winkelmann et al., 2010) may significantly reduce the uncertainty of modeling sea level rise associated with ice sheet dynamics.

2.2.3 Limitations of process-based models

2.2.3.1 Unsatisfactory match between model predictions and observations

Despite the strengths of physical models described above, their performance in predicting sea level rise is in general unsatisfactory, especially when it comes to predictions associated with the contribution by the ice sheets. According to Rahmstorf et al. (2007), satellite data showed a linear sea level rise rate of 3.3 ± 0.4 mm/year for the period 1993–2006, significantly larger than the IPCC's prediction of 1-2 mm/year (Church et al., 2001). Using AOGCM (HadCM3) simulations and process-based models of sea level rise, Gregory et al. (2006) computed the average rate of sea level to be 0.5 mm/yr rise for the 20th century, considerably lower than the average rate of 1.7 mm/yr estimated from observations for the same period (Church and White, 2006). Note that similar process-based models of sea level rise were adopted by the IPCC (Meehl et al., 2007). Based on the kinematic constraints on ice sheet melting, Pfeffer et al. (2008) proposed that an improved estimate of the range of sea level rise to 2100 should be between 0.8 and 2.0 m, if increased ice dynamics are considered. This range of 0.8-2.0 m is remarkably higher than the 0.18-0.59m range predicted by the IPCC (Meehl et al., 2007). The deviation of IPCC's sea level predictions from corresponding estimations based on observational

records is an indication that the process-based models might not characterize the physical mechanisms adequately.

In fact, there have been active discussions over an issue related to process-based models of sea level change, the attribution problem (Leuliette and Miller, 2009; Leuliette and Willis, 2011; Miller and Douglas, 2004; Mitrovica et al., 2006; Munk, 2002). The attribution problem of global sea level rise, sometimes noted as the sea level budget problem or the "sea level enigma", refers to the issue that the sum of thermal expansion and contributions from land ice is smaller than the estimated global mean sea level rise based on observations. For example, in the IPCC's Fourth Assessment Report (Bindoff et al., 2007), the former is smaller by 0.7 ± 0.7 mm/yr than the latter for the period of 1961-2003. This attribution problem suggests our understanding of certain physical mechanisms driving sea level rise is still insufficient. Consequently, cautions should be observed when the corresponding process-based models are employed to project future sea level change.

2.2.3.2 Insufficient understanding of physical mechanisms

Following the description of the unsatisfying performance by process-based sea level models in previous section, this section is focused on their limitations in representing certain physical mechanisms. These limitations are potential causes for the issues in process-based models. As mentioned previously, this category of models generally have success in characterizing the fraction of sea level rise caused by thermal expansion. However, because of limited understanding of physical mechanisms, they have major drawbacks in modeling sea level rise related to the behaviors of land ice.

For the modeling of sea level change caused by the melting of glaciers and ice caps, one major challenge is their relatively small spatial scale. Current physical models, such as AOGCM, have coarse horizontal resolution (about 200 by 200 km) (von Storch et al., 2008), which is significantly larger than most individual glaciers and ice caps. As a result, they are represented crudely in physical models. Furthermore, there are currently more than 130,000 glaciers worldwide (World Glacier Monitoring Service, 2012), and they have different structural and morphological characteristics. The large number and variety of glaciers make it unrealistic to model each of them individually. This leads to the empirical modeling of global sea level rise caused by glaciers and ice caps against global average surface temperature change, as mentioned previously. However, global total mass balance sensitivity calculated following the empirical modeling approach is greater than physical model results, which cannot be explained satisfactorily by current state of knowledge (Meehl et al., 2007).

The contribution of ice sheet dynamics is one of the most significant gaps in our current understanding of physical mechanisms behind sea level change. This dynamics is not a simple heat-uptake from the atmosphere. It has complicated underlying mechanisms involving ice cracks, water flow within the ice, ice sliding over the bedrock, etc (Alley et al., 2005; Alley and Joughin, 2012; von Storch et al., 2008). Major challenges for ice sheet dynamics modeling include stresses within ice sheets, different grid sizes for atmospheric signals and ice sheets, surface and subglacial hydrology, and ice shelf interactions with ocean circulation (U.S. Climate Change Science Program, 2008).

Because of the insufficient understanding of physical mechanisms, the IPCC applied simplistic approximation for calculation of corresponding sea level change (Meehl et al., 2007). The modeling of ice sheet dynamics by the IPCC relied heavily on parameterization. For instance, a scenario independent term (0.32 ± 0.35 mm/yr) is added

to the predicted contributions from ice sheet surface mass balance, which is derived from the portion of the present ice sheet mass balance estimated to be due to dynamic changes during the period 1993–2003. This approach assumes that this term can reflect recent ice flow acceleration, and that this contribution will remain unchanged. Both assumptions are problematic when compared to recent observations. Recent studies show that ice sheet appear to be experiencing accelerated mass loss (King et al., 2012; Rignot and Kanagaratnam, 2006; Rignot et al., 2011; Velicogna and Wahr, 2006), raising even more concerns about the process-based models' ability to accurately project future sea level change. In addition, the ice sheet models are generally applied in "off-line" mode, meaning that they do not provide feedbacks to the AOGCMs. However, a study has shown that the time scale of projected melting of the Greenland Ice Sheet may be different in coupled and off-line simulations (Ridley et al., 2005).

Based on their literature review, Jevrejeva et al. (2012) stated "at present, there are very few estimates of dynamical ice sheet loss which are not simply statistical extrapolations or expert opinion, and all models lack a proper representation of key processes such as calving." This summarizes the limitations of current physical ice sheet models rather well.

2.2.3.3 The uncertainty issue of process-based models

The process-based models aim to simulate sea level change by summing up the major components: thermal expansion, mass contribution from glaciers and ice sheets (Meehl et al., 2007). As described in previous sections, the modeling approaches for glaciers and ice sheets have significant limitations. An additional issue is the uncertainty of measurement data. For the process-based models, measurements of all components are needed, which is a tremendous challenge for the scientific community. For instance, the satellite imagery approach for glacier ice measurement only reveals the surface area, and

the total volume is still uncertain, with estimates ranging from 24 to 60 cm sea level equivalent (Rahmsorf, 2012b). The large ice sheets are also very challenging to measure. Recognizing the uncertainties both in measurements and models, the IPCC's Fourth Assessment Report stated "the upper values of the ranges given are not to be considered upper bounds for sea level rise." There are also concerns within the scientific community that the IPCC projections for the 21st century sea level rise may be an underestimated range (Horton et al., 2008; Jevrejeva et al., 2012; Moore et al., 2010; Rahmstorf et al., 2007; Zecca and Chiari, 2012).

2.2.4 Summary

Global sea level change models based on physical processes conceptually divide the total global mean change into contributions by thermal expansion of the ocean, mountain glaciers and ice caps, and ice sheets. These models then calculate the contribution to sea level change by each component separately with different physically based formulations which may also include empirical components. The process-based models have the merit of explicitly linking specific physical mechanisms with mathematical formulations. They are useful tools to investigate the mechanisms behind sea level change. However, the physical mechanisms of sea level change associated with ice sheet dynamics are not sufficiently understood, and observational records for land ice have limitations both in quantity and in quality. Consequently, parameterization is heavily involved in modeling sea level change contributed by land ice change. The resulted model predictions of sea level did not match observations very well. Based on literature review, current process-based models are not good choices for projecting future sea level change. Improvement of land ice measurement technology, modifications of process-based models based on new measurement data, and alternative modeling approaches are among the potential advances needed to project future sea level with more confidence.

2.3 Semi-empirical models

2.3.1 Review of semi-empirical models

Since process-based models cannot yet adequately characterize the complex physical mechanisms behind sea level change, an alternative way to model sea level change has been proposed, namely "semi-empirical" approach. The semi-empirical models utilize numerical and statistical techniques to characterize the link between global sea level and global temperature based on historical observations, which will then be used to project the future. The term "semi-empirical" comes from the fact that the model formulation originates from basic physical considerations but parameters of the model needs to be determined empirically from data (Rahmstorf et al., 2012). The rationale behind empirical modeling is that all major contributors to sea level rise will respond to temperature change (Grinsted et al., 2010). Accordingly, by quantifying the correlation between sea level rise and temperature, all known and unknown mechanisms of sea level rise could be incorporated into the analysis (Rahmstorf, 2007).

Most previous studies on semi-empirical modeling of sea level rise mainly focused on the relationship between global average sea level and global average surface temperature (Etkins and Epstein, 1982; Gornitz et al., 1982; Grinsted et al., 2010; Jevrejeva et al., 2009; Jevrejeva et al., 2010; Rahmstorf et al., 2007; Vermeer and Rahmstorf, 2009; Winkelmann and Levermann, 2013). In the study by Etkins and Epstein (1982), based on data between 1890 and 1980, the rate of global mean sea level rise was hypothesized to be linearly dependent on the rate of global mean surface temperature change and the rate of polar ice sheet mass change. Gornitz et al. (1982) found that global mean sea level is positively correlated with global mean surface air temperature based on observational data from 1880 to 1980. Based on observed data sets for the period of 1880 to 2001, Rahmstorf (2007) proposed that the rate of global mean sea level rise is highly dependent

on global mean surface air temperature, quantified by a coefficient of 3.4 mm/yr/°C. In a subsequent study by Vermeer and Rahmstorf (2009), the original model (Rahmstorf, 2007) was modified by adding a rapid-response term, which assumes that the rate of global mean sea level rise is also linearly proportional to the rate of global mean temperature rise and this makes the model perform better in capturing short-term variability of sea level. Grinsted et al. (2010) constructed their semi-empirical model of sea level rise and temperature with more parameters than those used previously, but they essentially assumed that the rate of global mean sea level rise is linearly dependent on global mean surface air temperature, same as that presented by Rahmstorf (2007). Their model was later modified to link sea level rise directly with global radiative forcing change (Jevrejeva et al., 2009). Utilizing their ice sheet model simulation results, Winkelmann and Levermann (2013) proposed a model with linear response functions to estimate sea level change contributions by thermal expansion and solid ice discharge from the ice sheets, which can be included in the category of semi-empirical models.

Formulations of major semi-empirical models are summarized in the table below, where t denotes time, H or $H(t)$ is the global mean sea level at time t, T or $T(t)$ is the global mean surface temperature at time t, ΔH and ΔT are the changes of H and T, respectively, T_0 and t_0 are constant temperature and time, respectively. Other letters are all model parameters to be determined empirically from data, except those that are explained explicitly in the table. Please refer to the corresponding references for detail explanations of model parameters.

Table 2.2 Major semi-empirical models of sea level change in the literature

Year of publication	Model formulation	Notation	Model parameter	Reference
1982	$\Delta H = a\Delta T + b\Delta M$	ΔM is the change of ocean mass.	$a = 18\ mm/^{\circ}C;\ b = 2.6\times10^{-15}\ mm/kg$	(Etkins and Epstein, 1982)
1982	$H(t) = aT(t - t_0) + b$	--	$a = 160\ mm/^{\circ}C;\ b = 3\ mm;\ t_0 = 10\ yr$	(Gornitz et al., 1982)
2007	$\frac{dH}{dt} = a(T - T_0)$	--	$a = 3.4\ mm/yr/^{\circ}C;\ T_0 = -0.5^{\circ}C$	(Rahmstorf, 2007)
2009	$\frac{dH}{dt} = a(T - T_0) + b\frac{dT}{dt}$	--	$a = 5.6\ mm/yr/^{\circ}C;\ b = -49\ mm/^{\circ}C;$ $T_0 = -0.41^{\circ}C$	(Vermeer and Rahmstorf, 2009)
2009	$\frac{dH}{dt} = \frac{1}{\tau}(aT + b - H)$	--	$a = 3100\ mm/^{\circ}C;\ b = 3680\ mm;$ $\tau = 1193\ yr$	(Grinsted et al., 2010)
2010	$\frac{dH}{dt} = \frac{1}{\tau}(aF + b - H)$	F is the global mean radiative forcing.	$a = 500\ mm/(W/m^2);\ b = 500\ mm;$ $\tau = 200\ yr$	(Jevrejeva et al., 2010)
2013	$\frac{dH}{dt} = \int_0^t c\left(\frac{t - t'}{t_0}\right)^{\alpha} f(t')\,dt'$	$f(t')$ is the external forcing related to global temperature perturbation.	$\alpha = -0.7, 0.1, -0.7$ for thermal expansion, Antarctic and Greenland Ice sheet, respectively.	(Winkelmann and Levermann, 2013)

The ranges of projected global mean sea level rise in the 21st century by published semi-empirical models are summarized in Table 2.2. In this figure, the projections generally span the range of 50 to 150 cm, with the widest range of 30-215 cm.

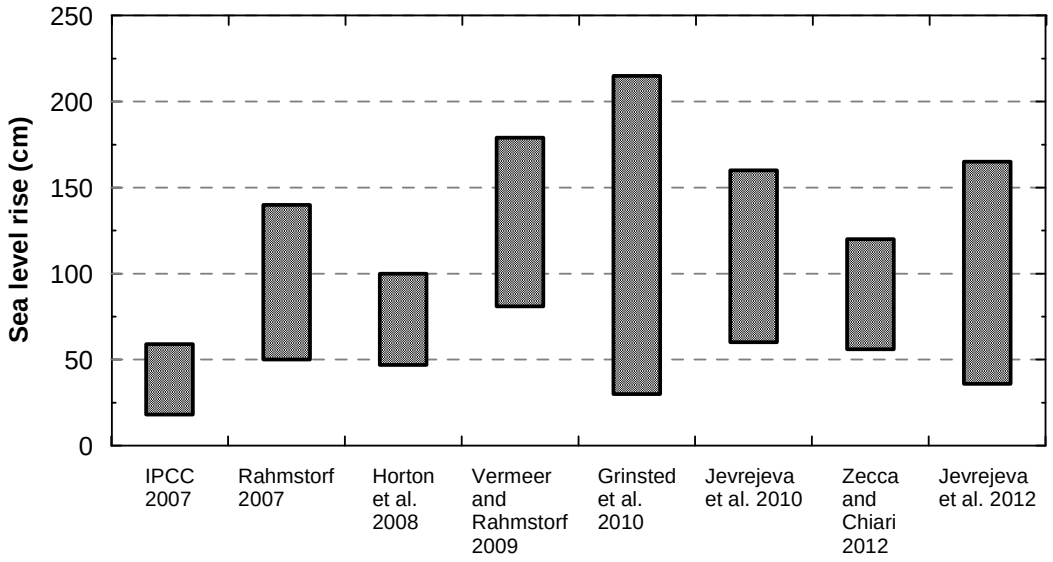

Figure 2.1 Projections of sea level rise in the 21st century by semi-empirical models (please refer to original publications for details of definition of sea level rise, climate scenarios, confidence level, etc.)

2.3.2 Limitations of semi-empirical models

The semi-empirical models have relatively simple model formulation and their parameters need to be configured empirically. Projections of sea level rise in the 21st century by these models, as shown in Figure 2.1, are generally larger than those obtained by process-based models. These facts have raised concerns among scientists, and there have been discussions about the limitations of semi-empirical models.

2.3.2.1 Physical basis

Since semi-empirical models of sea level change do not characterize each related physical process explicitly and separately, there have been concerns about whether they comply with established physical laws. For instance, Church et al. (2011) argue that non-climate-change-related sea level rise, such as water impoundment by dams, GIA, groundwater depletion, should be removed from the calibration dataset for semi-empirical models, and they found certain studies fail to apply a correction for groundwater depletion (Church et al., 2011). Based on a statistical analysis, Schmith et al. (2012) recently proposed that the global mean surface air temperature adjusts to the average temperature of the upper ocean, which is proportional to sea level change due to thermal expansion. This proposition indicates that global mean surface air temperature may adjust to sea level change, in opposition to the physical formulation of the semi-empirical model by Rahmsorf (2007), where sea level adjusts to temperature change. In addition, same with the process-based models mentioned previously, the semi-empirical models so far are also generally applied in "off-line" mode. They do not consider possible feedbacks of sea level to temperature or to itself. The effects of this offline mode application remain to be investigated and quantified.

2.3.2.2 Linearity of the models

The linear relationship between the rate of sea level change and global mean temperature in some semi-empirical models has also been questioned. Church et al. (2011) pointed out two processes influencing sea level cannot be represented as linear, the reduction of glacier area and the decrease of the ocean heat uptake efficiency. Other studies suggested that the nonlinear process of ice sheet dynamics may contribute significantly to sea level change, which will invalidate the linear formulation in the semi-empirical models (Hansen, 2007; Jevrejeva et al., 2012). Hansen (2007) stated that although the

contribution of ice sheet dynamics to sea level change was small until the past few years, it has doubled in the past decade, thus the interaction will unlikely follow a linear trend in response to global warming. Rahmstorf (2010) acknowledged that the linear relationship in the semi-empirical model does not capture the possible rapid nonlinear ice-flow changes expected by some glaciologists in the future, and he further suggested that the linear semi-empirical model will underestimate sea level rise if the rapid nonlinear ice-flow changes actually happen.

2.3.2.3 Statistical techniques

In the literature, questions also exist regarding the adequacy of statistical techniques used in some semi-empirical studies. The major issue is the application of ordinary least square (OLS) method to nonstationary time series for parameter estimation, e.g., the method applied in the study by Rahmstorf (2007). Several scientists argued that the study by Rahmstorf (2007) inappropriately applied OLS method to nonstationary time series of temperature/sea level records, hence the study may give misleading results (Schmith et al., 2012; von Storch et al., 2008). When the OLS method is applied to nonstationary time series, the residuals can potentially have positive autocorrelation, violating the basic assumption of independent identically distributed (IID) errors for OLS method (von Storch et al., 2008). However, based on theories of statistics, the OLS estimator for continuous dependent variables (e.g., rate of sea level rise) is inefficient when the IID assumption is violated, but it remains unbiased and consistent (Powers and Xie, 2008). According to this conclusion, applying OLS method for the estimation of semi-empirical model parameters will not result in biased parameters, but it will lead to inaccurate uncertainty estimate. To improve the statistical methodology, Rahmstorf et al. (2012) adopted the generalized least square (GLS) method instead of OLS for parameter estimation, which theoretically accounts for autocorrelation in the residual series

(Cwpertwait and Metcalfe, 2009). The results of Rahmstorf et al. (2012) indicate that parameter estimates by GLS are very similar with those by OLS, but parameter uncertainty estimation by GLS has been improved.

2.3.2.4 Strengths of semi-empirical models

The first advantage of semi-empirical approach to sea level change over process-based models is that they reproduce historical sea level records well. Simulated sea level rise rate during 1993–2006 by semi-empirical models is 3–4 mm/yr, very close to the rate of 3.3 mm/yr calculated from satellite altimetry, while process-based models' estimate of the rate is 1.9 mm/yr (Jevrejeva et al., 2012). Semi-empirical models also have the merit of implicitly accounting for the impacts of all the climate-related factors and their possible feedbacks on sea level change (Zecca and Chiari, 2012) since historical data imbeds this information into the model during calibration.

The linear relationship in semi-empirical models cannot be guaranteed to hold in the future (Rahmstorf et al., 2007; Rahmstorf et al., 2012), just as the assumptions used by the process-based models may not be valid under future scenarios (Meehl et al., 2007). Nonetheless, semi-empirical models reasonably represent behaviors of thermal expansion and glacier and ice sheet melting exhibited in the historical records. Specifically, the sea level response of complex physical models related to thermal expansion is well reproduced by the semi-empirical method (Rahmstorf, 2007), and the linear dependence of land ice on temperature is similar to that used in glacier modeling studies and by the IPCC (Rahmstorf, 2010). Based on their derivation, von Storch et al. (2008) suggested that a linear relationship should exist between the near-surface air-temperature and the global mean heat flux into the ocean for the linear relationship in semi-empirical models to hold. They then cited references indicating the heat-flux into the ocean is correlated

with the global mean near-surface temperature, although the physical mechanisms behind this correlation remain to be explained (von Storch et al., 2008). Semi-empirical models have also been tested recently using different formulations, statistical techniques, and choices of input data sets for temperature and sea level, and the projections of different versions of semi-empirical models were found to be robust (Rahmstorf et al., 2012).

The simplicity of semi-empirical models significantly decreases the requirement for computational power. As a result, systematic parameter sensitivity analysis and uncertainty assessment can be conducted in a timely manner, and projections under various future scenarios are computationally possible. This is particularly interesting as there have been active discussions on the uncertainty issue of complex physical models (such as those used by the IPCC) (Curry and Webster, 2011; Hegerl et al., 2011).

Because of these characteristics, semi-empirical approach can serve as an effective alternative to the still uncertain process-based climate model projections (Cazenave and Llovel, 2010). However, because the empirical relationship identified from historical records cannot be guaranteed to hold in the future (Rahmstorf, 2012), they should only serve as an alternative before our understanding of physical mechanisms are mature. Further more, the semi-empirical method should help to improve our understanding of physical mechanisms, so as to decrease empiricism in climate modeling.

2.3.3 Summary

Because of process-based models' limitations in representing ice change mechanisms and unsatisfying performance in reproducing historical sea level records, semi-empirical models are developed as an alternative approach. The semi-empirical models utilize numerical and statistical techniques to characterize the link between global sea level and

global temperature in historical observations, which is subsequently applied to project the future.

Semi-empirical models have their own limitations by nature. The most important limitation of semi-empirical models is that the relationship (usually linear) between sea level and temperature configured based on historical data cannot be guaranteed to hold in the future. Some technical aspects of semi-empirical models also need improvement. For example, non-climate-change-related sea level rise should be removed from the calibration dataset of semi-empirical models, and adequate statistical techniques should be chosen to address data with specific characteristics such as nonstationarity.

Despite their limitations, semi-empirical models have the advantage of reproducing historical sea level records well. Their proposed relationships do not conflict significantly with established physical laws in their concerned time frame. Projections of sea level in the 21st century by semi-empirical models are generally higher than those by the process-based models. Considering the widespread concerns that process-based models might underestimate future sea level rise, semi-empirical models provide an acceptable alternative before our understanding of physical mechanisms are mature. In addition, semi-empirical models are relatively new, and can be improved to represent the physical system more accurately. In this direction, the semi-empirical method can help to advance our understanding of physical mechanisms, so as to decrease empiricism in climate modeling.

2.4 Dynamic system models

As mentioned in previous paragraphs, both process-based and semi-empirical models of sea level change that appear in the literature generally operate in an “off-line” mode,

where sea level change is simulated as a function of temperature change. They do not consider possible impacts of sea level change on temperature or the feedback of sea level on itself. It has been known that sea level change can potentially influence the temperature through mechanisms such as change of surface albedo and moisture availability, alteration of ocean currents, and continental shelf CO_2 pump (National Research Council, 1990; Rippeth et al., 2008). For example, increased sea level is likely associated with ice loss, and ice loss can affect the climate through albedo change and water flux from continents to oceans (Grinsted et al., 2010), which in return may influence the temperature. A model that incorporates the interactions between sea level and temperature ("on-line" mode) can potentially yield better results than those by the models in "off-line" mode.

To incorporate the potential interactions between sea level and temperature and the possible feedbacks, the semi-empirical approach has been extended by recent studies. Like previous semi-empirical models, the new models also determine their parameters empirically from historical data. However, unlike previous semi-empirical models, the new ones take into account the possible interactions and feedbacks between sea level and temperature, thus treating the two as interactive dynamic systems (Aral et al., 2012; Schmith et al., 2012). To reflect the characteristic feature of this category of models, they are named as "dynamic system models" in this study.

In a study by Aral et al. (2012), through systematic analysis of historic data on temperature change and sea level rise, a linear dynamic system model is proposed to predict the two state variables, i.e. temperature and sea level, simultaneously. The governing equation of their model takes the following form

$$\begin{cases} \dfrac{dT}{dt} = a_{11}T + a_{12}H + c_1 \\ \dfrac{dH}{dt} = a_{21}T + a_{22}H + c_2 \end{cases} \tag{2.4}$$

where H and T are global mean sea level and surface temperature in a certain year, respectively; $\frac{dH}{dt}$ and $\frac{dT}{dt}$ are the rates of change in the same year; a_{ij}'s and c_j's are model parameters to be determined from historical records. Using this model, Aral et al. (2012) found that, while the rate of sea level rise is proportional to global mean temperature, it is also restrained by the current state of sea level with a constant of -0.0045/yr. They suggested that this negative constant implies the decelerating effect of current sea level on the evolution of its state. Their model results also indicated that sea level rise may slightly accelerate temperature rise (Aral et al., 2012).

In a more recent study, Schmith et al. (2012) proposed a first-order vector autoregressive (VAR) model for the relationship between sea level and temperature, and applied cointegration analysis to investigate the interactions between the two. The form of their model is very similar to that of Aral et al. (2012) when written in discrete form, with equations as below

$$\begin{pmatrix} \Delta T_t \\ \Delta h_t \end{pmatrix} = \Pi \begin{pmatrix} T_{t-1} \\ h_{t-1} \end{pmatrix} + \begin{pmatrix} \varepsilon_{Tt} \\ \varepsilon_{ht} \end{pmatrix} \tag{2.5}$$

where h_t and T_t are global mean sea level and surface temperature in a certain year t, respectively; Δh_t and ΔT_t are the changes from $t-1$ to t; ε_{Tt} and ε_{ht} are error terms; and Π is a 2×2 parameter matrix to be determined from historical records. Schmith et al. (2012) then used the error correction form of the VAR (abbreviated as VECM) to obtain parameters and investigated the relationship between sea level and temperature. Their model results indicated that temperature causally depends on sea level. The mechanistic

interpretation of this causal relationship is given in their study as: “the upper ocean temperature is strongly related to the sea level due to thermal expansion, and it dominates the surface air temperature because of its large heat capacity” (Schmith et al., 2012).

The dynamic system models inevitably inherit some limitations of previous semi-empirical models of sea level change. The relationship between rate of sea level change and impacting factors (states of sea level and temperature) is still proposed as linear, which cannot be guaranteed to hold in the future. Nonetheless, the dynamic system models have advanced the semi-empirical approach by considering feedbacks and interactions in the coupled sea level and temperature systems. Compared to previous semi-empirical models, the dynamic system models also have the additional capability of predicting temperature, which can be further improved by taking into account of other influencing factors. Because of these characteristics, dynamic system models can serve as viable options for sea level change simulation.

Because of the improvements, in dynamic system models the relationship between sea level change and temperature is not straightforwardly linear anymore, and the corresponding projections for the 21st century may also change. For example, projected sea level rise in the 21st century by a representative semi-empirical model (Rahmstorf, 2007) is compared with that by a representative dynamic system model (Aral et al., 2012) (Figure 2.2). In the figure, the range of sea level rise projection by Aral et al. (2012) is lower than that by Rahmstorf (2007), although they used the same temperature inputs. The difference is indicative of different systematic behaviors of dynamic system models from previous semi-empirical models.

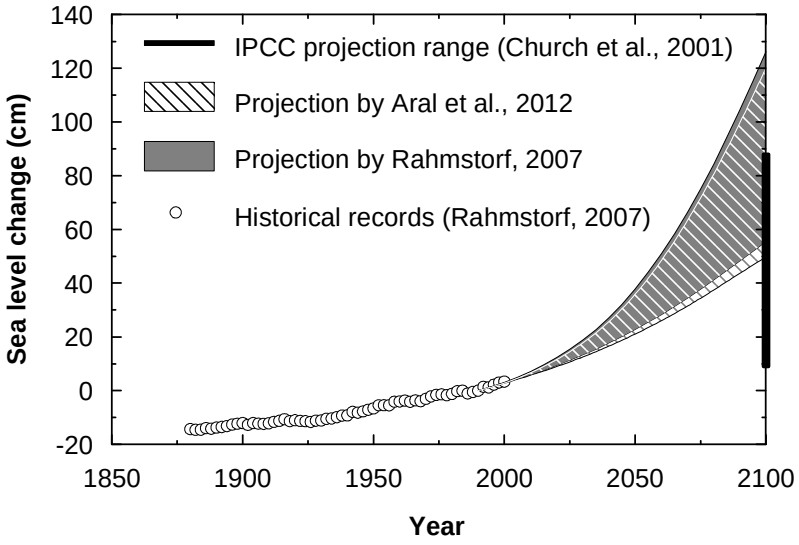

Figure 2.2 Comparison of sea level rise projections by semi-empirical and dynamic system model

2.5 Spatial variability of sea level

Another important aspect of sea level change modeling is the simulation of spatial variability of sea level, which is more relevant to local communities. Based on observational records, significant spatial variations exist in sea surface heights (Figure 2.3). During the period of 1992 to 2004, regional variations of sea level are found to be larger than the expected global-mean values (Wunsch et al., 2007). Model projections by the IPCC typically have regional sea level change varying within about ±0.15 m of the mean (Bindoff et al., 2007).

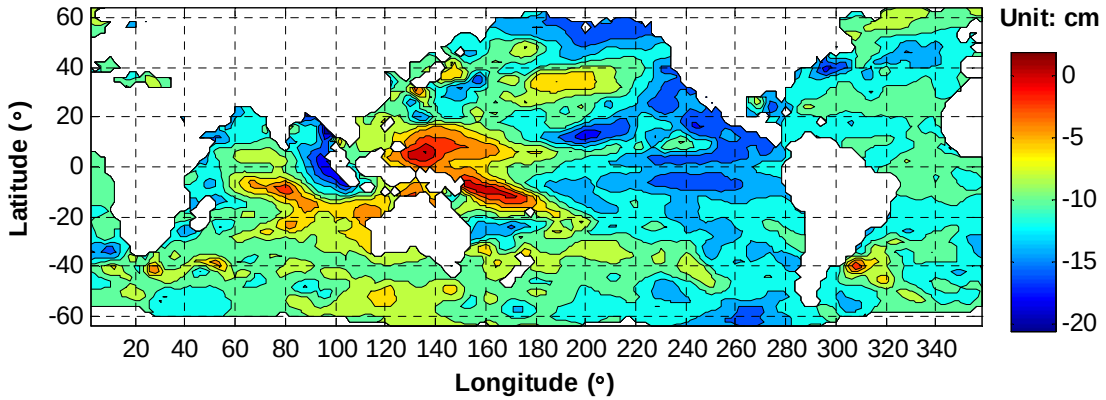

Figure 2.3 Yearly mean sea surface height at 1950 (Church et al., 2004)

Various mechanisms can contribute to the spatial patterns of sea level rise. Polar ice mass change is found to impact the spatial variation of sea level near the poles (Mitrovica et al., 2001). After a polar ice melting event, sea surface height will actually decrease within 2000 km of the melting ice sheet, and increase progressively as one migrates away from this region (Mitrovica et al., 2009). Local surface heating is important in explaining the interannual sea level variability in various regions of the Atlantic Ocean (Cabanes et al., 2006). Regional sea level pattern in the equatorial Pacific Ocean since 1993 is potentially caused by varying wind patterns associated with climate phenomena such as El Nino Southern Oscillation, which is largely reflected in regional patterns of ocean thermal expansion (Church et al., 2010). Analysis of model projections also revealed that spatial patterns in sea level are dominated by steric effects associated with the ocean's density field (Pardaens et al., 2011). By analyzing spatial sea level data during the period of 1992 to 2004, Wunsch et al. (2007) suggested general circulation change as another major contributor to the observed sea level variations.

Despite various studies on the geographical pattern of sea level change, physical models targeting the spatial patterns are still in their preliminary stages. For instance, in the Fourth Assessment Report by the Intergovernmental Panel on Climate Change (IPCC), geographical patterns of sea level change projected by different models are not similar in detail, with only 25% of spatial correlation coefficients between the pairs of models are larger than 0.5 (Meelh et al., 2007). Major research efforts are still needed to understand the underlying oceanographic and climate processes to improve the predictions of spatial variability in future sea level change (Milne et al., 2009). As an alternative to process-based physical models, semi-empirical models so far have only focused on global mean state of sea level (Grinsted et al., 2010; Jevrejeva et al., 2009; Rahmstorf et al., 2007; Rahmstorf et al., 2012; Vermeer and Rahmstorf, 2009). As a result, both process-based and semi-empirical sea level change models currently suffer significant drawbacks in characterizing spatial variations of sea level.

This study attempts to address the issue of spatial variations in sea level through a dynamic system modeling approach. The dynamic system approach is improved to incorporate spatial analysis capability, so that interactions among sea levels and surface temperatures in different regions of the oceans can be investigated. Our dynamic system approach avoids the unconstrained uncertainty caused by incorporating two many physical processes, as commonly seen in mechanistic models. Meanwhile, compared to typical spatial statistical approaches such as empirical orthogonal function analysis, the dynamic system approach has a stronger ability to relate the spatial variations of sea level rise to its underlying cause of global warming.

CHAPTER 3

PATTERN RECOGNITION AND DATA RECONSTRUCTION FOR SPATIAL SEA LEVEL RECORDS

3.1 Introduction

Sea level data can be grouped into different regions by various approaches for different analysis purposes of spatial pattern characterization. For instance, regional mean sea level comparison (Bursa et al., 1999) and identification of contributing factors to regional sea level differences (Menemenlis et al., 2007) require spatial data to be grouped into pre-defined regions. In the coming Chapter 4, the ocean will be divideed into 3 regions based on the three major ocean basins (the Indian, Pacific, and Atlantic Ocean) for one spatial analysis application. Under other circumstances, however, researchers may need to identify spatial patterns from the data based on attribute characteristics, which is previously unknown and cannot be arbitrarily defined. Despite numerous studies on spatial variations of sea level in the literature (Cabanes et al., 2006; Mitrovica et al., 2001; Mitrovica et al., 2009; Pardaens et al., 2011; Wunsch et al., 2007), few studies developed methodologies to identify spatial patterns automatically from spatial sea level data. To reveal spatial pattern of the sea level signal, a spatial pattern recognition technique based on clustering algorithms is proposed in this chapter to group the spatial sea level data. As an unsupervised learning method, clustering can help to divide the ocean into regions within which similarity of certain sea level attribute record is optimized. In addition, the dissimilarities between different regions are maximized. Because of the maximal intra-cluster similarity and inter-cluster dissimilarity (Liao, 2005), regions identified by clustering methods have distinct characteristics which may reflect the underlying climate phenomena.

Since spatial regions resulted from different region division approaches may reflect climate patterns contained in historical records, time series of average sea level for these regions have particular characteristics related to corresponding climate phenomena. Temporal patterns contained in long time series of mean sea level for these regions may provide support for studies of related climate phenomena. Unfortunately, however, spatial sea level data is scarce and time span of spatial data sets generally are also relatively short (Chambers et al., 2002; Hamlington et al., 2012; Meyssignac et al., 2012; Smith, 2000). To the contrary of spatial sea level data's scarcity, various studies have reconstructed global mean sea level and spatial sea surface temperature (SST) data with relatively long time span (Church and White, 2006; Church and White, 2011; Gregory et al., 2012; Smith et al., 2008). Previous researches indicated that sea level's spatial patterns are closely related to the thermosteric effect (Levitus et al., 2005; Levitus et al., 2009; Lombard et al., 2005), which motivates us to reconstruct regional mean sea level from spatial SST data. Previous studies have commonly used the empirical orthogonal function (EOF) method to reconstruct spatial sea level data (Church et al., 2004; Hamlington et al., 2012; Llovel et al., 2009; Smith, 2000). The EOF approach works well for filling data gaps, but is not an appropriate choice for reconstructing regional mean sea level from the global mean value. To address this issue, a method based on neural network analysis is adopted to reconstruct regional mean sea level from global mean sea level and spatial SST data.

The clustering algorithm developed in this chapter can identify characteristic spatial patterns from spatial sea level data. It is also capable of evaluating the relative strengths of different spatial climate signals. The neural network approach can successfully reconstruct spatial average sea level of different regions, and is potentially useful for related climate studies. In this study, the reconstructed regional mean sea levels for the

three major ocean basins and the clustered regions are used to calibrate our spatial dynamic system model as described in Chapter 4.

3.2 Clustering spatial sea level data

Clustering techniques group objects into different clusters based on their similarity in the feature space (Chuang et al., 2006). In this study, the spatial sea level data by Church et al. (2004) is applied to test our clustering methodology. The date set contains monthly records of sea level on a 1°×1° lat-long grid from 1950 to 2001. Since only the annual average sea level data is considered in the clustering process, each object has 52 records. Our feature space can consequently be viewed as 52-dimensional. To be consistent with the subsequent studies, the spatial data by Church et al. (2004) were resampled, which leads to a final spatial coverage of 2-358°E and 64°S-64°N on a 2°×2° lat-long grid. The total number of spatial grids with sea level records is about 8000. Our task can be then defined as grouping these 8000 grids into different clusters based on their attribute in the 52-dimensional feature space.

The fuzzy C-means algorithm (Bezdek et al., 1984) was first applied to cluster our spatial sea level data. As a classical clustering technique, fuzzy C-means calculates the probability of an object belonging to each cluster based on the minimization of a cost function. It has been widely used in pattern recognition applications such as medical image segmentation (Phillips et al., 1995), gene identification (Dembele and Kastner, 2003), audio signal processing (Haque and Kim, 2013), and geographic information systems (Di Martino and Sessa, 2009). Fuzzy C-means implements probabilistic membership assignment to avoid arbitrarily forcing a certain object to be included only in one cluster, a practice by hard clustering techniques such as K-means (Selim and Ismail, 1984). Because of this feature, fuzzy C-means has been shown to perform better than K-

means (Hamerly and Elkan, 2002). However, the fuzzy C-means method has a major disadvantage when processing spatial data for it cannot utilize the spatial information. Information in the geographical space is often correlated, and features in neighboring spatial locations tend to be similar. In the classical fuzzy C-means algorithm, objects contiguous to each other are treated the same as those far apart, thus spatial contiguity information is ignored.

To utilize the spatial information in target data, an improved version of fuzzy C-means algorithm by Pham (2001) is adopted here. The mathematical formulation of the spatial fuzzy C-mean algorithm is as below:

$$J_{Total} = \sum_{i=1}^{n}\sum_{k=1}^{K} r_{ik}^{m} \left\| \boldsymbol{x}_i - \boldsymbol{\mu}_k \right\|^2 + \frac{\beta}{2}\sum_{i=1}^{n}\sum_{k=1}^{K} r_{ik}^{m} \sum_{j=1}^{n}\sum_{l\neq k}^{[1,K]} p_{ij} r_{jl}^{m} \tag{3.1}$$

$$\sum_{k=1}^{K} r_{ik} = 1 \tag{3.2}$$

$$\boldsymbol{\mu}_k = \frac{\sum_{i=1}^{n} r_{ik}^{m} \boldsymbol{x}_i}{\sum_{i=1}^{n} r_{ik}^{m}} \tag{3.3}$$

where i, j, and l all indicate the spatial identity of an grid ($n = 8000$), k is the identity of a cluster (K is a fixed integer larger than 1), $\boldsymbol{x}_i$ is the sea level data vector at grid i, $\boldsymbol{\mu}_k$ is the sea level data vector at the center of cluster k in the feature space, r_{ik} is the probability of grid i belonging to cluster k, p_{ij} is the spatial contiguity multiplier (1 if grid i is contiguous to grid j, 0 if grid i is not contiguous to grid j), m is the parameter controlling the degree of fuzziness, and β is the spatial penalty (a large number forces high similarity between contiguous grids).

Because of the temporal trend and spatial variation in the original sea level data (Figure 3.1), they need to be processed before entering the clustering procedure. Since the aim of this study is to identify a stable spatial pattern of the sea level over time, annual global mean sea level was subtracted from the data set to isolate spatial variability from global trend. The spatial variance of sea level changes over time, indicating that the 52 dimensions of the feature space have varying magnitudes. As a result, the shapes of prospective clusters are likely to be non-spherical in the feature space, which can cause a major problem for the algorithm in Equation (3.1). The spatial fuzzy C-means algorithm's cost function is based on the Euclidean norm of the difference between the objects and cluster centers ($\|\boldsymbol{x}_i - \boldsymbol{\mu}_k\|^2$) and resulting clusters will consequently be spherical in the feature space. To address this issue, the Euclidean norm is changed to the Mahalanobis norm. The Mahalanobis norm is suitable when dimensions of the feature space (attributes of objects) are unequally variable, and it also addresses the issue of potential correlations between different dimensions (Equihua, 1990). The modified cost function of the spatial fuzzy C-means algorithm then becomes:

$$J_{Total} = \sum_{i=1}^{n}\sum_{k=1}^{K} r_{ik}^{m} \left(\boldsymbol{x}_i - \boldsymbol{\mu}_k\right)^T \mathbf{A}_k \left(\boldsymbol{x}_i - \boldsymbol{\mu}_k\right) + \frac{\beta}{2}\sum_{i=1}^{n}\sum_{k=1}^{K} r_{ik}^{m} \sum_{j=1}^{n}\sum_{l\neq k}^{[1,K]} p_{ij} r_{jl}^{m} \tag{3.4}$$

$$\mathbf{A}_k = \mathbf{F}_k^{-1} \tag{3.5}$$

$$\mathbf{F}_k = \frac{\sum_{i=1}^{n} r_{ik}^{m} \left(\boldsymbol{x}_i - \boldsymbol{\mu}_k\right)\left(\boldsymbol{x}_i - \boldsymbol{\mu}_k\right)^T}{\sum_{i=1}^{n} r_{ik}^{m}} \tag{3.6}$$

where $\mathbf{F}_k$ is the weighted covariance matrix for $\left(\boldsymbol{x}_i - \boldsymbol{\mu}_k\right)$ and the norm inducing matrix $\mathbf{A}_k$ is the inverse of $\mathbf{F}_k$. This algorithm essentially adopts the Mahalanobis distance as the measurement of the difference between an object and a cluster center.

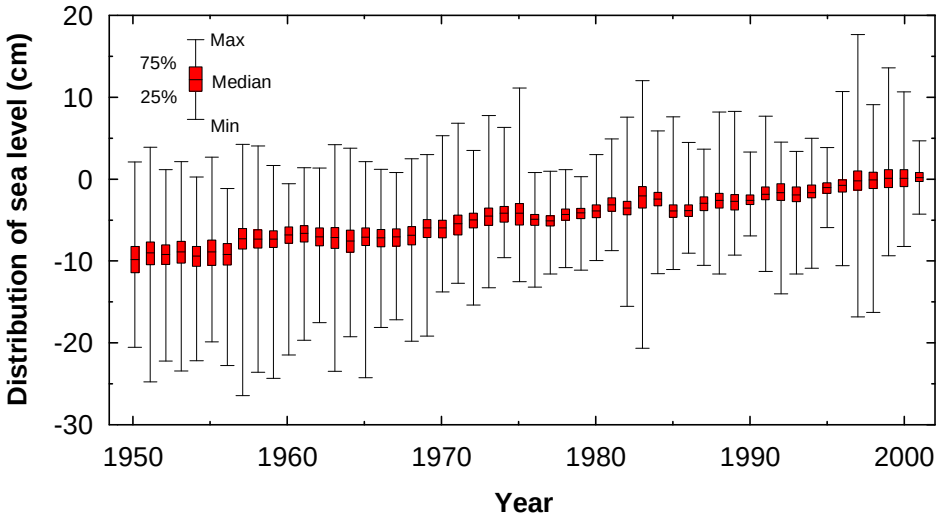

Figure 3.1 Spatial distribution of sea level data over time (data from Church et al., 2004)

Grouping of the spatial grids can be achieved by minimizing the cost function in Equation (3.2) with respect to r_{ik} . The well-known Gustafson-Kessel algorithm (Gustafson and Kessel, 1978) is adopted in constraining the norm inducing matrix $\mathbf{A}_k$ and adopted the numerical scheme by Babuska et al. (2002) to ensure numerical stability. Iterative algorithm to solve for r_{ik} thus achieving the grouping task is shown below.

Table 3.1 Iterative steps of the clustering algorithm

Iterative step	Implementation
0	Randomly generate r_{ik}, with the constraint of Equation (3.2).
1	Compute cluster center $\boldsymbol{\mu}_k$ following Equation (3.3).
2	Compute the weighted covariance matrix $\mathbf{F}_k$ following Equation (3.6).
3	Compute the norm inducing matrix as $\mathbf{A}_k = \left[\det\left(\mathbf{F}_k\right)\right]^{1/d} \mathbf{F}_k^{-1}$ (d is the dimensionality of the feature space).
4	Update r_{ik} by minimizing the cost function in Equation (3.4).
5	Go to Step 1 until convergence.

Cluster validation. Two critical tasks of the clustering practice are: (i) to determine the targeting number of clusters; and (ii) to verify that the resulted clusters are valid. For our clustering algorithm, this cluster number needs to be configured a priori, so external measures are needed to identify the optimal cluster number. A widely adopted approach to identify the appropriate cluster number is cluster validation (Baarsch and Celebi, 2012; Kim et al., 2004; Rawashdeh and Ralescu, 2012). This approach reveals that task (i) can be accomplished using the outcome of task (2). Through cluster validation, the optimal cluster number is determined among various candidate values based on an evaluation metric of their final clustering results. This metric, often referred to as the "cluster validity index", generally evaluates clustering results based on their intra-cluster compactness and inter-cluster separation. Various forms of cluster validity index exist in the literature, and among the most commonly used ones are Dunn's Index (Dunn, 1974), Davies-Bouldin Index (Davies and Bouldin, 1979), Silhouette Index (Rousseeuw, 1987), and Xie-Beni Index (Xie and Beni, 1991). The Silhouette Index is chosen for its simplicity and graphical functionality. The Silhouette Index for a certain object *i* is calculate as

$$s_i = \frac{(b_i - a_i)}{\max(a_i, b_i)} \tag{3.7}$$

where a_i is object i's average distance to other objects in the same cluster, and b_i is object i's average distance to all the objects in other clusters. The value of s_i ranges from -1 to 1, where a larger value indicates better cluster compactness and separation.

The validity of a cluster can be assessed by examining the Silhouette Index values of all the objects within it and the validity of the whole clustering result can be measured by the overall shape of the Silhouette graph (Figure 3.2). Note that in the process of cluster validation, the clustering algorithm (Equation (3.4)) was run without spatial penalty ($\beta = 0$), so that spatial patterns are identified solely based on the original data. Since the average Silhouette Index value of all objects is one important performance metric of the clustering algorithm, it is used as the criterion to select candidates for the optimal number of clusters. When grouping the spatial grids into 2, 3, 4, 5, 6, and 7 clusters, the calculated average Silhouette Index value is 0.33, 0.36, 0.42, 0.33, 0.33, and 0.35, respectively. So results with 3, 4, and 7 clusters have relatively higher validity index values. However, the patterns captured by clustering with 7 regions have relatively small spatial scale and the signals in them are accordingly week. Based on the principle of Occam's razor, 3 and 4 are chosen as the final candidates for the optimal number of clusters to characterize the spatial sea level data.

To finally decide the optimal number of clusters between the two candidates, the details of their Silhouette graphs (Figure 3.2) need to be examined. In the silhouette graphs, most of the objects have positive Silhouette Index value, except for some very small portions. Positive Silhouette Index value indicates that the distance between an object within a cluster and this cluster's center is smaller than the distance between this object and

another cluster's center. So a positive Silhouette Index suggests that the object is appropriately clustered. To the contrary, objects with negative Silhouette Index values received inappropriate cluster assignment. Although the result for clustering with 4 regions has a larger average Silhouette Index value than that for clustering with 3 regions, the former has larger regions of objects with significant cluster misassignment. As a result, the optimal cluster number is chosen as 3, and all the following cluster analysis is for the case with 3 clusters.

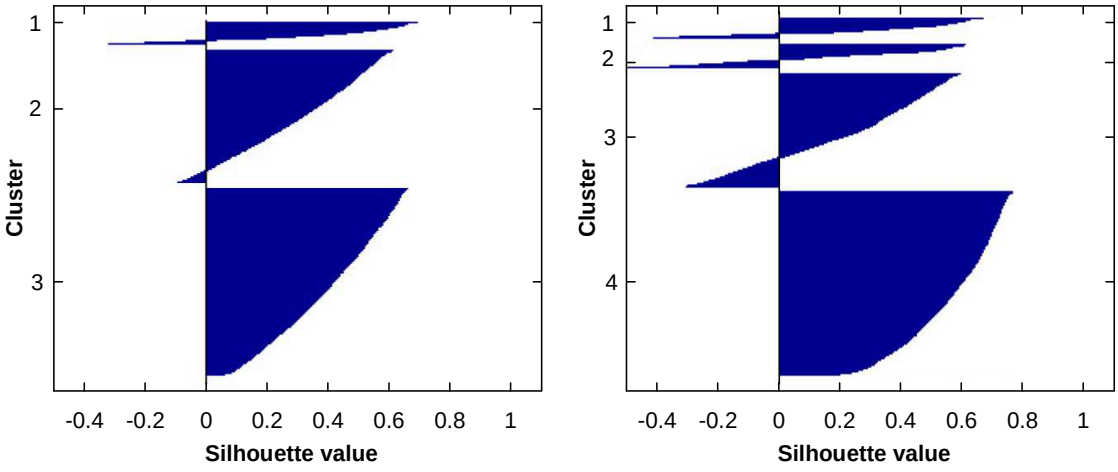

(a) (b)

Figure 3.2 Silhouette graph for the result of clustering with: (a) 3 clusters; (b) 4 clusters.

Physical implications of clustering results. Result of the clustering with 3 regions (with $\beta = 0$) is shown below (Figure 3.3). The spatial pattern shown in our clustering result (Figure 3.3) is closely related to important climate phenomena. Cluster 3's "belt" shaped zone in eastern tropical Pacific probably results from the distinct sea level change behaviors in that region caused by the El Niño-Southern Oscillation (ENSO) events. Meyssignac et al. (2012) demonstrated that sea level in the tropical Pacific region behaves as an east-west dipole that fluctuates following the ENSO mode of variability,

which supports our proposition. The isolated Cluster 1 is mainly located in the western tropical Pacific area, and is also likely related to the ENSO events, as well as the Pacific Decadal Oscillation (PDO). A study by Becker et al. (2012) confirmed that ENSO events strongly influence the interannual sea level variability of the western tropical Pacific. Sea level in this region is lower/higher than average during El Niño/La Niña events on the order of 20–30 cm. Merrifield et al. (2012) also found that sea level changes in the western tropical Pacific are related to PDO and low frequency fluctuations in the Southern Oscillation Index. Two other significant features in the clustering result are the isolated eastern tropical Indian Ocean and the longitudinally oriented region in northern Atlantic Ocean. Previous studies indicate that the former is associated with combined invigoration of the Indian Ocean Hadley and Walker cells (Han et al., 2010) and the later with North Atlantic Oscillation (NAO) (Bindoff et al., 2007).

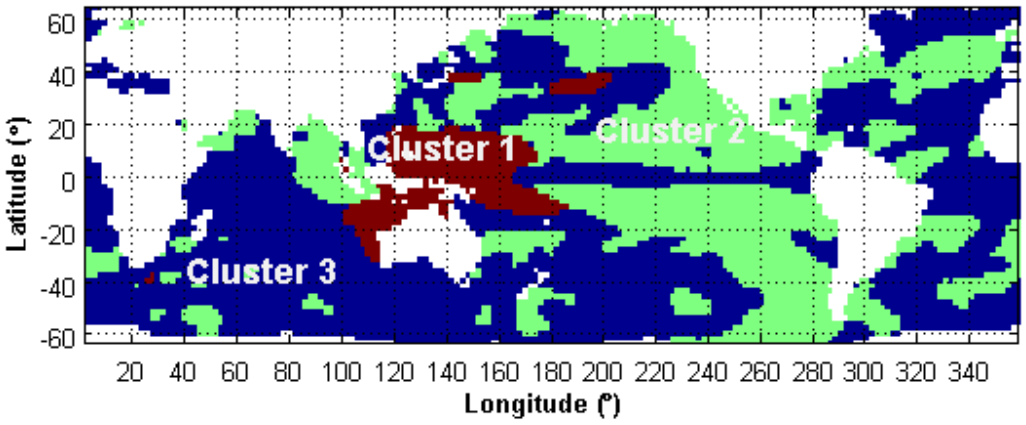

Figure 3.3 Result of clustering with no spatial penalty

Spatial penalty function to test the strength of signals. In our clustering algorithm (Equation (3.4)), the spatial penalty coefficient β sets the strength of the assumed similarity of sea level behavior between contiguous locations. When β is set as a large number, assumed similarity of contiguous is high, a small clustered region tend to be

merged into a large cluster contiguous to it if their sea level behaviors are not significantly different. Because of this functionality, β can be adjusted to filter out noise in the clustering result, and to test the significance of identified spatial patterns and their associate climate phenomena.

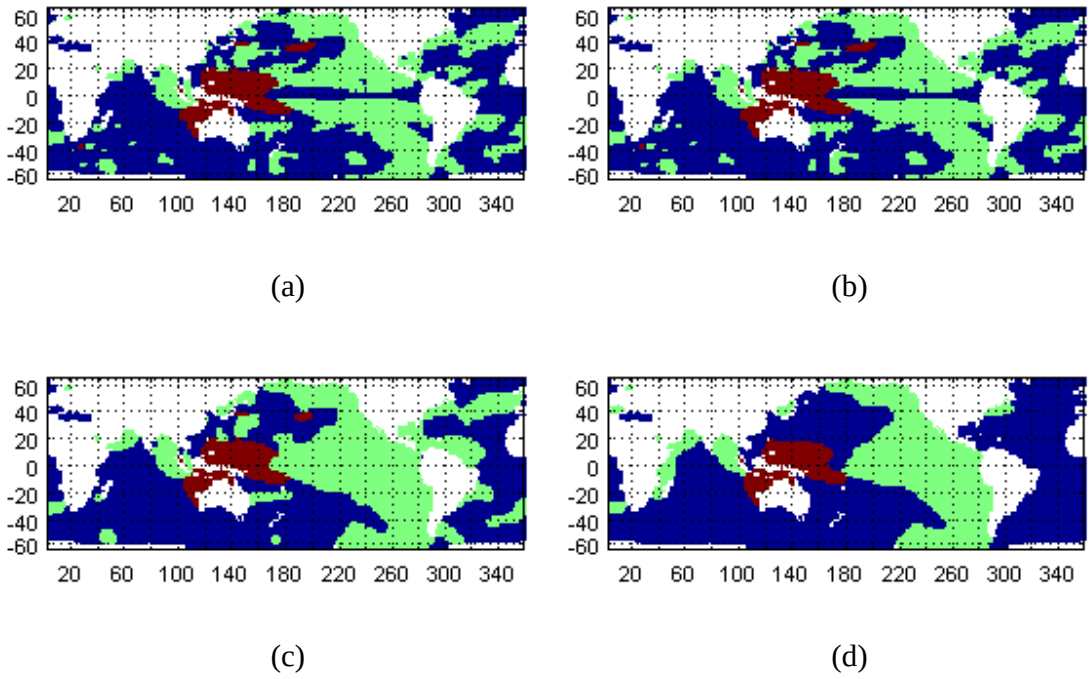

Figure 3.4 Results of clustering with the spatial penalty coefficient (β) set as: (a) 10; (b) 30; (c) 50; and (d) 100.

The impacts of the spatial penalty coefficient β on our clustering result were tested (Figure 3.4). As β increases, small regions of Cluster 1 and Cluster 2 are gradually merged into Cluster 3. So Cluster 3 can be viewed as the major body or the background signal of sea level, while Clusters 1 and 2 are associated with particular climate phenomena. When β is set at a large value of 100, the spatial patterns associated with North Atlantic Oscillation disappear, with the resulting Clusters 1 and 2 mainly reflecting

the spatial characteristics of ENSO events. This result reveals that, compared to regional climate phenomena like PDO and NAO, the ENSO events have stronger influences on the spatial variations of sea level. This conclusion is supported by the Intergovernmental Panel on Climate Change's (IPCC) findings in its Fourth Assessment Report (Meehl et al., 2007). Scientists in the IPCC found that ENSO-related ocean variability accounts for the largest fraction of variance in spatial patterns of thermosteric sea level (Bindoff et al., 2007). Since themosteric effect is the major contributor to spatial sea level variations (Bindoff et al., 2007; Meyssignac et al., 2012), this study's finding that ENSO has stronger impacts on spatial sea level variations than PDO and NAO is consistent with that of the IPCC.

3.3 Spatial sea level data reconstruction

Average sea levels for regions identified by our algorithm with β=100 are computed since this clustering eliminated insignificant noisy signals and retained spatial patterns of major climate phenomena (Figure 3.5). Compared to the average sea levels of three major ocean basins, those of the clustered regions show significant temporal patterns, which may provide support for studies of related climate phenomena. For this reason, long time series of mean sea level for these regions may be valuable. Unfortunately, as described above, time span of spatial sea level data is relative short. For instant, the sea surface height dataset constructed by Church et al. (2004) is only from 1950 to 2001. This shortage of spatial sea level data motivates us to resort to reconstruction techniques to establish longer time series of mean sea level for targeting regions.

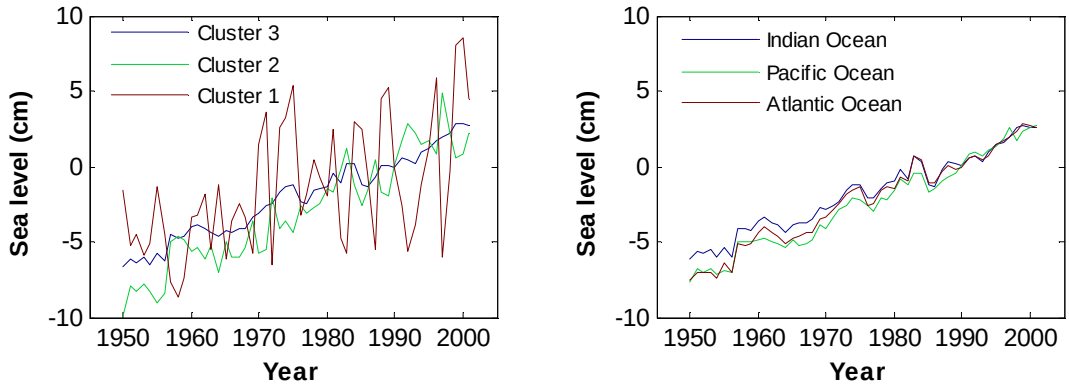

(a) (b)

Figure 3.5 Average sea levels of: (a) regions identified by clustering; (b) three major ocean basins

Previous studies on the reconstruction of records near sea level (SST, sea level pressure, and sea level) have utilized the technique of Empirical Orthogonal Function (EOF) (Smith et al., 1996; Kaplan et al., 2000; Church et al., 2004). This method constructs EOFs as eigenvectors of the spatial covariance matrix of data records from a certain time period, and uses these EOFs to reconstruct spatial data beyond the original period. In doing so, the EOF method assumes that the spatial covariance of data in the reconstruction period is the same as that in the observation period. Artificial neural network has also been applied to reconstruct regional mean sea level from tide gauge records (Wenzel and Shroter, 2010). The shared underlying principle of these different sea level reconstruction studies is that sea level at different regions of the ocean are related. Based on this principle, missing values of sea level at certain regions can be reconstructed using spatial records from other regions.

This study differs from previous spatial sea level reconstruction studies in that our target is not to reconstruct sea level for certain regions from available records of other regions.

Instead, the aim of this study is to reconstruct regional means of sea level based on the global mean value, which is logically similar to the downscaling techniques used in many other climate studies (Haylock et al., 2006; Schoof and Pryor, 2001; Wilby et al., 1998). Since the general temporal trend of sea level is constrained by the time series of global mean sea level, our task is only to figure out the spatial variations of sea level among the target regions. Previous study has shown that that thermosteric effect is the most important impact factor of sea level regional variability (Meyssignac et al., 2012). Sea surface temperature (SST), which reflects the thermosteric effect, has also been used to improve the accuracy of spatial sea level reconstruction (Hamlington et al., 2012). Accordingly, this study attempts to construct the regional variability of sea level based on the sea surface temperature (SST), which reflects the thermosteric effect.

As a powerful downscaling technique widely used in climate studies, artificial neural network (ANN) is also chosen in this study to reconstruct regional means of sea level from the global-mean records (Rahmstorf, 2007) and the regional means of SST (computed from Smith et al., 2008). The architecture of the neural network is shown (Figure 3.6). The feed-forward network is chosen to take the global mean sea level and the regional means of SST as input variables and give the mean values of sea level for the corresponding regions as outputs. Regional means of sea level computed from Church et al. (2004) serve as the calibration data, or “targets” for the outputs of neural network. The neural network is configured to contain only one hidden layer with 4 neurons for scarcity of calibration data.

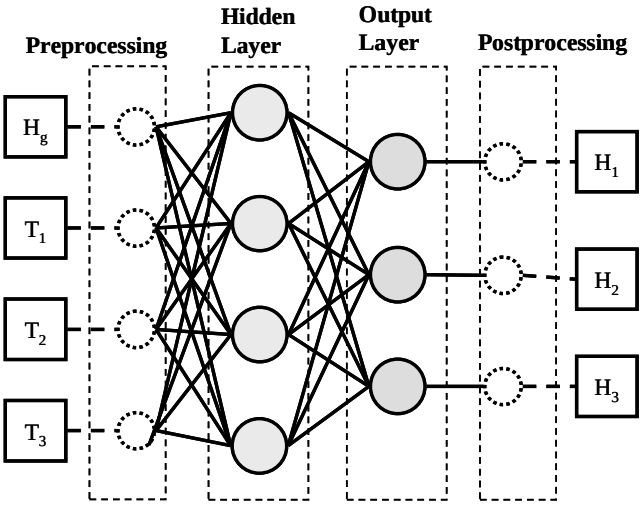

Figure 3.6 Architecture of the neural network for regional sea level reconstruction

The mathematical formulation behind the schematic of the neural network (Figure 3.6) is as below:

$$A = f_1\left(W_1 X + B_1\right) \tag{3.8}$$

$$Y = f_2\left(W_2 A + B_2\right) \tag{3.9}$$

$$f_1\left(x\right) = \frac{1}{1+e^{-x}} \tag{3.10}$$

$$f_2\left(x\right) = x \tag{3.11}$$

where X is the input data matrix, A is the data matrix produced by the hidden layer, Y is the output/target data matrix, W_1 and B_1 are weights and biases for the hidden layer of neurons, W_2 and B_2 are weights and biases for the output layer of neurons, f_1 is the transfer function for the hidden layer (log sigmoid function), and f_2 is the transfer function for the output layer (direct output without transformation).

The training mode of the neural network is set as back-propagation, with the optimization method of the Levenberg-Marquardt algorithm (Hagan et al., 1996). Since our methodology to reconstruct regional mean sea level is essentially a hindcast approach (using current data to reconstruct older data), the earliest 15% of the training data were reserved as the validation set to improve the generalization of the neural network. In addition, to address the local minimum issue of the Levenberg-Marquardt algorithm, every network training is repeated for 1000 random initial states of the neurons (weights and biases).

Impacts of SST and region division. After its architecture and training methodology are established, the neural network is first trained and tested using the available observation data for potentially important issues before it is actually applied in the reconstruction phase. The first issue examined is the importance of the regional average SST's as input variables in the neural network. Based on the training and the testing results, incorporating regional average SST's as input variables significantly improved the neural network's performance on reconstructing sea level data for region division based clustering (compare Figure 3.7 (a) and (b)). However, for region division based on major ocean basins, the difference caused by including SST's as input variables is almost negligible (Figure 3.7 (c) and (d)). This difference might be related to the fact that areas of regions identified based on ocean basins are all quite large. Weak signals tend to be averaged out for spatial means of large areas, so the spatial relationship between the mean sea levels of the three major ocean basins is relatively stable over time and is not significantly affected by decadal climate phenomena. As a result, regional average SST's do not provide a significant amount of additional information in characterizing the relationship between global mean sea level and regional mean sea levels of ocean basins. Another issue worth noticing is the impact of region division on neural network's performance. The neural network's performance for region division based on major

ocean basins is remarkably better than that for region division based on clustering (compare Figure 3.7 (a) and (c)). This difference is also likely to be related to the large areas of ocean basins and the resulted relatively significant and stable sea level signals, which are easier to characterize than those of regions identified by clustering.

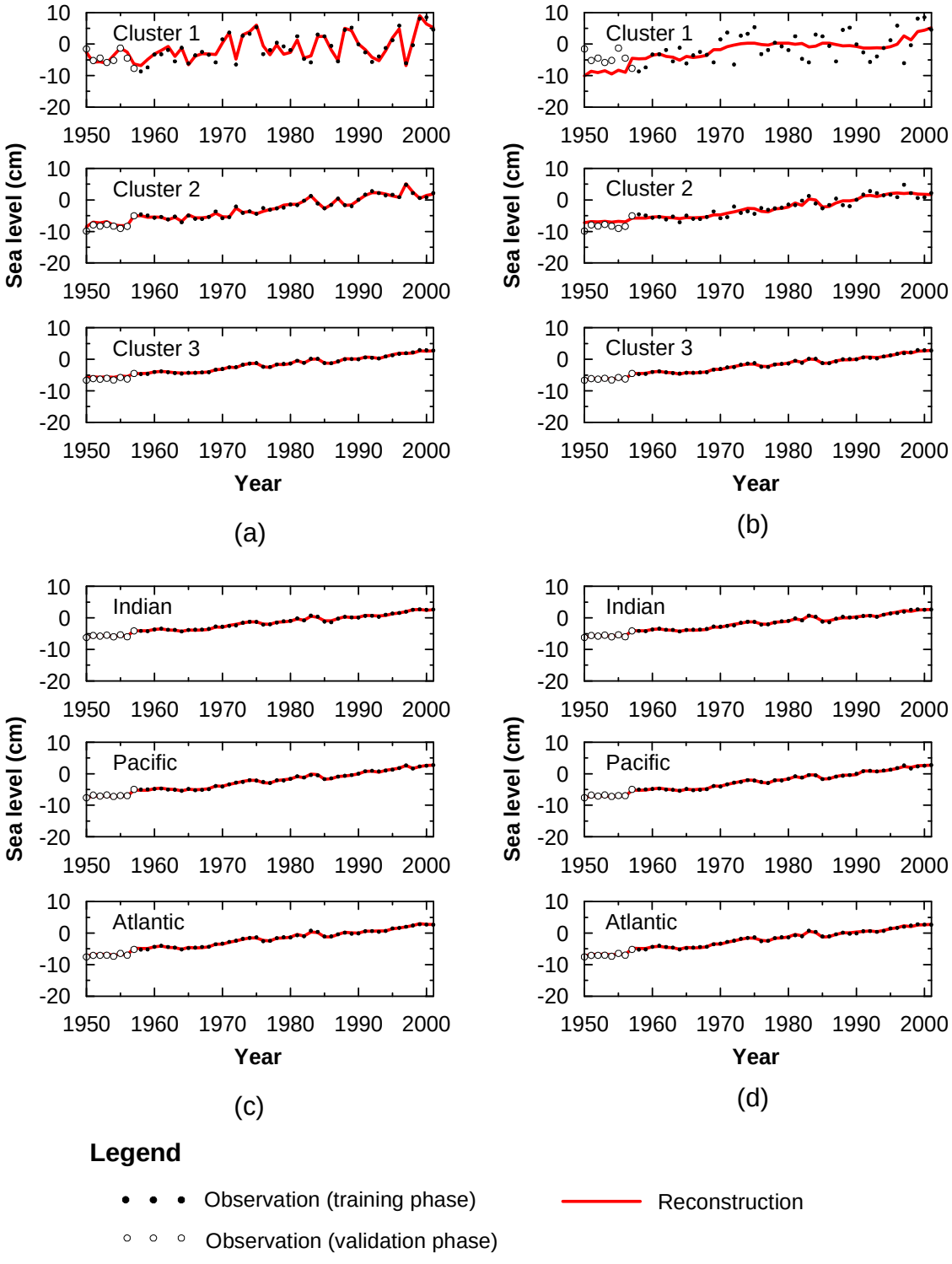

Figure 3.7 Training and testing of neural network: (a) region division based on clustering and SST's as input variables; (b) region division based on clustering but SST's not

included as input variables; (c) region division based on major ocean basins and SST's as input variables; (d) region division based on major ocean basins but SST's not included as input variables.

Final results of reconstruction. Based on the training and testing results (Figure 3.7), our neural network with SST's as input variables is able to reproduce the target observations in the training phase and the trained network has great generalization into the test phase. The neural network configuration was consequently fixed as shown in Figure 3.6, and all available observational data were used as inputs to train the network. The trained network was subsequently applied to reconstruct regional average sea levels from the year 1870 to 1949. The final reconstruction results are shown in Figure 3.8. Reconstructed data for both region division schemes have temporal patterns consistent with those shown in the observational records (Figure 3.8 (a) and (c)). Global mean sea level computed from reconstructed data under either region division scheme also matches the observational global mean sea level pretty well. These results are strong indications that the reconstruction of regional average sea level time series has been successful.

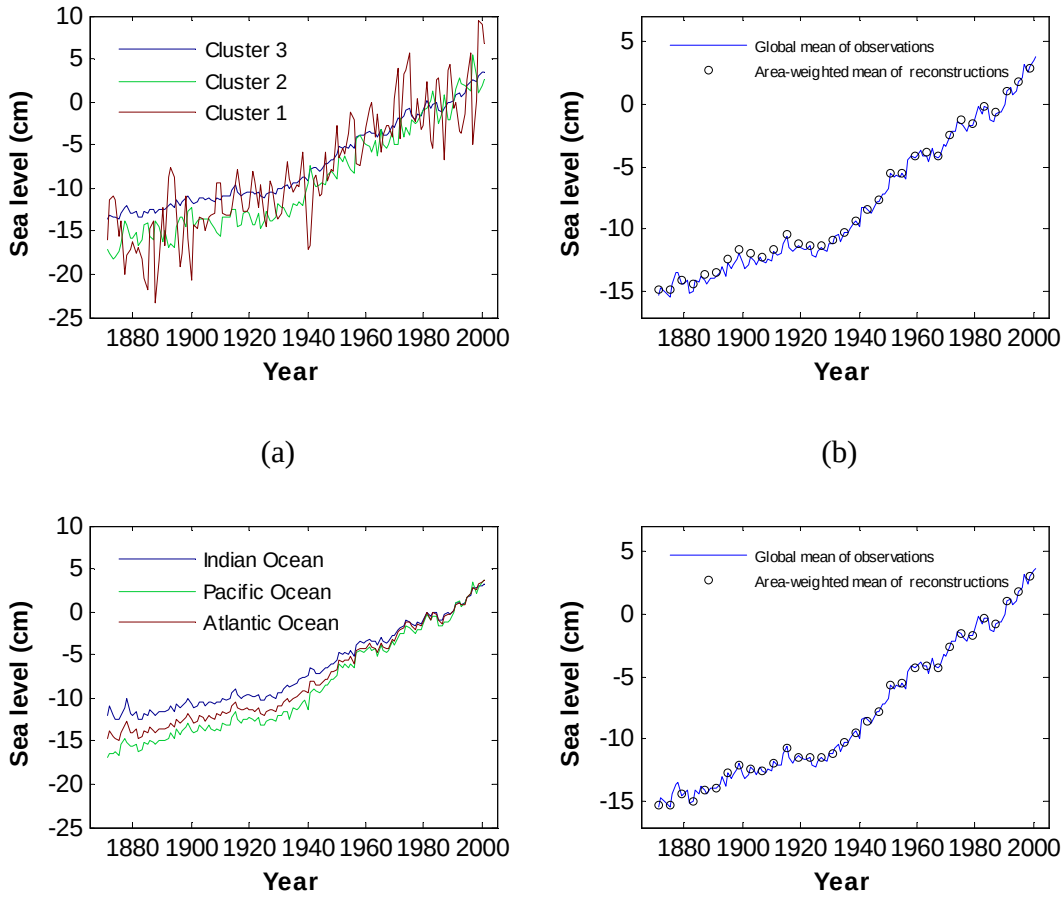

Figure 3.8 Results of data reconstruction: (a) reconstructed average sea levels for regions identified by clustering; (b) global average sea level computed from reconstructions for regions identified by clustering; (c) reconstructed average sea levels for regions based on major ocean basins; (d) global average sea level computed from reconstructions for regions based on major ocean basins.

3.4 Conclusions

To address this need of characterizing spatial pattern automatically from observational data, a pattern recognition technique based on clustering algorithms s is developed to characterize patterns in spatial sea level data in this chapter. This methodology is capable of clustering sea level data with changing magnitude of spatial variations over time, and has the functionality to assess the impacts of spatial constraints through its spatial penalty term. The optimal number of cluster division is selected using a cluster validity metric called Silhouette Index. When applied to a spatial sea level data set by Church et al. (2004), this methodology was able to identify spatial patterns in the data that are related to climate phenomena such as El Nino-Southern Oscillation (ENSO), Pacific Decadal Oscillation (PDO), and North Atlantic Oscillation (NAO). By the functionality of the spatial penalty term in our clustering algorithm, ENSO is evaluated to be the strongest spatial signal in the data, which is consistent with findings of previous studies.

To resolve the issue of short time span of regional average sea level time series, a neural network approach is adopted to reconstruct regional mean sea level from time series of global mean sea level. Utilizing the correlative relationship between sea level and sea surface temperature (SST), the neural network takes regional average SST's and global average sea level as input variables, and it generates regional average sea levels as outputs. The network is demonstrated to reproduce observational data well at the training stage and has good generalization performance at the validation stage. For region division based on clustering result, as well as that based on the three major ocean basins, the neural network approach reproduced observational data well and showed good generalization performance. Both of these two reconstructed data sets are used in Chapter 4 for the calibration of our spatial dynamic system model. Further analysis showed that data reconstruction for clustered regions is more difficult than that for the major ocean

basins because of the small areas of certain clusters. SST's were shown to be indispensable for clustered regions' data reconstruction, but they did not significantly affect the data reconstruction for major ocean basins, as weak signals tend to average out for large areas. This neural network approach, combined with the clustering methodology, provides a viable tool for future research on spatial variations of sea level.

CHAPTER 4

SPATIAL SEA LEVEL RISE ANALYSIS USING DYNAMIC SYSTEM MODEL

4.1 Introduction

It is reported in the literature that sea level rise (SLR) is not spatially uniform. Consequently the development of modeling techniques to predict future regional sea levels becomes critical. Previous studies have shown that models based on physical processes may not yet predict regional sea level changes with confidence (Vermeer and Rahmstorf, 2009). As discussed in Chapter 2, this type of mechanistic modeling has its own limitations by its nature, since the scientific understanding of certain physical processes (i.e., dynamics of ice sheets, glacial melting, thermodynamics of sea-volume analysis, hydrologic impacts etc.) is still limited to allow an accurate quantitative analysis in a regional scale (Grinsted et al., 2010; Schmith, et al., 2012). An alternative way to model SLR is the empirical or semi-empirical approach, which utilizes numerical and statistical techniques to reveal correlations between SLR and temperature.

Previous studies on semi-empirical modeling of sea level rise mainly focused on the unidirectional impacts of global mean surface temperature on the global mean sea level (Etkins and Epstein, 1982; Gornitz et al., 1982; Grinsted et al., 2010; Jevrejeva et al., 2009; Jevrejeva et al., 2010; Rahmstorf et al., 2007; Vermeer and Rahmstorf, 2009). As another application of semi-empirical models, the interactive relationship between global mean sea level and global mean surface air temperature was characterized in a dynamic system model (DSM) proposed by Aral et al. (2012), where both the rate of SLR and surface air temperature change are hypothesized to be linearly dependent on global mean

sea level and surface air temperature among other external effects. Their results demonstrated the advantages of this two-way interactive approach over previous unidirectional semi-empirical analyses. The assumption in DSM was that the interactive feedback mechanisms are expected to occur between the state variables of the target system. This two-way interaction concept originally proposed in Aral. et al. (2012) was later confirmed in an independent study by Schmith, et al., (2012). The discrete model used to solve the DSM by Aral et al. (2012) has the same structure of the model used in the study by Schmith et al. (2012). In their study Schmith et al. (2012) also stated that the surface air temperature adjusts to the average temperatures of the upper ocean (because oceans represent a much larger heat capacity than atmosphere), indicating that sea level rise will affect temperature. Thus, the DSM concept is validated by two independent studies in the recent literature. The DSM analysis was later successfully extended to explicitly incorporate external forcing effects, i.e. radiative forcing (Guan et al, 2013). This application also demonstrated the versatility of the DSM approach in analyzing the SLR problem under different modeling strategies.

Despite its advantages over previous empirical models, the global DSM model has the limitation of being "zero-dimensional," thus it cannot be used in spatial analysis of SLR. As discussed in Chapter 2, significant spatial variations exist in sea surface heights, which are potentially associated with underlying mechanisms such as local surface heating, polar ice mass change, and general circulation change. Despite various studies on the geographical pattern of sea level change, physical models targeting the spatial patterns are still in their preliminary stages. Major research efforts are needed to improve the predictions of spatial variability in future sea level changes.

In this chapter, the dynamic system model (DSM) approach (Aral et al., 2012; Guan et al., 2013) is extended to conduct spatial analysis. Spatial variability of sea level and sea

surface temperature is incorporated into the DSM so that interactions among sea levels and sea surface temperatures in different regions of the oceans can be investigated. Instead of focusing on complicated physical mechanisms behind the spatial variability of SLR, the proposed model utilizes a spatially characterized DSM to potentially address this issue. For instance, the previously mentioned physical mechanisms, such as polar ice melting, local surface heating, and general circulation change of the oceans, will not be characterized specifically in our model. However, most of these physical mechanisms are directly or indirectly connected with the sea surface height (sea level) and the surface temperature (SST) of the oceans. If a spatial DSM successfully simulates the system behaviors of sea surface heights and SST's, the major physical mechanisms affecting these two variables should have been appropriately characterized by the model. This indicates that the model without explicit characterization of physical mechanisms can nonetheless be physically valid. Our hypothesis is that the complex system behavior of this problem is embedded in the historical records of the state variables (sea levels and SST's). If models are constructed successfully to capture historical system behaviors of sea levels and SST's, subsequent predictive spatial analysis can be made within certain error bounds. The key point in such an application is the degrees of freedom incorporated into the selected model. As a first step in this direction, two model configurations are proposed which differ in the definition of the external forcing function and the related analyses are described in the following sections of this chapter.

4.2 Model Formulation

To investigate the spatial characteristics of SLR, the DSM model is extended to include spatially distributed state variables. In the spatial DSM model the global scalar state variables used in previous studies (Aral et al., 2012; Guan et al., 2013) are represented as vector variables and the scalar coefficients of the previous DSM will be represented in

terms of matrices. This extension enables the model to characterize the spatial interactions between sea levels and temperatures in different regions of the ocean. In this chapter, two configurations/applications of this spatial DSM model are presented, one with an external forcing function term and the other without an explicit term of external forcing function.

When the external forcing function is not considered to be an independent term, the matrix form of the spatial DSM can be given as

$$\begin{aligned} \frac{d}{dt}\overline{H}(t) &= \mathbf{A}\overline{H}(t) + \mathbf{B}\overline{T}(t) + \mathbf{C}_H \\ \frac{d}{dt}\overline{T}(t) &= \mathbf{D}\overline{H}(t) + \mathbf{E}\overline{T}(t) + \mathbf{C}_T \end{aligned} \tag{4.1}$$

where $\overline{H}(t)$ and $\overline{T}(t)$ are vectors of regional means of sea level and SST, respectively, at time t; **A** and **B** are coefficient matrices characterizing contributions to the rate of sea level change as a function of $\overline{H}(t)$ and $\overline{T}(t)$, respectively; **D** and **E** are coefficient matrices characterizing contributions to the rate of SST change as a function of $\overline{H}(t)$ and $\overline{T}(t)$, respectively; $\mathbf{C}_H$ and $\mathbf{C}_T$ are constant vectors indicating contributions to the changing rate of sea level and SST from sources other than the current states of sea level and SST respectively.

When the external forcing function is considered as an independent factor affecting sea levels and SST's, the spatial DSM model can be given as

$$\begin{aligned} \frac{d}{dt}\overline{H}(t) &= \mathbf{A}\overline{H}(t) + \mathbf{B}\overline{T}(t) + \mathbf{C}_H \\ \frac{d}{dt}\overline{T}(t) &= \mathbf{D}\overline{H}(t) + \mathbf{E}\overline{T}(t) + \mathbf{Q}\overline{U}(t) + \mathbf{C}_T \end{aligned} \tag{4.2}$$

where **Q** is a control matrix related to external forcing and $\overline{U}(t)$ represents the independent external forcing function which takes a modified form of radiative forcing (Equation (4.4)). The two assumptions adopted in the formulation of Equation (4.2) are: (i) the forcing function, i.e. increased greenhouse gas concentrations in the atmosphere, will not directly affect sea level but rather affect SST which in turn will cause sea level rise. This assumption was confirmed in the study by Schmith et al. (2012) and Guan et al. (2013); and, (ii) the forcing function will not be spatially variable but will be defined as a globally uniform term. This assumption is more of a physical interpretation than a mathematically restriction, because carbon dioxide, which is the target greenhouse gas in this study, is a well-mixed greenhouse gas and has near uniform spatial distribution (Church et al., 2001).

In this study, the spatial model is applied to the case of three major oceans (Figure 4.1) and also the case if three clustered regions discussed in Chapter 3. For these cases Equation (4.2) will take the form:

$$\begin{Bmatrix} \frac{dH_1}{dt} \\ \frac{dH_2}{dt} \\ \frac{dH_3}{dt} \end{Bmatrix} = \begin{bmatrix} a_{11} & a_{12} & a_{13} \\ a_{21} & a_{22} & a_{23} \\ a_{31} & a_{32} & a_{33} \end{bmatrix} \begin{Bmatrix} H_1 \\ H_2 \\ H_3 \end{Bmatrix} + \begin{bmatrix} b_{11} & b_{12} & b_{13} \\ b_{21} & b_{22} & b_{23} \\ b_{31} & b_{32} & b_{33} \end{bmatrix} \begin{Bmatrix} T_1 \\ T_2 \\ T_3 \end{Bmatrix} + \begin{Bmatrix} C_{H1} \\ C_{H2} \\ C_{H3} \end{Bmatrix}$$

$$\begin{Bmatrix} \frac{dT_1}{dt} \\ \frac{dT_2}{dt} \\ \frac{dT_3}{dt} \end{Bmatrix} = \begin{bmatrix} d_{11} & d_{12} & d_{13} \\ d_{21} & d_{22} & d_{23} \\ d_{31} & d_{32} & d_{33} \end{bmatrix} \begin{Bmatrix} H_1 \\ H_2 \\ H_3 \end{Bmatrix} + \begin{bmatrix} e_{11} & e_{12} & e_{13} \\ e_{21} & e_{22} & e_{23} \\ e_{31} & e_{32} & e_{33} \end{bmatrix} \begin{Bmatrix} T_1 \\ T_2 \\ T_3 \end{Bmatrix} + \begin{Bmatrix} q_1 \\ q_2 \\ q_3 \end{Bmatrix} u + \begin{Bmatrix} C_{T1} \\ C_{T2} \\ C_{T3} \end{Bmatrix} \quad (4.3)$$

where H_i and T_i are sea level and SST, respectively, for the three regions (i =1, 2, 3) (In this application, i = 1, 2, 3 represents the Indian, Pacific, and Atlantic Ocean respectively); the first subscript index of the coefficient matrix elements indicates the target region,

while the second subscript index indicates the contributing region, e.g., b_{23} indicates the impact of the third region's temperature (T_3) on the rate of sea level change of the second region (dH_2/dt); coefficients a's, d's, and e's can be interpreted in a similar manner; C_{Hi} and C_{Ti} are constant terms for the rate of change of sea level and temperature in region i; q_i measures the i'th region's SST change contributed by the global external forcing function u. As an important impacting factor on temperature change u is the same for all regions, and it takes a modified form of the radiative forcing definition (Guan et al., 2013):

$$u(t) = \left[5.35 \ln\left(c(t)/c_0\right)\right]^{\beta} \tag{4.4}$$

where $c(t)$ is the global average atmospheric carbon dioxide concentration at year t, c_0 is the baseline global average atmospheric carbon dioxide concentration set as 278 ppm(v), and β is a coefficient to be determined during model calibration.

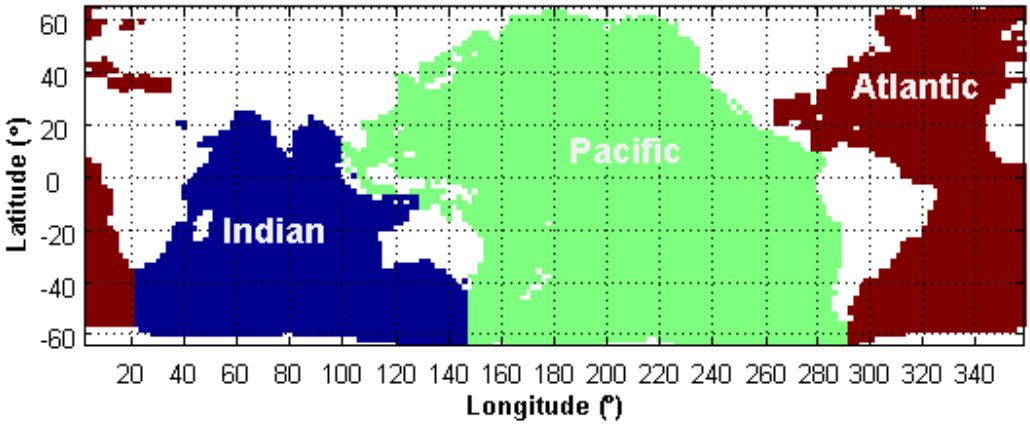

Figure 4.1 Region division based on the three major ocean basins.

4.3 Model calibration and validation

From the mathematical perspective, the spatial model (Equation (4.1), (4.2), and (4.3)) is essentially a non-homogeneous system of first-order linear ordinary differential equations (ODEs). To solve this system of ODEs, the first step is to obtain the values of the elements (model coefficients) in matrices $\mathbf{A}$, $\mathbf{B}$, $\mathbf{D}$, $\mathbf{E}$, $\mathbf{Q}$, $\mathbf{C}_H$, and $\mathbf{C}_T$. This step is the calibration stage of the proposed model. After the model is calibrated, the system of ODEs can be solved analytically or numerically to compute the values of the state variables H_i's and T_i's, given the initial condition of the system. This will be the prediction stage. The procedure of model calibration is described in this section, and the analytical and numerical methods used for model prediction are discussed in Section 4.4.

4.3.1 Calibration and validation methodology

To calibrate the spatial DSM model (Equation (4.3)), it is first transformed into a matrix form as shown below for computation convenience. The components of Equation (4.3) are denoted as

$$\mathbf{X} = \begin{Bmatrix} H_1 \\ H_2 \\ H_3 \\ T_1 \\ T_2 \\ T_3 \end{Bmatrix} \tag{4.5}$$

$$\mathbf{X}' = \begin{Bmatrix} dH_1/dt \\ dH_2/dt \\ dH_3/dt \\ dT_1/dt \\ dT_2/dt \\ dT_3/dt \end{Bmatrix} \tag{4.6}$$

$$\mathbf{K} = \begin{bmatrix} a_{11} & a_{12} & a_{13} & b_{11} & b_{12} & b_{13} \\ a_{21} & a_{22} & a_{23} & b_{21} & b_{22} & b_{23} \\ a_{31} & a_{32} & a_{33} & b_{31} & b_{32} & b_{33} \\ d_{11} & d_{12} & d_{13} & e_{11} & e_{12} & e_{13} \\ d_{21} & d_{22} & d_{23} & e_{21} & e_{22} & e_{23} \\ d_{31} & d_{32} & d_{33} & e_{31} & e_{32} & e_{33} \end{bmatrix} \tag{4.7}$$

$$\mathbf{F}(t) = \begin{bmatrix} C_{H1} \\ C_{H2} \\ C_{H3} \\ C_{T1} + q_1 u(t) \\ C_{T2} + q_2 u(t) \\ C_{T3} + q_3 u(t) \end{bmatrix} \tag{4.8}$$

where $\mathbf{X}$ is a vector state variable whose elements are H_i's and T_i's, $\mathbf{X}'$ is the first-order derivative of $\mathbf{X}$ with respect to time t, $\mathbf{K}$ is the coefficient matrix, $\mathbf{F}(t)$ is the non-homogeneous vector term of the system incorporating the impacts of the external forcing function $\overline{U}(t)$ and constant terms C_{Hi}'s and C_{Ti}'s. Following this notation, Equation (4.3) can be expressed as:

$$\mathbf{X}' = \mathbf{K}\mathbf{X} + \mathbf{F}(t) \tag{4.9}$$

To obtain the coefficients in Equation (4.9), the truncated Taylor series approximation is applied for $\mathbf{X}'$, which gives

$$\mathbf{X}' \cong \frac{\mathbf{X}(t+\Delta t) - \mathbf{X}(t)}{\Delta t} \tag{4.10}$$

Combining the three equations (4.8), (4.9), and (4.10) renders

$$\frac{\mathbf{X}(t+\Delta t)-\mathbf{X}(t)}{\Delta t}=\mathbf{K}\mathbf{X}(t)+\begin{bmatrix} C_{H1} \\ C_{H2} \\ C_{H3} \\ C_{T1}+q_1 u(t) \\ C_{T2}+q_2 u(t) \\ C_{T3}+q_3 u(t) \end{bmatrix} \tag{4.11}$$

Separating constants from variables,

$$\frac{\mathbf{X}(t+\Delta t)-\mathbf{X}(t)}{\Delta t}=\mathbf{K}\mathbf{X}(t)+\begin{bmatrix} 0 \\ 0 \\ 0 \\ q_1 \\ q_2 \\ q_3 \end{bmatrix} u(t)+\begin{bmatrix} C_{H1} \\ C_{H2} \\ C_{H3} \\ C_{T1} \\ C_{T2} \\ C_{T3} \end{bmatrix} \tag{4.12}$$

Rearranging the equation results in

$$\frac{\mathbf{X}(t+\Delta t)-\mathbf{X}(t)}{\Delta t}=\begin{bmatrix} & 0 & C_{H1} \\ & 0 & C_{H2} \\ \mathbf{K} & 0 & C_{H3} \\ & q_1 & C_{T1} \\ & q_2 & C_{T2} \\ & q_3 & C_{T3} \end{bmatrix}\begin{bmatrix} \mathbf{X}(t) \\ u(t) \\ 1 \end{bmatrix} \tag{4.13}$$

By setting $\Delta t = 1yr$, the equation above is transformed into a discrete equation

$$\mathbf{X}(t+1)-\mathbf{X}(t)=\begin{bmatrix} & 0 & C_{H1} \\ & 0 & C_{H2} \\ \mathbf{K} & 0 & C_{H3} \\ & q_1 & C_{T1} \\ & q_2 & C_{T2} \\ & q_3 & C_{T3} \end{bmatrix}\begin{bmatrix} \mathbf{X}(t) \\ u(t) \\ 1 \end{bmatrix} \tag{4.14}$$

Equation (4.14) represents a linear system. Since observational records for $\mathbf{X}(t)$, $\mathbf{X}(t+1)$, and $u(t)$ are available at different years, all the constants in Equation (4.14) (model parameters) can be obtained using the linear least squares method (Aral et al., 2012). The computational procedure of the least squares method is described as below.

Transposing both sides of Equation (4.14) leads to

$$\left[\mathbf{X}(t+1)-\mathbf{X}(t)\right]^{\mathrm{T}}=\begin{bmatrix}\mathbf{X}(t)\\ u(t)\\ 1\end{bmatrix}^{\mathrm{T}}\begin{bmatrix}\mathbf{K} & \begin{matrix}0 & C_{H1}\\ 0 & C_{H2}\\ 0 & C_{H3}\\ q_1 & C_{T1}\\ q_2 & C_{T2}\\ q_3 & C_{T3}\end{matrix}\end{bmatrix}^{\mathrm{T}} \tag{4.15}$$

This equation can be rearranged as

$$\left[\mathbf{X}(t+1)^{\mathrm{T}}-\mathbf{X}(t)^{\mathrm{T}}\right]=\begin{bmatrix}\mathbf{X}(t)^{\mathrm{T}} & u(t) & 1\end{bmatrix}\begin{bmatrix}\mathbf{K} & \begin{matrix}0 & C_{H1}\\ 0 & C_{H2}\\ 0 & C_{H3}\\ q_1 & C_{T1}\\ q_2 & C_{T2}\\ q_3 & C_{T3}\end{matrix}\end{bmatrix}^{\mathrm{T}} \tag{4.16}$$

The equation above is the equation for the system approximation at year t. For the calibration data set spanning k years, $t=1,2,\cdots,k$. The system of equations for the calibration data set can then be formulated as

$$\begin{bmatrix}\mathbf{X}(2)^{\mathrm{T}}-\mathbf{X}(1)^{\mathrm{T}}\\ \mathbf{X}(3)^{\mathrm{T}}-\mathbf{X}(2)^{\mathrm{T}}\\ \cdots\\ \mathbf{X}(k)^{\mathrm{T}}-\mathbf{X}(k-1)^{\mathrm{T}}\end{bmatrix}=\begin{bmatrix}\mathbf{X}(1)^{\mathrm{T}} & u(1) & 1\\ \mathbf{X}(2)^{\mathrm{T}} & u(2) & 1\\ & \cdots & \\ \mathbf{X}(k-1)^{\mathrm{T}} & u(k-1) & 1\end{bmatrix}\begin{bmatrix}\mathbf{K} & \begin{matrix}0 & C_{H1}\\ 0 & C_{H2}\\ 0 & C_{H3}\\ q_1 & C_{T1}\\ q_2 & C_{T2}\\ q_3 & C_{T3}\end{matrix}\end{bmatrix}^{\mathrm{T}} \tag{4.17}$$

For notational convenience, the following equations are formulated:

$$\mathbf{\Omega} = \begin{bmatrix} \mathbf{X}(2)^{\mathrm{T}} - \mathbf{X}(1)^{\mathrm{T}} \\ \mathbf{X}(3)^{\mathrm{T}} - \mathbf{X}(2)^{\mathrm{T}} \\ \cdots \\ \mathbf{X}(k)^{\mathrm{T}} - \mathbf{X}(k-1)^{\mathrm{T}} \end{bmatrix} \tag{4.18}$$

$$\mathbf{\Pi} = \begin{bmatrix} \mathbf{X}(1)^{\mathrm{T}} & u(1) & 1 \\ \mathbf{X}(2)^{\mathrm{T}} & u(2) & 1 \\ & \cdots & \\ \mathbf{X}(k-1)^{\mathrm{T}} & u(k-1) & 1 \end{bmatrix} \tag{4.19}$$

The linear least squares solution of Equation (4.17), which represents the model application with the external forcing function, can then be obtained as

$$\begin{bmatrix} & 0 & C_{H1} \\ & 0 & C_{H2} \\ \mathbf{K} & 0 & C_{H3} \\ & q_1 & C_{T1} \\ & q_2 & C_{T2} \\ & q_3 & C_{T3} \end{bmatrix}^{\mathrm{T}} = \left(\mathbf{\Pi}^{\mathrm{T}}\mathbf{\Pi}\right)^{-1}\mathbf{\Pi}^{\mathrm{T}}\mathbf{\Omega} \tag{4.20}$$

For the model application without explicit external forcing function (Equation (4.1)), the linear least squares solution can be computed as

$$\begin{bmatrix} & C_{H1} \\ & C_{H2} \\ \mathbf{K} & C_{H3} \\ & C_{T1} \\ & C_{T2} \\ & C_{T3} \end{bmatrix}^{\mathrm{T}} = \left(\mathbf{\Gamma}^{\mathrm{T}}\mathbf{\Gamma}\right)^{-1}\mathbf{\Gamma}^{\mathrm{T}}\mathbf{\Omega} \tag{4.21}$$

where

$$\Gamma = \begin{bmatrix} \mathbf{X}(1)^{\mathrm{T}} & 1 \\ \mathbf{X}(2)^{\mathrm{T}} & 1 \\ \cdots & \\ \mathbf{X}(k-1)^{\mathrm{T}} & 1 \end{bmatrix} \tag{4.22}$$

For the model application with external forcing function, there is an extra parameter to be calibrated, which is β in Equation (4.4). The value of this parameter is calibrated by supplying the model with atmospheric CO_2 concentration input under a 2 °C temperature increase scenario (NASA, 2012) and forcing the global average of predicted temperature increases to match the expected temperature increase.

To test the generalization ability of our proposed model, a cross-validation method is adopted, which uses part of the observational data to calibrate the model and the rest of the data to validate it. The corresponding mathematical procedure is to first use the calibration data set to obtain coefficients in Equation (4.14) through the least squares method described above. The coefficients obtained are then applied to make predictions for the validation period following the procedure described later in Section 4.4. The prediction results are compared with the observational data in the corresponding time period to evaluate the model's generalization ability. A good agreement between predictions and observations in the validation period indicates that the model generalizes well, and it is thus validated.

4.3.2 Observational data for model calibration and validation

In this study, the spatial sea level dataset was obtained from the Commonwealth Scientific and Industrial Research Organization (CSIRO) of Australia. This dataset, reconstructed by Church et al. (2004), contains sea surface height records for different

regions of oceans. It compiles monthly sea level records from January 1950 to December 2001 for the ocean between 65°S and 65°N, with a spatial resolution of 1°×1° (lat-long). From this data set the seasonal signal has been removed and it also has inverse barometer correction and glacial isostatic adjustment (GIA) made to tide gauge data. Church et al. (2004) used near-global coverage from monthly satellite data of sea level (TOPEX/Poseidon dataset) from 1993 to 2001 to estimate the global covariance structure of observed sea level variability. This covariance structure was then applied to interpolate longer monthly tide gauge records from 1950 to 2001 that are relatively sparse in number (less than 500) to a final data set with spatial coverage and resolution mentioned above. As a measurement of errors in this dataset, it was compared with the satellite data over 1993-2000. The error of the original satellite data is less than 5 cm (NASA, 2013).The correlation between the two data sets has a global area-weighted average of 0.60; while the correlation is above 0.9 in the tropical Pacific and Indian Ocean (Church et al., 2004). Errors of the tide gauge data used were not discussed, but a preliminary estimation can be obtained. The Inter-governmental Panel on Climate Change (IPCC) stated that tide gauges can be based on different technologies such as float, pressure, acoustic, radar and that "the Global Sea Level Observing System (GLOSS) specifies that a gauge must be capable of measuring sea level to centimetre accuracy (or better) in all weather conditions" (Meehl et al., 2001). Since the tide gauge data source in Church et al. (2004) contributed significantly in the GLOSS data, it is expected that the tie gauge data used by Church et al. (2004) have accuracy at the centimeter level.

For spatial temperature records, sea surface temperature (SST) was used instead of surface air temperature data that was used in previous studies (Aral et al. 2012; Guan et al. 2013). The reason behind this choice is that SST is one of the direct ocean temperature indictors and it has a spatial coverage matching to that of the sea surface height datasets. The spatial SST dataset is obtained from Version v3b of Extended Reconstructed Sea

Surface Temperature (ERSST) developed by National Climate Data Center of NOAA, USA, which is based on the International Comprehensive Ocean-Atmosphere Data Set (ICOADS) release 2.4 (Smith et al., 2008). This data set has monthly SST records from January 1854 to December 2009 for the ocean between 0-358°E and 88°S-88°N on a 2°×2° lat-long grid. SST records in this dataset are presented as anomalies computed with respect to the 1971-2000 month climatology (Xue et al., 2003). As a measurement of errors in this data set, the global root mean squared error (RMSE) was computed for the ERSST by Smith and Reynolds (2003), which is about 0.08 °C at 1880 and decreases to about 0.02 at 2000.

In the current study the yearly average data are used in order to demonstrate the methodology, so yearly means of the two datasets are computed as arithmetic means of the data in each consecutive 12 months (January to December). To render the spatial coverage of the two datasets consistent, only records at those overlapping grid points are selected, giving both of the final datasets a spatial coverage of 2-358°E and 64°S-64°N on a 2°×2° lat-long grid. In addition, all the data used in this study was preprocessed so that they are relative to the global mean value at the year of 1990. After both datasets are prepared, regional means of them are calculated to serve as the observational data for model calibration and validation.

As described above, the time span of the sea surface height dataset obtained from CSIRO is very short (1950-2001), especially when compared with that of the SST dataset period obtained from NOAA which is from 1854 to 2009. When analyzing global-mean sea level and temperature datasets (Rahmstorf 2007; Aral et al. 2012), it became clear that the CSIRO sea surface records from 1950 to 2001 will not be sufficient to capture the historical trends. To address the issue of data shortage, the reconstructed regional mean sea levels in Chapter 3 were used to calibrate our spatial DSM model.

To calibrate the model with external forcing function (Equation (4.2)), global mean atmospheric CO_2 concentration data (1880-2000) are obtained from the Goddard Institute for Space Studies of the U.S. National Aeronautics and Space Administration (NASA, 2012). Future CO_2 concentrations (2001-2100) projected by the carbon cycle model ISAM (Jain et al., 1994) are used for our model projections, which are obtained from the IPCC (2012). CO_2 concentrations in both datasets are in unit of parts per million by volume (ppmv), and their annual average values are used in this study.

4.4 Analytical and numerical methods for model prediction

After the model coefficients are calibrated, an analytical solution approach can be used to predict H_i's and T_i's at any given time. However, finding the analytical solution is time consuming, and it has to be conducted for each different application. More importantly, potential further development of the spatial DSM model might make it difficult or even impossible to obtain an analytical solution. For instance, if the coefficients of the spatial DSM model are configured as time-dependent, the procedure described in this section will no longer be suitable for the solution. Facing these challenges, the alternative numerical method is potentially a better choice. As a result, the numerical method is used for all model predictions in this study. Nonetheless, for applications whose analytical predictions can be easily obtained, the analytical solution can be utilized to validate the adopted numerical method. For this reason, both the analytical and the numerical methods of model prediction are presented in this section. Following this discussion, the methodology applied to construct the confidence interval of model prediction is described lastly in this section.

4.4.1 Analytical prediction method

In this section, the procedure to obtain the analytical predictions by the spatial DSM model (Equation (4.3)) is described. In Equation (4.3), $\mathbf{K}$ and $\mathbf{F}(t)$ are continuous over time. In addition, the initial condition $\mathbf{X}(t_0)$ is known. These conditions constitute an initial value problem, which has been proved to have a unique solution (Zill, 2008). According to the classical theories on the solution for non-homogeneous system of linear ODEs (Zill, 2008), the analytical solution of Equation (4.9) has the form

$$\mathbf{X} = \mathbf{X}_c + \mathbf{X}_p \tag{4.23}$$

where $\mathbf{X}_c$ is the general solution of the associated homogeneous linear system

$$\mathbf{X}' = \mathbf{K}\mathbf{X} \tag{4.24}$$

and $\mathbf{X}_p$ is any particular solution of the non-homogeneous system. The approaches to solve for $\mathbf{X}_c$ and $\mathbf{X}_p$ are described in the following paragraphs.

The general solution of the associated homogeneous ODEs (Equation (4.24)), also called the complementary function, has different formats for three different cases of $\mathbf{K}$ with respect to its eigenvalue features.

(i) $\mathbf{K}$ ($n \times n$ matrix) has n distinct real eigenvalues. The solution of Equation (4.24) is

$$\mathbf{X} = c_1\mathbf{V}_1 e^{\lambda_1 t} + c_2\mathbf{V}_2 e^{\lambda_2 t} + \cdots + c_n\mathbf{V}_n e^{\lambda_n t} \tag{4.25}$$

where λ's (λ_1, λ_2, …, λ_n) and $\mathbf{V}$'s ($\mathbf{V}_1, \mathbf{V}_2$, …, $\mathbf{V}_n$) are the distinct eigenvalues and corresponding eigenvectors of matrix $\mathbf{K}$; c's (c_1, c_2, …, c_n) are arbitrarily chosen constants.

(ii) **K** has repeated real eigenvalues. For a repeated eigenvalue λ with multiplicity of m, if it has m corresponding linearly independent eigenvectors ($\mathbf{V}_1, \mathbf{V}_2, \ldots, \mathbf{V}_m$), the general solution of the system will contain the linear combination of the solutions

$$\begin{aligned} \mathbf{X}_1 &= \mathbf{V}_1 e^{\lambda t} \\ \mathbf{X}_2 &= \mathbf{V}_2 e^{\lambda t} \\ &\cdots \\ \mathbf{X}_m &= \mathbf{V}_m e^{\lambda t} \end{aligned} \tag{4.26}$$

If the repeated eigenvalue with multiplicity of m has only 1 eigenvector, then the general solution of the system contains the linear combination of the solutions

$$\begin{aligned} \mathbf{X}_1 &= \mathbf{V}_1 e^{\lambda t} \\ \mathbf{X}_2 &= \mathbf{V}_1 t e^{\lambda t} + \mathbf{V}_2 e^{\lambda t} \\ &\cdots \\ \mathbf{X}_m &= \mathbf{V}_1 \frac{t^{m-1}}{(m-1)!} e^{\lambda t} + \mathbf{V}_2 \frac{t^{m-2}}{(m-2)!} e^{\lambda t} + \cdots + \mathbf{V}_m e^{\lambda t} \end{aligned} \tag{4.27}$$

The vector $\mathbf{V}_2$ is the eigenvector associated with eigenvalue λ. The vectors $\mathbf{V}_2$, $\mathbf{V}_3$, …, $\mathbf{V}_n$ are called "generalized eigenvectors" corresponding to the eigenvalue λ, and they can be computed through the algorithm below:

$$(\mathbf{K} - \lambda \mathbf{I})\mathbf{V}_i = \mathbf{V}_{i-1}, \ \forall i = 2, 3, ..., m \tag{4.28}$$

If the repeated eigenvalue with multiplicity of m has p eigenvectors (1<p<m), the solutions can be obtained using an algorithm similar with the one above.

(iii) **K** has complex eigenvalues. If $\lambda = \alpha + i\beta$ is a complex eigenvalue of the coefficient matrix **K** and **V** is its corresponding eigenvector, the general solution contains two linearly independent solutions

$$\mathbf{X}_1 = \left[\mathbf{V}_R \cos \beta t - \mathbf{V}_I \sin \beta t\right] e^{\alpha t}$$
$$\mathbf{X}_2 = \left[\mathbf{V}_I \cos \beta t + \mathbf{V}_R \sin \beta t\right] e^{\alpha t} \tag{4.29}$$

where $\mathbf{V}_R$ and $\mathbf{V}_I$ are real number vectors containing the coefficients of the real and the imaginary parts of $\mathbf{V}$, respectively.

Particular solution of the non-homogeneous linear system can be obtained using two approaches: (i) undetermined coefficients; and, (ii) variation of parameters. Because variation of parameters is generally a more powerful approach, that solution process is adopted in this study. Procedures of this method are briefly described as blow following Goodwine (2011). The linearly independent solutions of the homogeneous part of the system can be arranged to form the "fundamental matrix" of the system. For instance, in the case where the coefficient matrix $\mathbf{K}$ has distinct eigenvalues, the fundamental matrix is formed as

$$\mathbf{\Phi}(t) = \left[\mathbf{V}_1 e^{\lambda_1 t} \quad \mathbf{V}_2 e^{\lambda_2 t} \quad \cdots \quad \mathbf{V}_n e^{\lambda_n t}\right] \tag{4.30}$$

As mentioned previously, the eigenvectors $\mathbf{V}$'s are all $n \times 1$ vectors. $\mathbf{\Phi}(t)$ is accordingly an $n \times n$ matrix. The variation of parameters approach assumes that the particular solution of the system should have the form

$$\mathbf{X}_p = \mathbf{\Phi}(t)\mathbf{U}(t) \tag{4.31}$$

where $\mathbf{U}(t)$ is initially unknown. Finding $\mathbf{U}(t)$ will give us the particular solution of the system. Through derivation (Goodwine, 2011), it can be shown that

$$\mathbf{U}(t) = \int \mathbf{\Phi}^{-1}(t)\mathbf{F}(t)\,dt \tag{4.32}$$

The particular solution can then be calculated as

$$\mathbf{X}_p = \mathbf{\Phi}(t) \int \mathbf{\Phi}^{-1}(t)\mathbf{F}(t)\,dt \tag{4.33}$$

Combining the general solution for the homogeneous part of the system and the particular solution, the general solution of the system is

$$\mathbf{X} = \mathbf{\Phi}(t)\mathbf{C} + \mathbf{\Phi}(t)\int \mathbf{\Phi}^{-1}(t)\mathbf{F}(t)\,dt \tag{4.34}$$

where $\mathbf{C}$ is an $n\times 1$ vector containing arbitrary constants, $\mathbf{\Phi}(t)$ is the fundamental matrix of the system, and $\mathbf{F}(t)$ is the non-homogeneous vector term of the system. Note that constant of integration is not needed in the evaluation of this equation (Zill, 2008).

4.4.2 Numerical prediction method

The spatial DSM model can be solved numerically using the classical forward Euler method (Butcher, 2008). Using the forward Euler method, the first-order derivative of the matrix $\mathbf{X}$ is approximated as

$$\mathbf{X}' \cong \frac{\mathbf{X}(t+\Delta t) - \mathbf{X}(t)}{\Delta t} \tag{4.35}$$

Equation (4.9) is then transformed into

$$\frac{\mathbf{X}(t+\Delta t) - \mathbf{X}(t)}{\Delta t} = \mathbf{K}\mathbf{X}(t) + \mathbf{F}(t) \tag{4.36}$$

To solve the initial value problem, the equation above can be rearranged as

$$\mathbf{X}(t+\Delta t) = (\Delta t\mathbf{K} + \mathbf{I})\mathbf{X}(t) + \Delta t\mathbf{F}(t) \tag{4.37}$$

Numerical experiments have shown that decreasing the time step Δt to be less than 1 does not significantly increase the accuracy of the numerical solution. Since the annual mean of $\mathbf{X}$ is investigated in this study, Δt is chosen as 1 year for this application.

To project future sea levels and SST's, the initial inputs of the model are regional mean sea levels and SST's at the starting year. With the inputs of observations at the starting year t ($\mathbf{X}(t)$), the calibrated constant coefficients in matrices $\mathbf{K}$ and $\mathbf{F}(t)$ of Equation (4.37), and the external forcing function calculated at t ($u(t)$),the immediate outputs $\mathbf{X}(t+\Delta t)$ can be calculated by setting Δt at a certain value (chosen as 1 year in this study). Following the same procedure, predicted regional mean sea levels and SST's ($\mathbf{X}(t+\Delta t)$) can be used as inputs to make further predictions at $t+2\Delta t$. This process can be repeated to make predictions for the desired time interval.

4.4.3 Confidence interval for model prediction

The uncertainty of model prediction is quantified via the construction of confidence intervals. A basic assumption in this analysis is that the magnitude and the distribution of errors do not change significantly from the model calibration stage to the prediction stage. Based on this assumption, model errors in the calibration stage can be used to construct the confidence intervals of model predictions. Following the procedures by Ryan (1990), the confidence intervals for model predictions can be constructed as below. First, the model error indicators for sea level and SST are calculated as their mean squared errors (MSE) $\hat{\sigma}_{Hi}^2$ and $\hat{\sigma}_{Ti}^2$. For a sea level prediction at the year n ($H_i(n)$), its confidence interval at the $(1-\alpha)$ confidence level is

$$H_i(n)_{CI,\alpha} = H_i(n) \pm t_{\alpha/2,k-p-1}\sqrt{\hat{\sigma}_{Hi}^2\left(\begin{bmatrix}\mathbf{X}(n)^{\mathrm{T}} & 1\end{bmatrix}\left(\Gamma^{\mathrm{T}}\Gamma\right)^{-1}\begin{bmatrix}\mathbf{X}(n)\\ 1\end{bmatrix}+\frac{1}{k}+1\right)} \tag{4.38}$$

where $t_{\alpha/2,k-p-1}$ is the critical value of the Student's t distribution, k is the total years of observations in the calibration stage, p is the number of parameter used for that specific

prediction ($p = 7$ here), and the definitions of $\mathbf{X}(n)$ and Γ can be found in Equation (4.5) and (4.22), respectively.

The confidence intervals for SST predictions are calculated differently for the model applications with and without external forcing functions. Following the same notation as the previous paragraph, for the model application without external forcing function, the confidence interval for SST prediction at the year n ($T_i(n)$) is

$$T_i(n)_{CI,\alpha} = T_i(n) \pm t_{\alpha/2,\, k-7-1} \sqrt{\hat{\sigma}_{Ti}^2 \left(\begin{bmatrix} \mathbf{X}(n)^{\mathrm{T}} & 1 \end{bmatrix} \left(\Gamma^{\mathrm{T}} \Gamma \right)^{-1} \begin{bmatrix} \mathbf{X}(n) \\ 1 \end{bmatrix} + \frac{1}{k} + 1 \right)} \tag{4.39}$$

For the model application with external forcing function, the corresponding confidence interval is

$$T_i(n)_{CI,\alpha} = T_i(n) \pm t_{\alpha/2,\, k-8-1} \sqrt{\hat{\sigma}_{Ti}^2 \left(\begin{bmatrix} \mathbf{X}(n)^{\mathrm{T}} & u(n) & 1 \end{bmatrix} \left(\Pi^{\mathrm{T}} \Pi \right)^{-1} \begin{bmatrix} \mathbf{X}(n) \\ u(n) \\ 1 \end{bmatrix} + \frac{1}{k} + 1 \right)} \tag{4.40}$$

where $u(n)$ and Π are defined in Equation (4.4) and (4.19), respectively.

4.5 Results and discussion

Model results for both of the two applications described in Section 4.2 are presented in this section. The first application utilizes the model given in Equation (4.1), which does not include the forcing function explicitly. The model was first calibrated with reconstructed data from 1880 to 1992, using the least squares method described in Section 4.3.1. The confidence intervals of model simulations were also calculated following the methodology discussed in Section 4.4.3. The calibrated model was then

applied for the time period of 1993-2001, and the results obtained were compared with corresponding observations for the purpose of validation. As shown in Figure 4.2, model results match observations well in both the calibration period and the validation period. The RMSE of the overall fitting in the calibration phase for sea level is 1.33 cm, and that for SST is 0.12 °C. In the validation phase, the corresponding numbers are 0.98 cm and 0.10 °C, respectively.

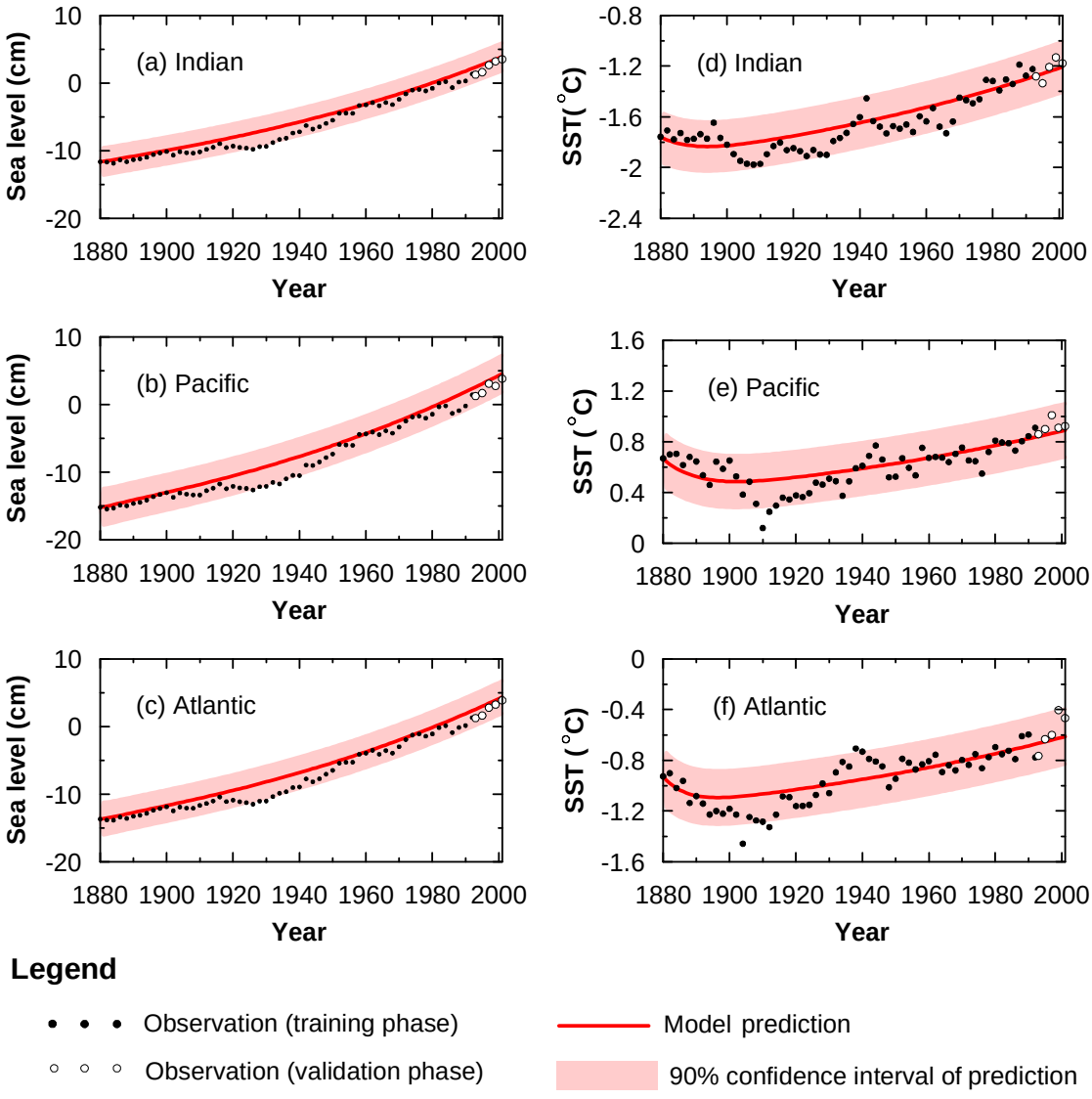

Figure 4.2 Spatial model results in the training phase and the validation phase.

To fully utilize the observational datasets, coefficients for the dynamic system model, Equation (4.1), were finally calibrated using all the data from 1880 to 2001. The resulting coefficient matrices are shown in Table 4.1. While the rate of sea level rise in the global DSM model by Aral et al. (2012) is negatively correlated with its current state, this negative feedback trend is not the same for every region in our spatial DSM model. In Table 4.1, two of the total three elements on the diagonal of matrix **A** are positive suggesting that feedback by a single region is not necessarily negative. An interesting observation is that, for the matrix **E**, which quantifies the impacts of different regions' SST on their rate of SST rise, the diagonal elements are all negative, indicating that the three regions' SST rise rates all receive negative feedbacks from their current states of SST. From the perspective of control theory, this negative feedback feature indicates that the response of the temperature system is controllable when external controls are implemented on the system. Note that the diagonal elements of matrices **B** and **D** do not follow a systematic pattern. This illustrates the importance of representing appropriate interactions between different regions in modeling spatial variations of SLR. Because of this complex nature of spatial interactions, the methodology that may be used to model global means of sea level and SST would not be appropriate to predict the spatially distributed sea levels and temperatures of these regions. That is treating different regions of the oceans as if they are isolated regions would not be a reasonable approach and interactive analysis needs to be performed as discussed in this study. Eigenvalue analysis reveals that the most dominant eigenvalues for matrices **A**, **B**, **D**, **E** are -0.37, 0.38, -0.17, -0.27, respectively. Based on these eigenvalues, sea levels and SST's generally have negative impacts on the changing rate of themselves (**A** and **E**). While increase of SST leads to increase of sea level rise rate (**B**), increase of sea level will decrease the SST rise rate (**D**).

Table 4.1 Coefficient matrices obtained from model calibration

Rate of Rise	**Contributing variable**						
	H			T			Constant
	A (yr^{-1})			**B** (cm/°C/yr)			$\mathbf{C_H}$ (cm/yr)
dH/dt	0.22	0.20	-0.41	0.29	-0.35	0.22	1.02
	0.63	-0.12	-0.41	0.30	-0.20	-0.12	0.57
	0.60	0.23	-0.77	0.40	-0.45	0.11	1.15
	D (°C/cm/yr)			**E** (yr^{-1})			$\mathbf{C_T}$ (°C/yr)
dT/dt	-0.03	-0.07	0.11	-0.26	0.12	-0.01	-0.46
	-0.04	-0.06	0.10	0.01	-0.07	-0.02	0.05
	0.05	0.02	-0.06	-0.01	-0.02	-0.11	-0.07

The analytical formula for model prediction can be obtained by rearranging the matrices in Table 4.1 and following the procedures described in Section 4.4.1. Specifically, for the spatial DSM model without explicit external forcing function (Equation (4.1)), the corresponding coefficient matrix $\mathbf{K}$ computed from Table 4.1 has four distinct real eigenvalues ($\lambda_1 \sim \lambda_4$) and two conjugate complex eigenvalues ($\lambda_5 / \lambda_6 = m \pm ni$). Accordingly, $\mathbf{K}$ has four linearly independent real eigenvectors ($\mathbf{V}_1 \sim \mathbf{V}_4$) and a complex-conjugate pair of eigenvectors ($\mathbf{V}_5 / \mathbf{V}_6 = \mathbf{M} \pm \mathbf{N}i$). As a result, Equation (4.23), (4.25), and (4.29) are applied to construct the analytical formula as

$$\begin{Bmatrix} H_1(t) \\ H_2(t) \\ H_3(t) \\ T_1(t) \\ T_2(t) \\ T_3(t) \end{Bmatrix} = \sum_{j=1}^{4} c_j \mathbf{V}_j e^{\lambda_j t} + c_5 \left[\mathbf{M} \cos nt - \mathbf{N} \sin nt \right] e^{mt} + c_6 \left[\mathbf{N} \cos nt + \mathbf{M} \sin nt \right] e^{mt} + \mathbf{X}_p \quad (4.41)$$

The particular solution $\mathbf{X}_p$ can be obtained using the variation of parameters method discussed in Section 4.4.1, and the constants c_j's, c_5 and c_6 can be computed using the initial conditions of H_i's and T_i's.

To test the accuracy of our numerical method described in Section 4.4.2, the numerical predictions are compared with the analytical predictions computed using Equation (4.41) (Figure 4.3). Based on the comparison, the numerical predictions match the analytical predictions very well, indicating that the numerical method adopted is accurate enough for this application.

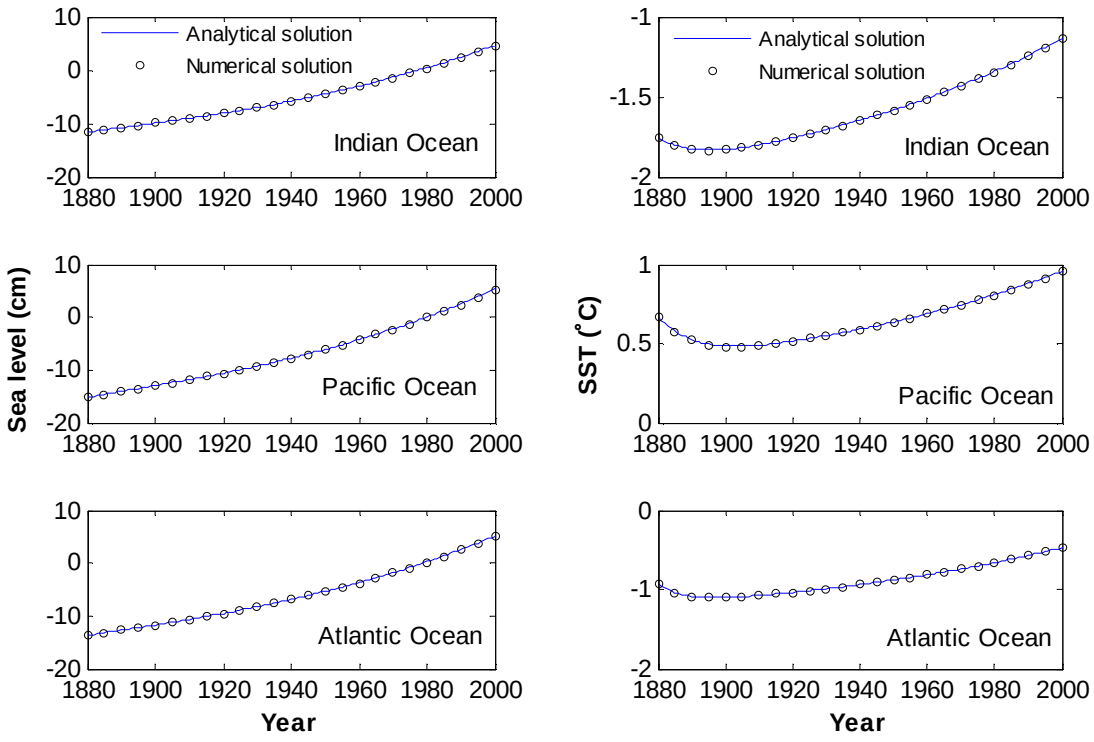

Figure 4.3 Analytical and numerical predictions of the model without external forcing function for the variable of: (a) sea level; (b) SST.

The predictions made using this model assume that the anthropogenic factors during the prediction period behave similarly to those in the calibration period. Carbon dioxide emission scenarios used for projections in the IPCC analysis (Meehl et al., 2007) is not considered here. However, this is not a restriction since the procedure described in Aral, et al. (2012) can be used to implement this analysis for this case as well. Applying the calibrated DSM (Table 4.1), sea level and SST for all three regions are projected in the 21st century (Figure 4.4). All three regions of the ocean will experience significant sea level and SST rise in the 21st century, but the magnitude of rise varies from region to region. The projected magnitude (with 90% confidence interval) of sea level rise from

2001 to 2100 for Indian, Pacific, and Atlantic Ocean are 38±3 cm, 47±4 cm, 43±3 cm, respectively; those for SST rise of the corresponding regions are 1.8±0.3 °C, 1.3±0.3 °C, 1.6±0.3 °C. The magnitude of SLR in the Indian Ocean is significantly lower than those in the other two regions, while the magnitude of SST rise is the lowest in the Pacific Ocean. The outcome that the highest SST rise among regions will not lead to the highest sea level rise is again an indication that different regions of the oceans cannot be treated as isolated zones. To compare our results with those by previous studies, the global average of predicted sea levels or SST's is calculated as the area-weighted average of regional means of sea level or SST. The global mean sea level in 2100 relative to 1990 is 48 cm with 90% confidence interval of 45-51 cm. This result matches the predicted central value of 48cm (with a range of 9-88 cm) by the IPCC (Church and Gregory, 2001) perfectly well. Our prediction of sea level is also close to the range of 50-140 cm by Rahmstorf (2007) and that of 40-45 cm by the global dynamic system analysis study of Aral et al. (2012). The small difference between results of this model and that in Aral et al. (2012) is probably caused by the use of different types of temperature data. As mentioned previously in Section 4.3.2, sea surface temperature (SST) was used in this study, while surface air temperature data was used in the study by Aral et al. 2012. The lower prediction of sea level by our model compared to that by Rahmstorf (2007) is likely associated with the incorporation of feedback mechanisms into our model. This difference might indicate the importance of feedback mechanisms to the dynamic system of sea level and SST.

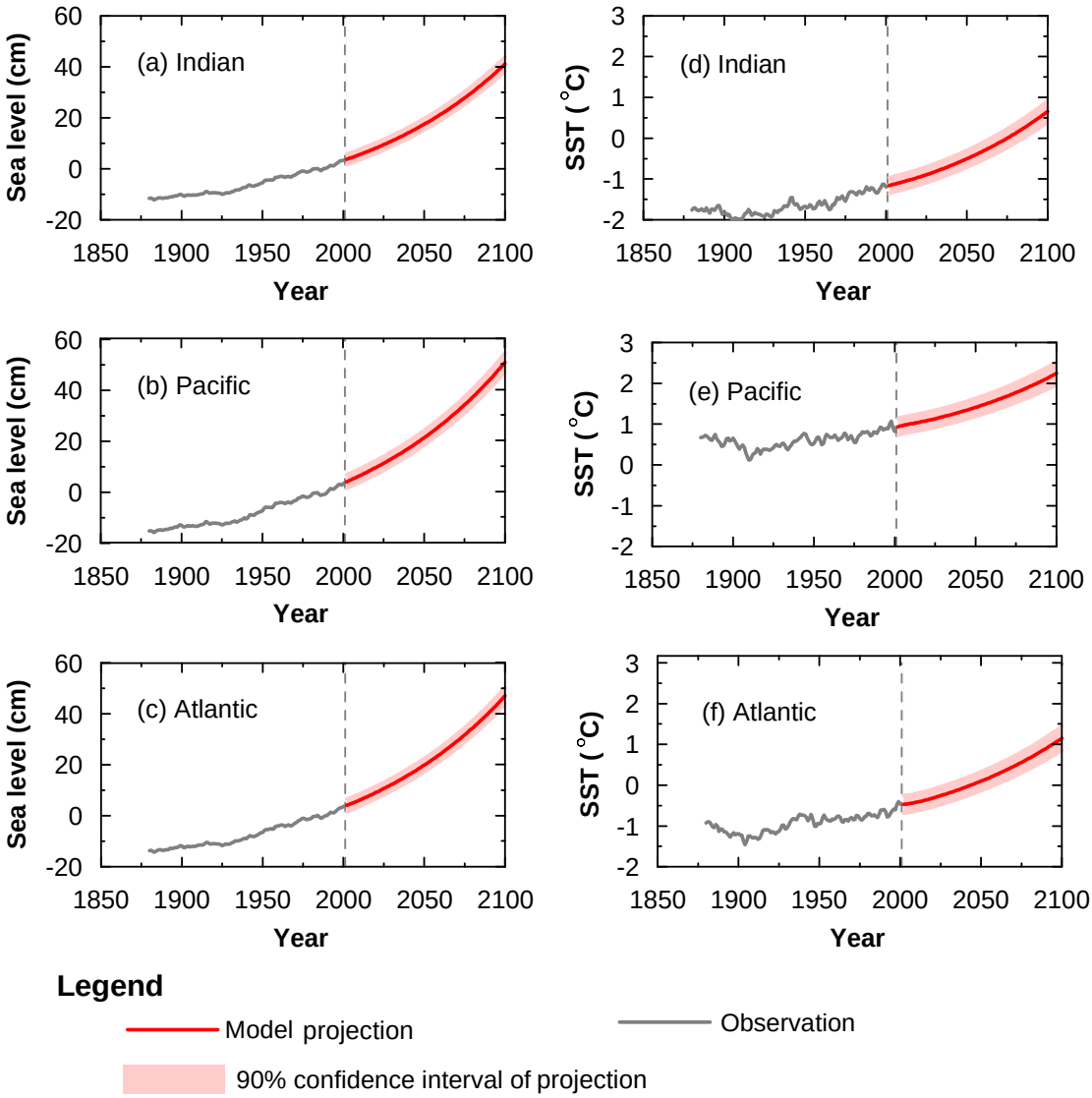

Figure 4.4 Projections of regional means by the spatial DSM without external forcing function.

In the second application the model given in Equation (4.2) is applied. Using the methodology described in Section 4.3.1, the term β in Equation (4.4) was calibrated as 1.21. After β is determined, the model in Equation (4.2) was calibrated with the sea level (reconstructed using ANN, see detail descriptions in previous paragraphs), SST, and global mean CO_2 concentration data from 1880 to 1992 using the methodology described

in Section 4.3.1. The calibrated model was then validated using observation from 1993 to 2001. Model results match observations well in both the calibration and the validation period (Figure 4.5). The RMSE of the overall fitting in the calibration phase for sea level is 1.07 cm, and that for SST is 0.11 °C. In the validation phase, the corresponding numbers are 0.35 cm and 0.09 °C, respectively.

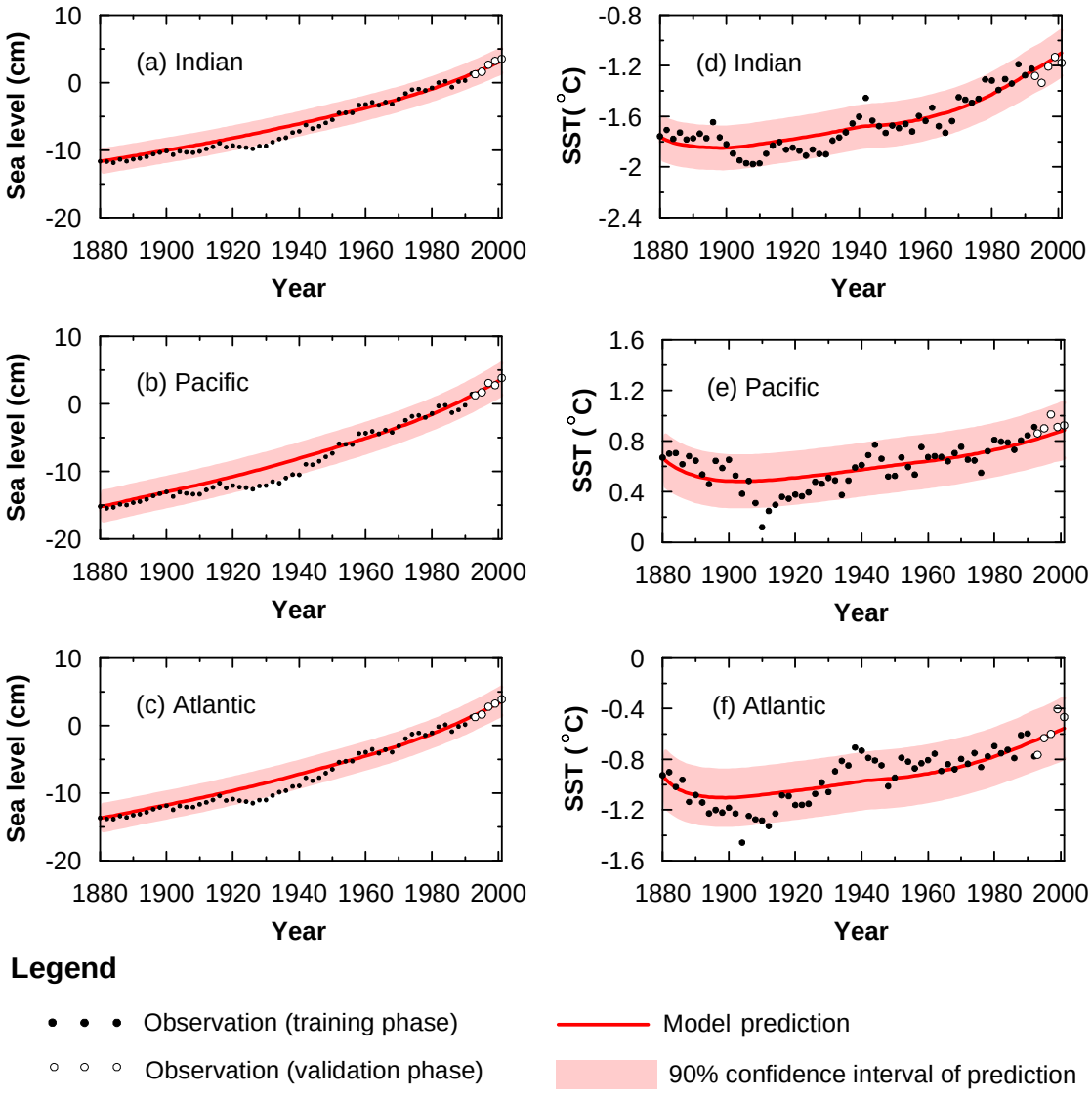

Figure 4.5 Results of spatial model with external forcing function in the training and the validation phase.

The calibrated coefficient matrices in Equation (4.2) are shown in Table 4.1. As expected, adding external forcing function to the model does not change the values of matrices $\mathbf{A}$, $\mathbf{B}$, or $\mathbf{C_H}$. However, changes are likely to occur in $\mathbf{D}$, $\mathbf{E}$, and $\mathbf{C_T}$, as adding external forcing will theoretically re-attribute contributions to SST change among sea level, SST, constant term, and the external forcing. Compared to values in Table 4.1, $\mathbf{D}$ and $\mathbf{C_T}$ in Table 4.2 have significant changes, while no significant change is observed in $\mathbf{E}$. Elements in $\mathbf{D}$ now exhibit a more discernible pattern, as values on the diagonal are all negative. These negative diagonal elements indicate that the three regions' rates of SST rise all receive negative feedbacks from their current states of sea level. The absence of significant change in $\mathbf{E}$ suggests that adding external forcing does not affect SSTs' behavioral impacts on themselves. The three elements of $\mathbf{Q}$ are all positive, an indication that increased global mean CO_2 concentration will lead to increased rates of SST rise for all regions. The fact that q_3 is larger than q_1 and q_2 reveals that the Atlantic Ocean's rate of SST change are more sensitive to global CO_2 concentration change than the Indian and the Pacific Ocean. The most dominant eigenvalues for matrices $\mathbf{A}$ and $\mathbf{B}$ are the same with those for our first model (Equation (4.1)). The most dominant eigenvalues for matrices $\mathbf{D}$ and $\mathbf{E}$ are -0.18 and -0.29, respectively, which do not differ significantly from their previous values in the first model (Equation (4.1)). This demonstrates that our model results are relatively robust.

Table 4.2 Calibrated coefficient matrices for spatial model with external forcing function

Rate of rise	**Contributing variable**							
	H			T			CO_2	Constant
	A (yr^{-1})			**B** (cm/°C/yr)			**N/A**	$\mathbf{C_H}$ (cm/yr)
dH/dt	0.22	0.20	-0.41	0.29	-0.35	0.22	N/A	1.02
	0.63	-0.12	-0.41	0.30	-0.20	-0.12	N/A	0.57
	0.60	0.23	-0.77	0.40	-0.45	0.11	N/A	1.15
	D (°C/cm/yr)			**E** (yr^{-1})			**Q** (°C/ppm/yr)	$\mathbf{C_T}$ (°C/yr)
dT/dt	-0.04	-0.06	0.10	-0.29	0.12	0.01	0.073	-0.56
	-0.04	-0.06	0.10	0.01	-0.07	-0.02	0.010	0.04
	0.05	0.03	-0.07	-0.04	-0.03	-0.09	0.076	-0.17

Predictions made by the model with external forcing function reflect the changing trends of the anthropogenic factors during the prediction period. In this study, the future anthropogenic factors are represented by projected future CO_2 concentrations in the atmosphere. Specifically, our model used projected global mean CO_2 concentrations in the 21st century under six scenarios (Figure 4.6) proposed by the IPCC. The six scenarios include four marker scenarios (A1B, A2, B1, and B2) and two illustrative scenarios (A1T and A1FI). The A1 family of scenarios is commonly characterized by a homogeneous future world focused on economic growth, with three alternative technological emphases: fossil intensive (A1FI), non-fossil energy sources (A1T), or balanced energy sources (A1B). A2 assumes a very heterogeneous world that favors economic growth over environmental quality. B1 describes a homogeneous future world that values environmental sustainability, and B2 describes a heterogeneous world that is oriented toward environmental protection. These four marker scenarios are recommended as the basis of climate model projections, and detailed story lines behind different scenarios can

be found in the IPCC's Special Report on Emission Scenarios (SRES) (Nakicenovic et al., 2000).

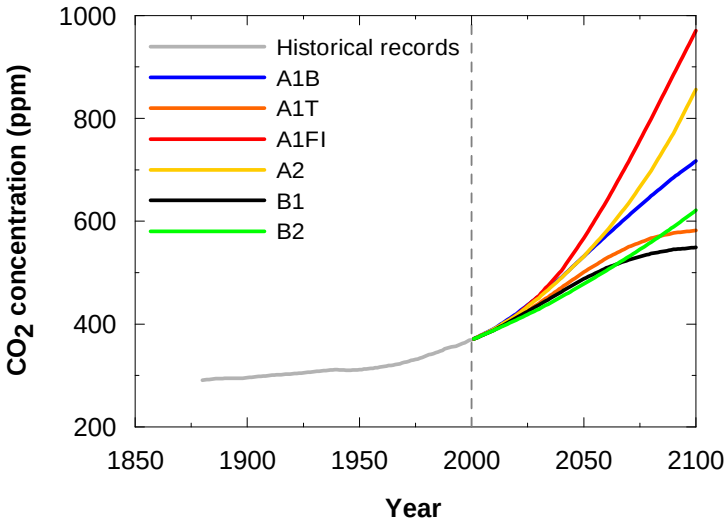

Figure 4.6 Global mean atmospheric CO_2 concentrations under different scenarios

Projected sea levels and SST's under the A1B scenario are drawn in Figure 4.7 to show the temporal behaviors of different regions, where all predicted SST and sea level curves progress smoothly over time. This "smoothness" is expected since our model targets projecting long-term trends rather than short-term oscillations. The same smoothness was observed for predictions of sea levels and SST's under all the other five scenarios.

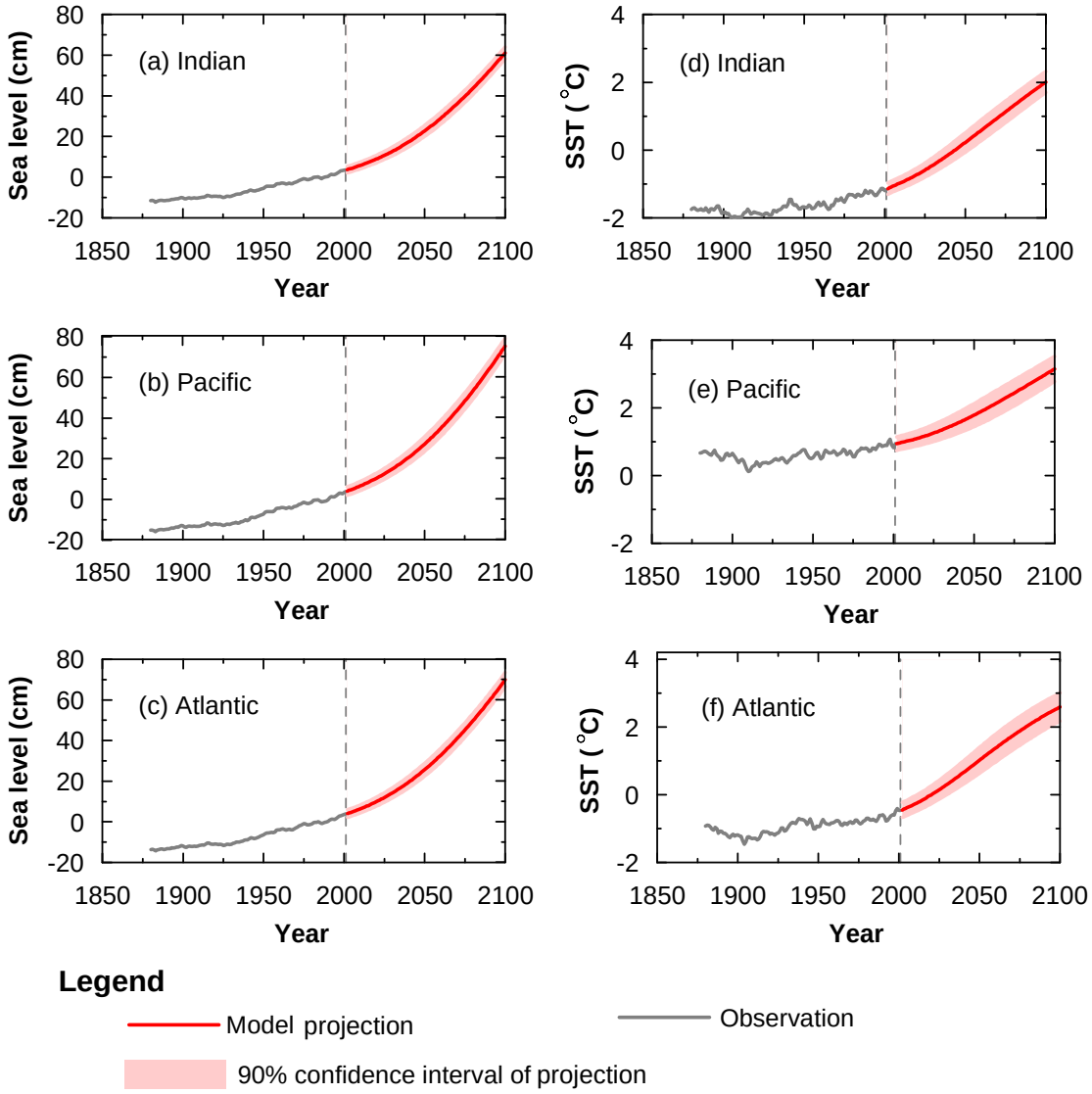

Figure 4.7 Temporal patterns of model predictions under the A1B scenario.

The final predicted sea levels and SST's (relative to the global mean values at 1990) under all the six SRES scenarios are presented in Figure 4.8. The highest and the lowest projected SST's occur under scenarios A1FI and B1, respectively, responding to the highest and the lowest predicted global mean CO_2 concentrations. Accordingly, the highest sea levels are predicted under the scenario A1FI, ranging from 71 cm to 86 cm (relative to 1990 global mean sea level); the lowest predicted sea levels are under the

scenario B1, varying from 51 cm to 64 cm. Both the predicted sea levels and SST's of the Indian Ocean are significantly lower than those of the Pacific Ocean and the Atlantic Ocean under all six scenarios. The relative magnitudes of SST's between the Pacific Ocean and the Atlantic Ocean vary under different scenarios. While the predicted sea levels of the Pacific Ocean are slightly higher than those of the Atlantic Ocean under all the scenarios, the differences are not significant. Another interesting result is related to projected temperatures under A1T, B1, and B2 scenarios. Compared to other scenarios, the projected atmospheric CO_2 concentrations are significantly lower under A1T. B1, and B2 scenarios, and the predicted SST's are accordingly lower. However, the spatial heterogeneity of predicted SST's under these three scenarios is significantly higher than that under the other three scenarios. The calculated global mean SLR from 2001 to 2100 is 67 cm, 60 cm, 78 cm, 70 cm, 56 cm, and 57 cm under scenario A1B, A1T, A1FI, A2, B1, and B2, respectively. This range of 56-78 cm is within the range of 9-88 cm by the IPCC (Church and Gregory, 2001) but is above their central value of 48 cm.

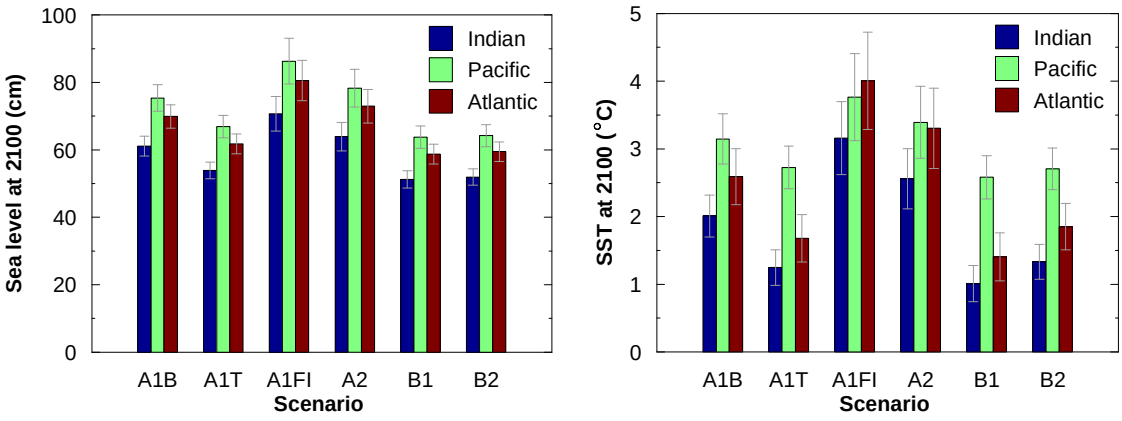

(a) (b)

Figure 4.8 Projections by model with external forcing under IPCC SRES scenarios for regional means of: (a) sea level; (b) SST (error bar: 90% confidence interval).

Regions of the ocean resulted from different division schemes have different spatial relevance, and they may reflect different climate patterns contained in historical records. So it is interesting to compare our model projections under different region division schemes. For this reason, the spatial DSM model was configured to investigate the behaviors of the system under the six SRES scenarios for a different region division scheme based on the spatial clustering result in Chapter 3 (Figure 4.9). Because of the change in region division scheme, regional average sea levels and SST's under this configuration exhibited remarkably different temporal patterns from those under the region division scheme based on the three major ocean basins (Figure 3.5).

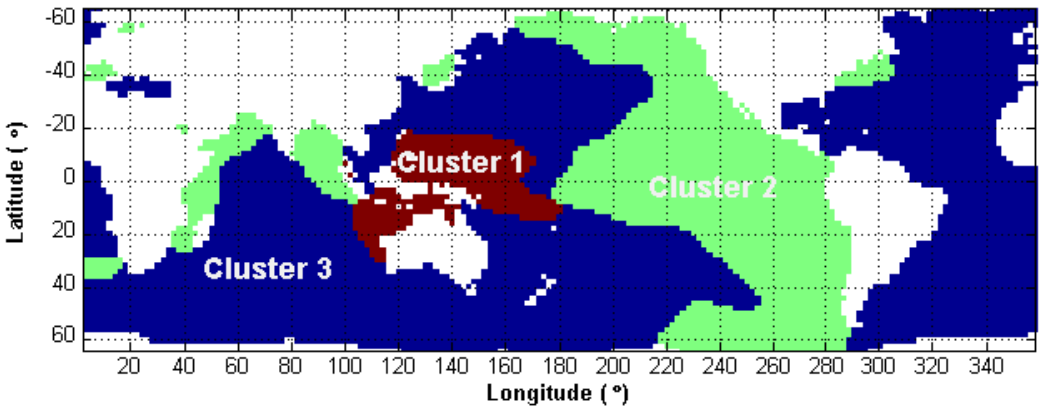

Figure 4.9 Region division based on spatial clustering.

Following the same procedure as that of the second model application, the spatial DSM model with the clustered region division scheme was calibrated and validated after a β coefficient was determined as 1.07 (Figure 4.10). Note that the sea level prediction errors in this application are noticeably larger than those in the application with region division scheme based on major ocean basins (Figure 4.5), especially for the case of Cluster 1. The RMSE of the overall fitting for sea level and SST are 1.39 cm and 0.11 °C in the

calibration phase, respectively; the corresponding numbers in the validation phase are 1.23 cm and 0.14 °C, respectively. For the case of Cluster 1's sea level, the RMSE of fitting is as large as 1.90 cm. For the previous model application with region division based major ocean basins, the RMSE of the overall fitting for sea level and SST are 1.33 cm and 0.12 °C in the calibration phase, respectively; the corresponding numbers in the validation phase are 0.98 cm and 0.10 °C, respectively. The significant increase of model errors in this application is probably caused by the oscillatory patterns shown in the time series of regional average sea levels (Figure 3.5 (a)). The temporal patterns of regional average sea levels are potentially associated with certain climate phenomena, thus they may be particularly useful for related studies. However, since the spatial DSM was originally designed to simulate long-term trends of sea levels and SST's, it is not specifically suited to capture the temporal oscillatory signals in the sea level records, which leads to increased model errors.

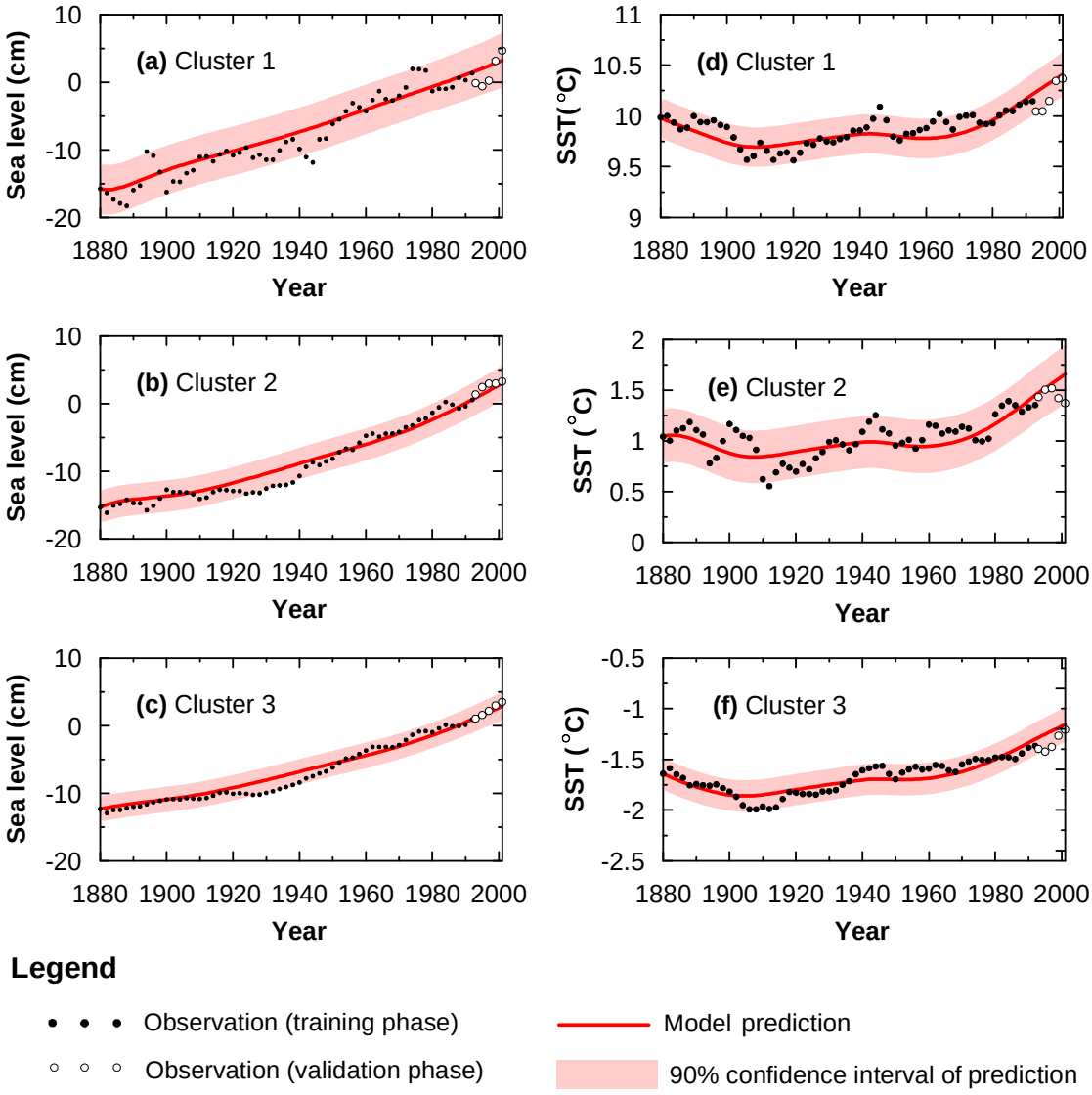

Figure 4.10 Results of spatial DSM model with the clustered region division scheme in the training and the validation phase.

The calibrated coefficient matrices for the spatial DSM model with clustered region division scheme are shown in Table 4.3. Because of the large prediction errors described in the previous paragraph, the calibrated coefficients theoretically should come with significant uncertainties. As a result, extra caution must be taken when interpreting the model coefficients and further using them for future projections.

Table 4.3 Coefficient matrices for spatial DSM with clustered region division scheme

Rate of rise	**Contributing variable**							
	H			T			CO_2	Constant
	A (yr^{-1})			**B** (cm/°C/yr)			**N/A**	$\mathbf{C_H}$ (cm/yr)
dH/dt	0.41	0.26	0.08	0.43	0.37	0.35	N/A	3.60
	1.07	0.67	0.20	1.11	0.96	0.90	N/A	9.35
	3.19	2.01	0.61	3.32	2.87	2.70	N/A	27.94
	D (°C/cm/yr)			**E** (yr^{-1})			**Q** (°C/ppm/yr)	$\mathbf{C_T}$ (°C/yr)
dT/dt	0.06	0.04	0.01	0.06	0.05	0.05	0.034	0.51
	0.21	0.13	0.04	0.20	0.17	0.16	0.112	1.70
	0.13	0.08	0.03	0.13	0.11	0.10	0.071	1.07

Projections of sea levels and SST's at year 2100 for the region division scheme based on spatial clustering are shown in Figure 4.11. Cluster 1 mainly represents a spatial footprint of the El Nino phenomenon (see Chapter 3), and it is located in the west tropical Pacific region. As a result, Cluster 1's historical average SST is significantly higher than those of the other two regions. Our projections also reflect the distinction between the SST of Cluster 1 and those of the other two regions (Figure 4.11 (b)). As expected, the highest projected sea level and SST both occur under the scenario A1FI. However, the differences between projections under different scenarios are not as significant as those observed for region division based on major ocean basins (Figure 4.8), especially for the case of sea level. This is also probably caused by the significant temporal oscillations in the mean sea levels of Cluster 1 and 2. Temporal oscillations in the observational data lead to larger uncertainties in the projections, which can potentially decrease the differences between projections under different scenarios. This result also suggests that the spatial DSM with the current configuration is not well suited to characterize the spatial behaviors of sea level under the clustered region division scheme.

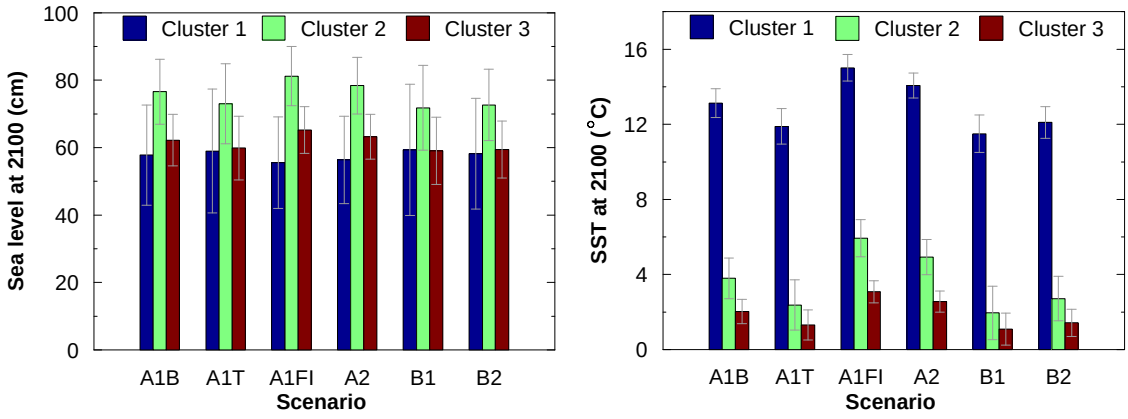

(a) (b)

Figure 4.11 Projections of regional means under region division based on spatial clustering: (a) sea level; (b) SST (error bar: 90% confidence interval).

4.6 Conclusions

A spatial form of the dynamic system model (DSM) is proposed to analyze spatial variations in sea level and temperature change. Using reconstructed spatial sea level and sea surface temperature (SST) data, the spatial DSM model was calibrated for two different configurations: (i) external forcing function embedded in the system matrix; and, (ii) external forcing function treated explicitly. The dynamic system matrices identified reveal that significant interactions exist among different regions of the oceans, and that feedback mechanisms observed in our previous global model do not necessarily apply to each single region. Instead, the feedback mechanisms exist in a more complex manner. When dynamic system matrices are analyzed from the control theory perspective, SST can be viewed as a negative feedback system. This indicates that the system response is controllable when external anthropogenic controls are implemented on the system.

For the model application with external forcing function embedded in the system matrices, sea levels and SST's are predicted for the 21st century based on the identified dynamic system matrices. Projection results indicate that both sea levels and SST's will rise significantly in the 21st century in all the three target regions of the ocean, but their magnitudes differ. The magnitude of sea level rise in the Indian Ocean is significantly lower than those in the Pacific and the Atlantic Ocean, while the magnitude of SST rise is the lowest in the Pacific Ocean. The global average of sea level rise projected from 2001 to 2100 is 48 cm with the 90% confidence interval of 45-51 cm, which is consistent with previous projections.

For the model application with external forcing function treated explicitly, sea levels and SST's for the three regions were projected using global mean CO_2 concentrations under six IPCC SRES scenarios. The highest and the lowest projected SST's occur under scenarios A1FI and B1, respectively, responding to the highest and the lowest predicted global mean CO_2 concentrations. The highest sea levels are predicted under the scenario A1FI, ranging from 71 cm to 86 cm (relative to 1990 global mean sea level); the lowest predicted sea levels are under the scenario B1, ranging from 51 cm to 64 cm. Predicted sea levels and SST's of the Indian Ocean under all six scenarios are significantly lower than those of the Pacific and the Atlantic Ocean. The relative magnitudes of SST's between the Pacific and the Atlantic Ocean vary under different scenarios, while the predicted sea levels of the Pacific Ocean are slightly higher than those of the Atlantic Ocean under all the scenarios. Calculate global mean sea level rise from 2001 to 2100 varies from 56 cm to 78 cm, which is in the upper portion of the IPCC's 9-88 cm range. A similar analysis was conducted for a model application with a region division based on spatial clustering. The temporal patterns of regional average sea levels are potentially associated with certain climate phenomena, thus they may be particularly useful for related studies. However, since the spatial DSM was originally designed to simulate long-

term trends of sea levels and SST's, it is not well suited to capture the temporal oscillatory signals in the sea level records. This speculation is supported by the large model calibration and validation errors, which suggests that further model development efforts are needed to utilize the information contained in the oscillatory signals.

CHAPTER 5

CASE STUDY ON THE INUNDATION IMPACTS OF PROJECTED SEA LEVEL RISE

5.1 Introduction

As the human society is facing potentially significant rise of sea level, such as those predicted in Chapter 4 of this study, accurate impact assessments of sea level rise (SLR) are critically needed worldwide. In these assessments, temporal characterization of the impact is as important as the spatial characterization for appropriate managerial decisions to be made in a timely manner.

A host of studies have analyzed the inundation impacts of potential SLR at global, regional, and local scales. Li et al. (2009) developed geographic information system (GIS) methods to assess inundation impacts of a hypothetical global SLR of one to six meters, and estimated that the inundated area would be between 1.055 (for one meter) to 2.193 (for six meters) million square kilometers. Dasgupta et al. (2009) also used GIS methods to identify inundation zones for 84 coastal regions of developing countries under projected SLR of 1-5 meters. Assessments of inundation caused by SLR have been conducted for various regions, including New Jersey, U.S. (Cooper et al., 2008), South Florida, U.S. (Zhang, 2011), the Florida Keys, U.S. (Zhang et al., 2012), and the Chinese coast (Yin et al., 2012). Studies have also quantified inundation areas under potential scenarios of SLR at a local scale, with target locations at metropolitan areas that include Maui, Hawaii (U.S.) (Cooper et al., 2013), New York City (U.S.) (Gornitz et al., 2002), Satellite Beach City, Florida (U.S.) (Parkinson and McCue, 2001), Collaroy/Narrabeen

Beach, Sydney (Australia) (Hennecke et al., 2004), and the cities of Tel Aviv and Haifa (Israel) (Lichter and Felsenstein, 2012).

Despite the large number of studies on inundation impact assessment of potential SLR, issues still exist in the methodologies that are used in these studies. Hypothetical magnitudes of SLR are commonly used to calculate the severity of inundation in some studies (Dasgupta et al., 2009; Li et al., 2009; Lichter and Felsenstein, 2012; Parkinson and McCue, 2011; Zhang et al., 2011). A series of hypothetical SLR scenarios may explore the range of possible inundation impacts, but this approach involves significant uncertainties in expected SLR projections. The hypothetical SLR scenarios are not very useful in identifying the most likely magnitude of SLR, since the likelihood of each scenario is not quantified. Another issue in previous inundation impact studies is that the difference between sea level datum and land elevation datum, as well as its impact on the results, is rarely addressed. While the difference in the reference point may produce negligible errors for small regions (Zhang, 2011) it may have a significant impact on results of studies that target large regions.

In this chapter, inundation impact assessment is conducted for three states along the United States (U.S.) east coast, namely Florida, Georgia, and New Jersey, where the SLR is a particularly concerning issue. Since future sea levels under different scenarios have already been projected in Chapter 4 of this study, the inundation impact assessment in this chapter does not have to be based on hypothetical sea levels. This will lead to a more relevant assessment of the inundation threats on the target study regions, which can provide critical and timely information for policy makers. Critical issues in the inundation assessment process, such as the data accuracy issue and the elevation datum issue mentioned above, are discussed, and related suggestions are given to future studies.

5.2 Study regions

Three states along the east coast of the United States (U.S.) are selected as representative regions for our inundation impact case study, namely, Florida, Georgia, and New Jersey (Figure 5.1). Florida is chosen because of its long coastline and the large area of flat and low-lying regions in its southern tip. Among the contiguous United States, Florida has the longest coastline of 1,350 miles (U.S. Census Bureau, 2012), which makes sea level rise a particularly concerning issue for the local community. The coastline of Georgia is about 100 miles in length, where the United States' fourth largest port by container traffic, the port of Savannah, is located. The state of New Jersey has the second highest population density (about 1,196 people per square mile of land area) in the U.S., and about 52% of its population lives in coastline counties. Other statistical information about the regions of study can be found in Table 5.1.

Table 5.1 Statistical information about the regions of study

Region of study	Land area [a] (sq mi)	Length of coastline [b] (mi)	Population [c]	Percentage of population on coastline counties [d]
Florida	53,603	1,350	9,829,000	75.7
Georgia	57,501	100	18,538,000	4.9
New Jersey	7,354	130	8,708,000	51.6

a, b, c: from U.S. Census Bureau (2012)

d: from U.S. Census Bureau (2010)

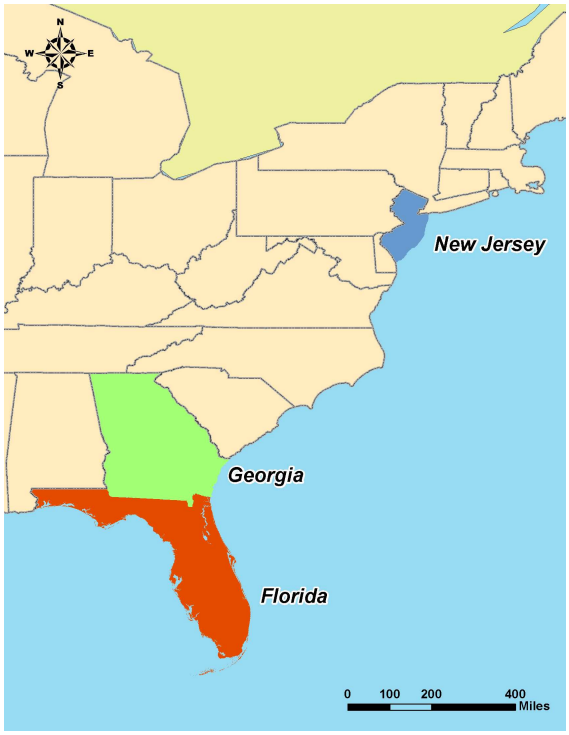

Figure 5.1 Geographic locations of study regions

5.3 Data acquisition

The aim of this chapter is to analyze the inundation impact caused by our spatial DSM model's projected SLR under different scenarios. Two types of spatial data are needed for this inundation impact assessment study, land elevation raster data and U.S. states' political boundary vector data. The political boundary data is obtained from the Topologically Integrated Geographic Encoding and Referencing (TIGER) database of the U.S. Census Bureau (2013).

The land elevation data for the states of New Jersey and Georgia were acquired from the 1/3 arc-second digital elevation model (DEM) data set of the U.S. Geological Survey (USGS) (2013). For the state of Florida, because of its relatively large area and the flat topography in its southern part, two sets of data were used to characterize its land

elevation: (i) the 1 arc-second DEM data set of the USGS (2013) and (ii) the high accuracy elevation data (HAED) from South Florida Information Access (SOFIA) of USGS (SOFIA, 2012). For most parts of the Florida peninsula, the 1 arc-second DEM data are used for inundation mapping. For the greater Everglades area, because of its flat topography, the elevation dataset with higher vertical resolution HAED is used to make the inundation mapping more accurate. The HAED dataset has a target accuracy of 15 cm, and the measured samples have a RMSE error of about 4 cm (Jones et al., 2012). The coverage of the HAED data is shown in Figure 5.2.

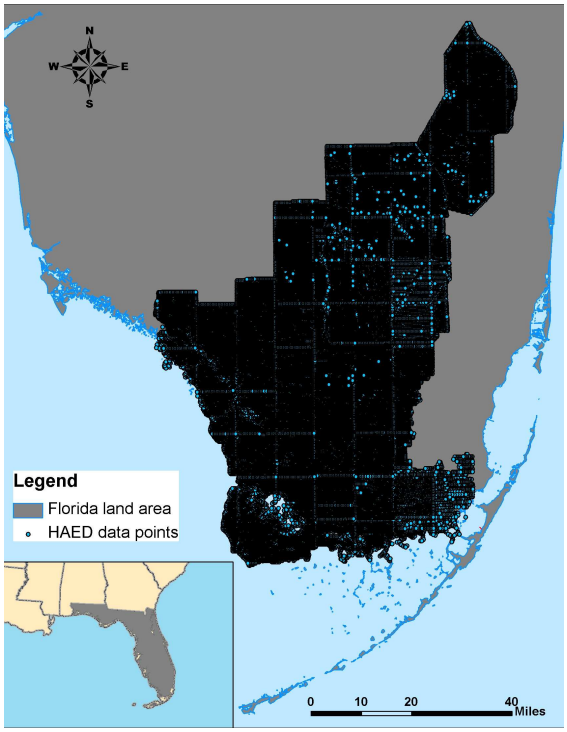

Figure 5.2 Coverage of the HAED dataset

5.4 Inundation impact assessment

5.4.1 Inundation mapping

Before the actual inundation mapping process is conducted, the land elevation data need to be processed first. Both the 1 arc-second and 1/3 arc-second DEM data were originally obtained in the 1° × 1° (long-lat) tile form. They were then merged into three DEM files whose spatial relevance matches that of the three study regions respectively, using the "mosaic to new raster" tool of the software ArcMap (Version 10.0) by ESRI (Redlands, California, USA). Note that all the spatial data processing and map production in this chapter were conducted using this ArcMap software. For the case of Florida, to utilize the HAED data, this vector data set (point shapefile) was first transformed into a DEM file with the spatial resolution of 1 arc-second. The resulted DEM file was then merged with the 1 arc-second DEM file by replacing the corresponding data in the latter. To improve the accuracy of the subsequent spatial processing, the three DEM files were projected to change their original coordinate system of GCS North American 1983 to the state plane coordinate systems. After this projection processing, the DEM files for Florida, Georgia, and New Jersey now have the coordinate systems of NAD1983 State Plane for Florida West (FIPS 0902), Georgia East (FIPS 1001), and New Jersey (FIPS 2900), respectively. The three projected DEM files were finally clipped by the political boundaries of the three target states to be spatially relevant and accurate.

After the preprocessing of land elevation data, the inundation mapping process was carried out using the "single-value surface model" (NOAA Coastal Services Center, 2010). This method uses only two types of data: sea surface elevation and land elevation (topography). Assuming topography of the land does not change as sea water intrudes, an area (a pixel in the DEM file) will be classified as inundated if its land elevation is smaller than the modeled sea surface elevation at the same location. All the pixels of each

DEM file were classified as above or below sea level, and the classification result was mapped. The number of pixels classified as below sea level on the map was then counted and multiplied by the area of a unit pixel to calculate the total inundation area.

5.4.2 Sea level datum

One important issue in the elevation comparison step of the inundation mapping process above is the consistent use of datum for these two elevation datasets. For the elevation comparison to be appropriate and the subsequent inundation area calculation to be accurate, the two datasets involved should be referenced to the same elevation datum. In this study, the local mean sea level (LMSL) datum was chosen as the datum to measure the magnitude of sea level rise. Mean sea level (MSL) is a tidal datum defined in the National Tidal Datum Epoch (NTDE) based on data collected over a 19-year tide cycle and it pertains to LMSL at the tide station at which it was observed (NOAA, 2013). The current NTDE for the U.S. is 1983-2001, and the LMSL defined in this epoch was adopted as the datum for our sea level height data. The land elevation datum for the DEM data used in this study is the North American Datum of 1988 (NAVD88). To examine the elevation difference between the two data, the elevation of LMSL relative to NAVD88 is calculated using the software VDatum by NOAA (VDatum, 2012).

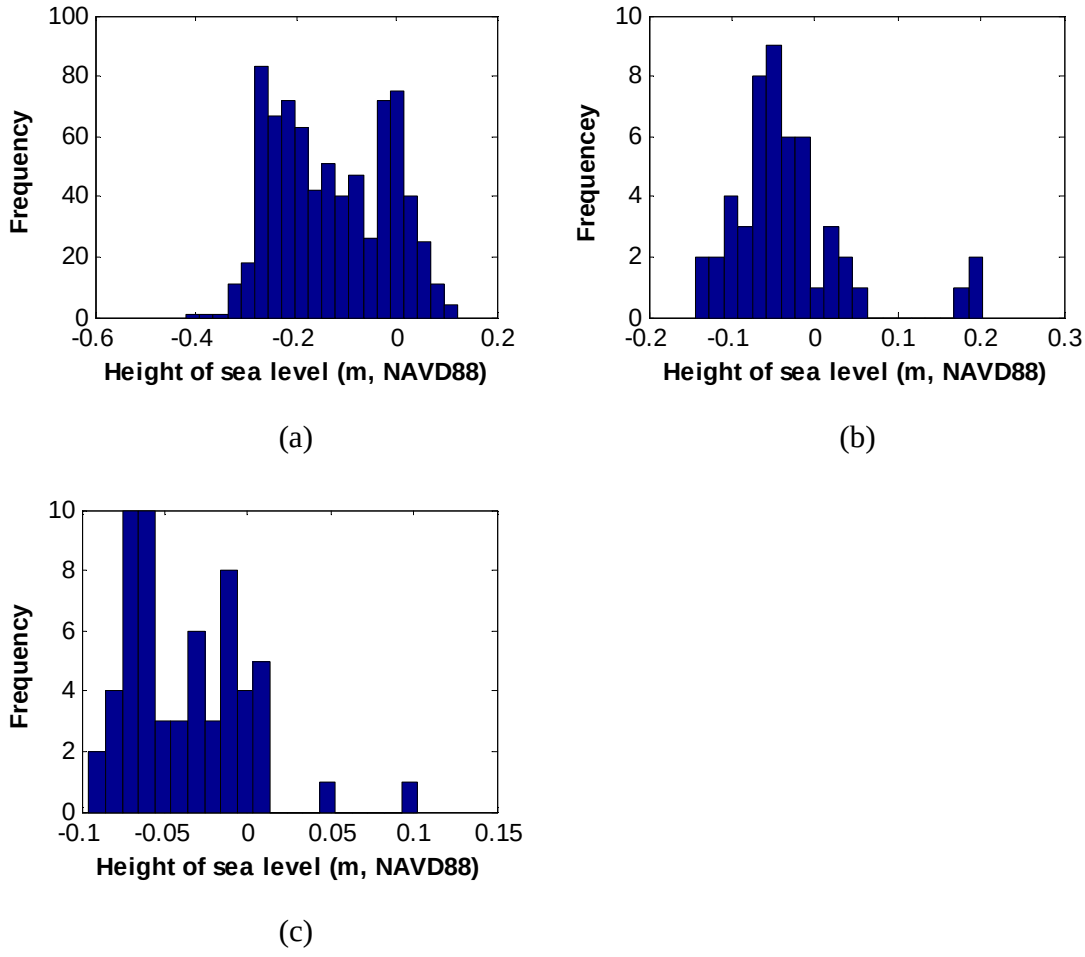

Figure 5.3 Elevation of LMSL relative to NAVD88 at tide stations along the coastline of: (a) Florida; (b) Georgia; and (c) New Jersey.

The results of the VDatum calculation are shown in Figure 5.3. The LMSL's at tide stations along the Florida coastline are significantly different than the NAVD88 datum, with the elevation difference on the order of magnitude of 10 cm. For the other two states Georgia and New Jersey, the corresponding difference is not as significant, which is on the order of magnitude of 1 cm. Based on these results, the insignificant difference between LMSL and NAVD88 was neglected for the states of Georgia and New Jersey. The land elevation data of Florida was further processed to account for the significant difference between LMSL and NAVD88 along its coastline. Since the VDatum software

only computes the difference for tide stations along the coastline, interpolation techniques are needed for inland areas. For this purpose, the elevation of LMSL relative to NAVD88 is first calculated at tide stations, which is generally within the "datum calibration regions" defined by NOAA (2011). In the second step, the "natural neighbor" interpolation technique (Ledoux and Gold, 2005) is used to calculate elevation of LMSL at other locations, including those that are inland. The interpolated LMSL elevation will help us compute the elevation of new sea level as the coastline moves landward under projected sea level rise. The interpolation result is shown in Figure 5.3. The interpolated elevation of LMSL was subtracted from the preprocessed DEM dataset of Florida, so the resulted DEM data is referenced to the datum LMSL. In the subsequent calculations, both land elevation data and sea surface elevation data can be viewed as relative to the datum of LMSL, so the elevation comparison between the two is appropriate.

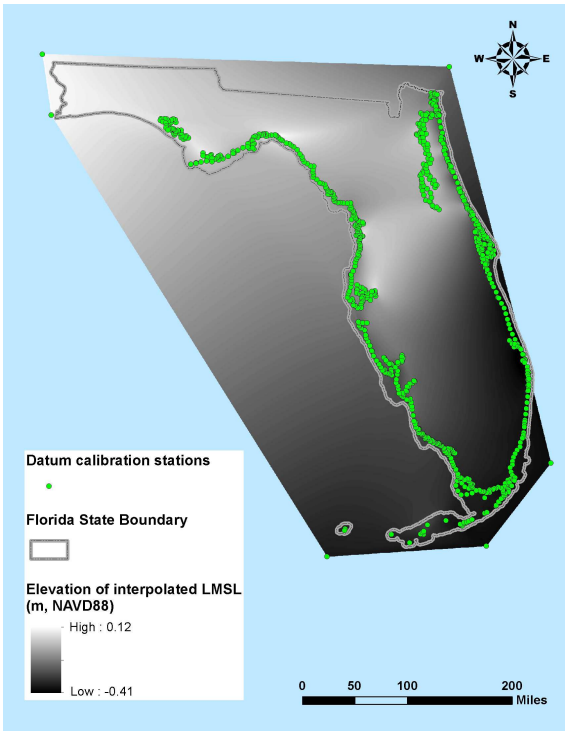

Figure 5.4 Interpolated LMSL elevation relative to NAVD88 for the state of Florida

5.4.3 Projected future sea levels

Sea levels projected under the six SRES scenarios in Chapter 4 are used in this chapter to assess the corresponding inundation impacts in the 21st century. Since the three selected study regions are all along the east coast of the U.S., the projected sea levels for the Atlantic Ocean are specifically chosen to make a spatially relevant assessment. As described in Section 5.4.2, and the LMSL defined in 1983-2001 epoch was adopted as the datum for our sea level height data. Accordingly, projected mean sea levels of the Atlantic Ocean by the spatial DSM model were recalculated to be relative to their averages from 1983 to 2001 (Figure 5.5). The projected sea levels at 2100 range from 58cm to 79 cm (relative to the 1983-2001 average). The highest sea level rise is projected under the A1FI scenario, and the lowest under the B1 scenario, which corresponds to the highest and the lowest projected CO_2 concentration in the atmosphere (Chapter 4), respectively.

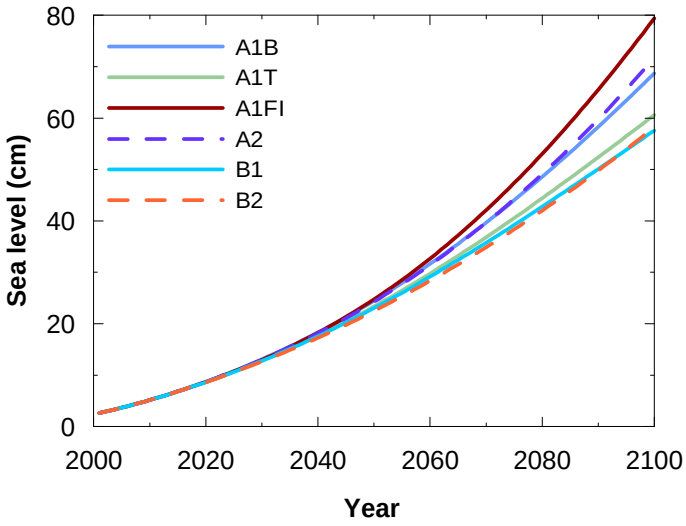

Figure 5.5 Projected mean sea level of the Atlantic Ocean under various IPCC SRES scenarios (relative to the 1983-2001 average)

5.5 Results and discussion

Based on the elevation comparison between the processed DEM data and the projected sea level, inundation mapping of Florida, Georgia, and New Jersey was conducted and the cumulative inundated land areas were plotted for different world development scenarios (Figure 5.7). Significant differences exist between the projected land inundation situations of the three target regions, which reflect the variations among their land topography. Under all the six scenarios, Florida will experience the most severe land inundation, with the total area of inundation from 2010 to 2100 calculated to be about 3,000 square miles. The area of inundation from 2010 to 2100 for Georgia ranges from 201 to 376 square miles, while that range for the state of New Jersey is from 142 to 202 square miles. To demonstrate the relative severity of land inundation, the percentage of inundated land area to the total current land area is calculated for each state (Figure 5.6). Based on the result, the percentage land inundation for Florida, Georgia, and New Jersey is projected to 5.4%, 0.3% - 0.6%, and 1.9% - 2.7%, respectively. As expected, the most serve land inundation will happen under scenario A1FI and the least severe under B1 for all the three study regions.

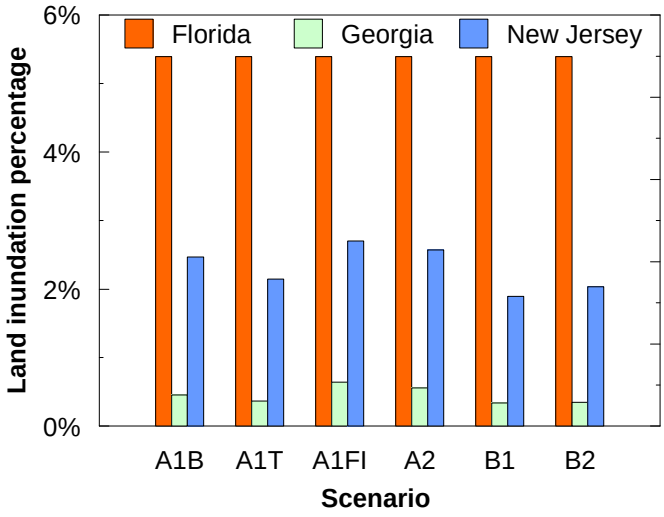

Figure 5.6 Land inundation percentage by 2100 under various IPCC SRES scenarios

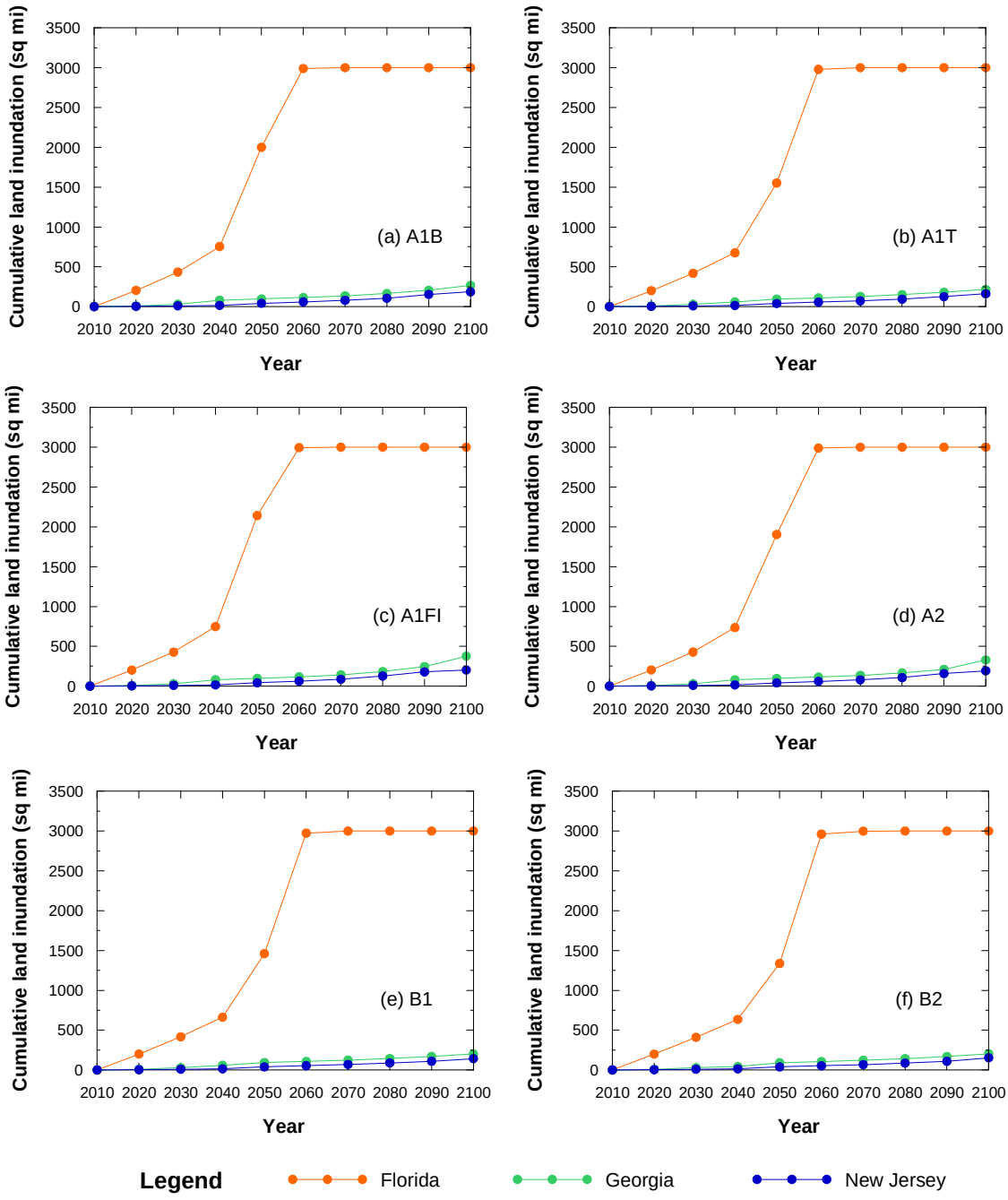

Figure 5.7 Cumulative land inundation since 2010 corresponding to projected sea level rise under the scenario: (a) A1B; (b) A1T; (c) A1FI; (d) A2; (e) B1; (f) B2.

In addition to the final magnitude of inundation, the temporal behavior of the inundation process is also critical for decision making. The inundation impact assessment results indicate that the temporal patterns of land inundation differ among the three study regions (Figure 5.7). For the case of Florida, the temporal inundation process follows a non-linear pattern. The rate of inundation starts to accelerate from 2040 and decelerate after 2060. Since no such non-linear pattern has been observed in the time series of projected Atlantic Ocean mean sea level, the non-linear inundation process should be caused by the characteristic topography of Florida. This type of non-linear inundation pattern was observed in a previous study by Zhang (2011) for the South Florida region, which also proposed that the nonlinearity is due to regional topography. The situation in this study is similar. For the study region of Georgia, there also appears to be an acceleration of land inundation after 2080, especially under the scenarios A1FI and A2. However, the magnitude of this acceleration is remarkably smaller than that for the case of Florida. No significantly non-linear pattern is observed in the time series of cumulative inundation area for New Jersey under all the six scenarios.

To examine the spatial patterns of the inundation process, land inundation maps under the "business-as-usual" A1B scenario are plotted for Florida (Figure 5.8), Georgia (Figure 5.9), and New Jersey (Figure 5.10). For Florida, the inundated areas are mainly located in the southern part, with the Everglades as the most severely affected region. This map also shows the spatial features associated with the non-linear temporal pattern of inundation described in previous paragraph. Notice the remarkable increase of inundation area from 2040 (Figure 5.8 (b)) to 2070 (Figure 5.8 (c)), which suggests that the acceleration of land inundation shown in Figure 5.7 is mainly caused by the inundation of the flat and low-lying Everglades area (southernmost region of Florida on the map). The inundation the Fort Lauderdale area (yellow region on the southeast coastline) also appears to contribute to the non-linear inundation process. For the case of Georgia, no particular

spatial pattern was observed, indicating an inundation threat that is relatively uniform in space. The inundation impact on New Jersey is more noticeable from 2070 and afterwards, with its southeast coastal region as the most vulnerable to inundation caused by projected sea level rise.

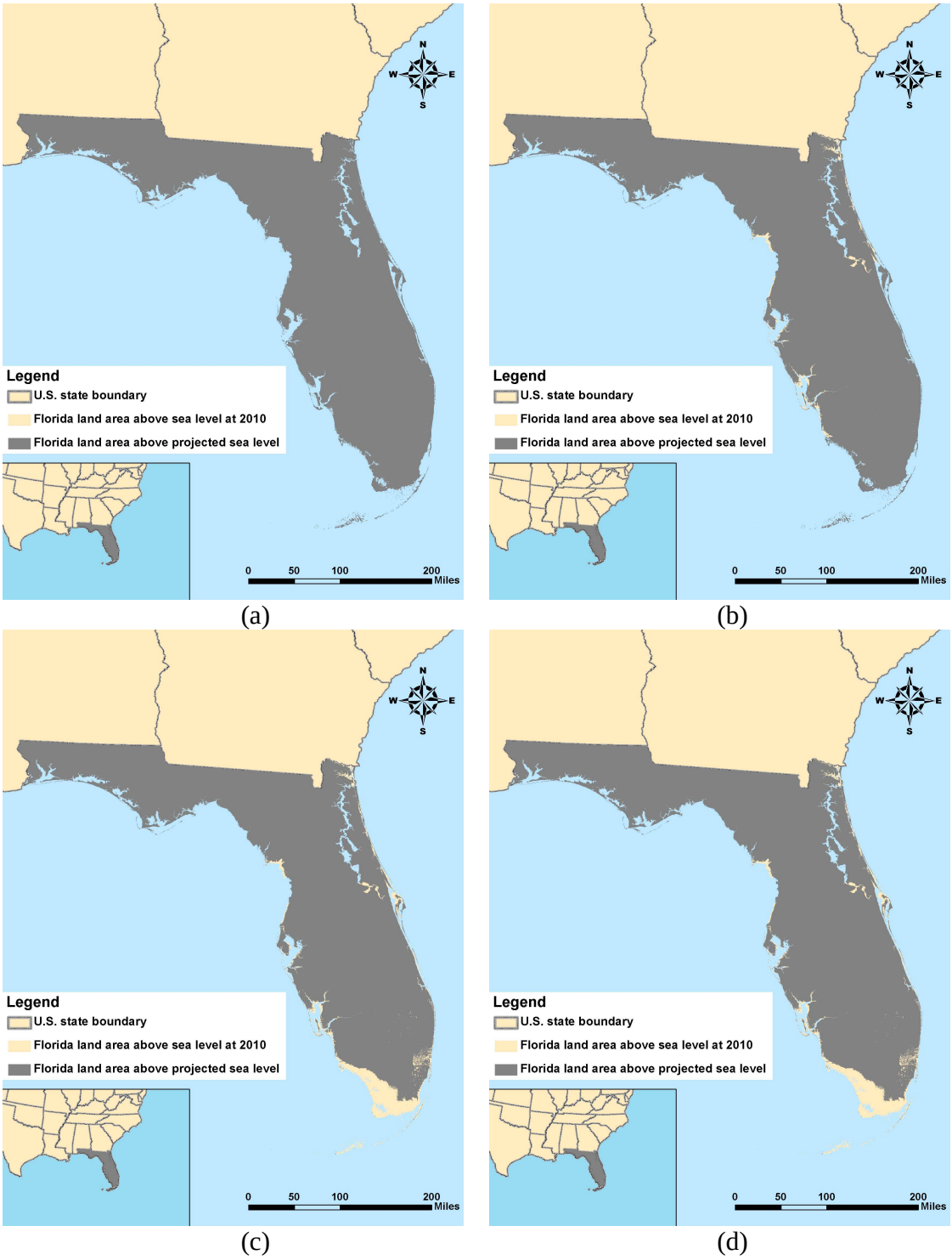

Figure 5.8 Inundation map of Florida under the A1B scenario for the year of: (a) 2010; (b) 2040; (c) 2070; and (d) 2100.

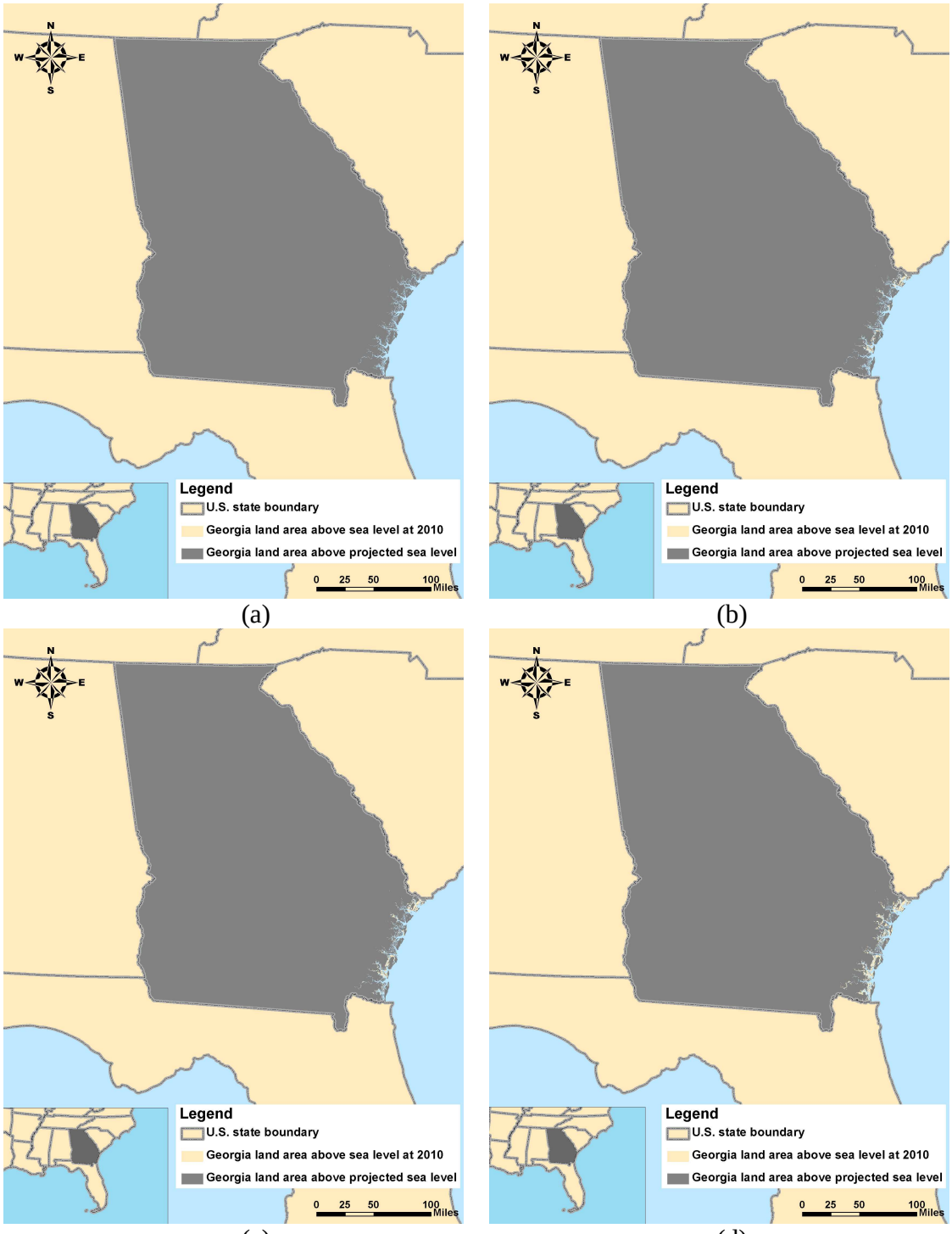

Figure 5.9 Inundation map of Georgia under the A1B scenario for the year of: (a) 2010; (b) 2040; (c) 2070; and (d) 2100.

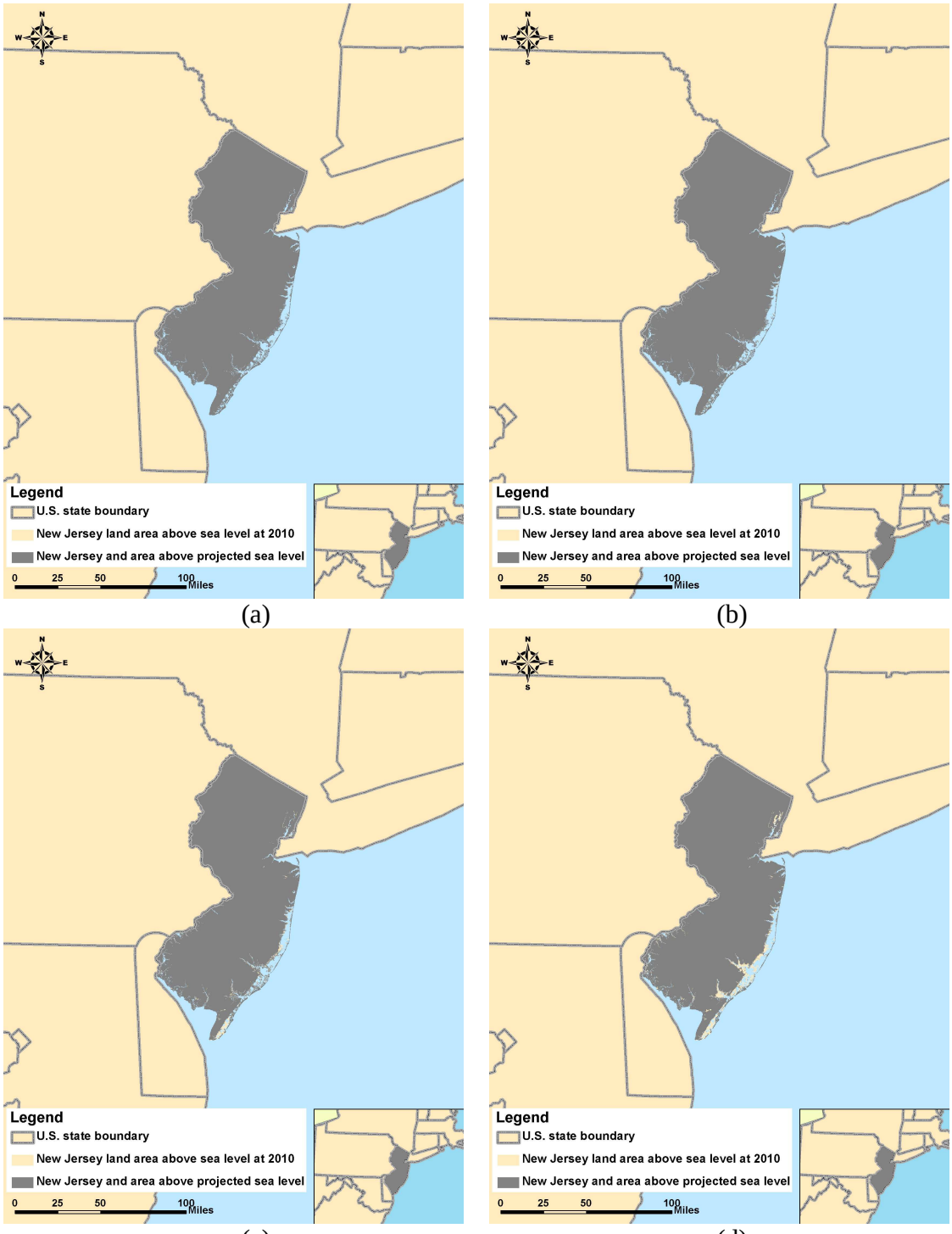

Figure 5.10 Inundation map of New Jersey under the A1B scenario for the year of: (a) 2010; (b) 2040; (c) 2070; and (d) 2100.

The importance of elevation datum. As mentioned in Section 5.4.2, the land elevation and sea level datasets involved in the inundation mapping process should be referenced to the same elevation datum. In previous studies (Zhang, 2011; Zhang et al., 2011), geodetic datum such as NAVD 88 has been directly used as the datum for sea level, for the difference between NAVD 88 and the local sea level is not significant. Similarly in this study, for regions such as Georgia and New Jersey, the difference between sea level datum LMSL and land elevation datum NAVD88 is also negligible, thus it is acceptable to simply use NAVD88 as the datum for sea level. However, for other regions where LMSL is noticeably different from NAVD88, such as Florida, use NAVD88 as the datum for sea level might lead to errors in inundation mapping. This issue is particularly important for the inundation mapping of large areas that have flat and low-lying land surface, such as the Everglades area. To illustrate the importance of the consistent use of elevation datum, two maps are plotted in Figure 5.11 for comparison. Notice that a significant part of Florida's current land area is classified as under sea level for the case of using NAVD88 as the datum of sea level (Figure 5.11 (a)). This result is apparently inaccurate, and it demonstrates the importance of referencing land elevation data and sea level data to the same datum. For future inundation assessment studies, the elevation datum issue must be carefully examined for their specific study regions before related assumptions are made.

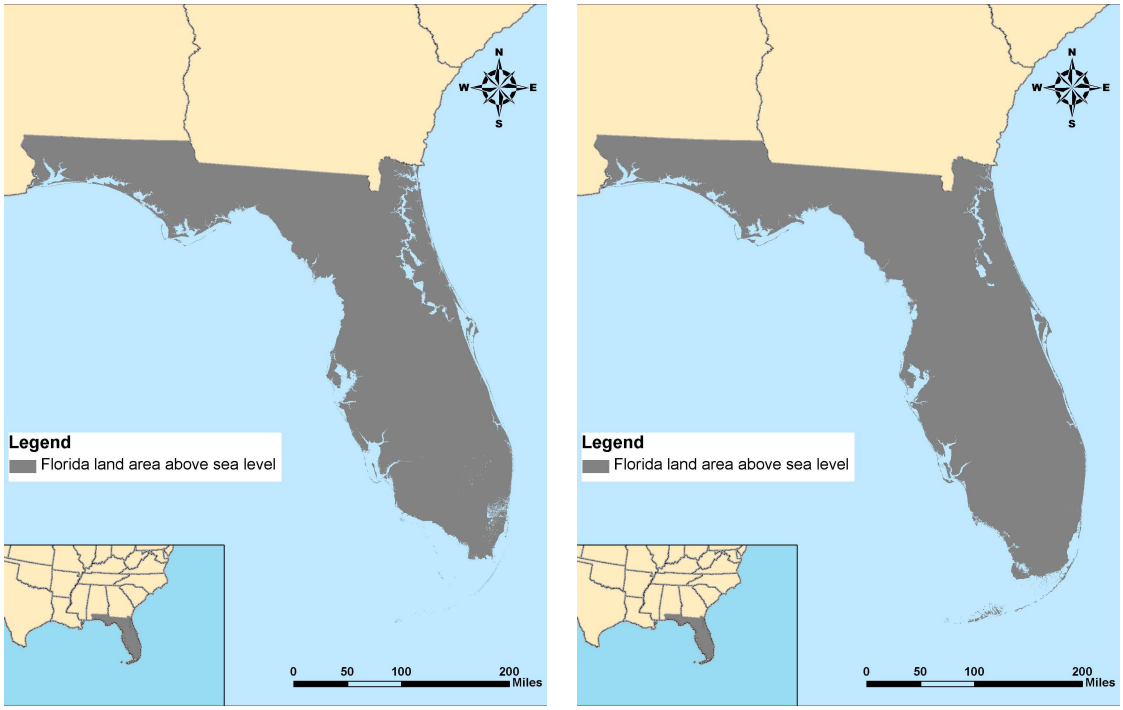

(a) (b)

Figure 5.11 (a) Calculated Florida land area with DEM elevation higher than 0 m; (b) calculated Florida land area with DEM elevation higher than the local mean sea level computed by VDatum.

Impacts of elevation data accuracy. It was described in Section 5.3 that a high accuracy data HAED was used to characterize the flat topography of Everglades area in Florida. The issue of elevation data accuracy is critically important for inundation mapping of flat and low-lying coastal regions, where errors in the elevation data can result in significant inaccuracy in the inundation assessment result. To assess the influence of elevation data accuracy on the inundation mapping result, a new set of inundation assessment is conducted for Florida, using the 1arc-second DEM data alone without the HAED data. The resulted time series of cumulative land inundation is plotted for different scenarios in Figure 5.12. Using land elevation data with lower accuracy significantly underestimated the magnitude of inundation in Florida, and it also changed the temporal pattern of the

inundation process. In light of the data accuracy issue, efforts should be devoted to the creation and compilation of high accuracy elevation data, such as the Light Detection and Ranging (LiDAR) data.

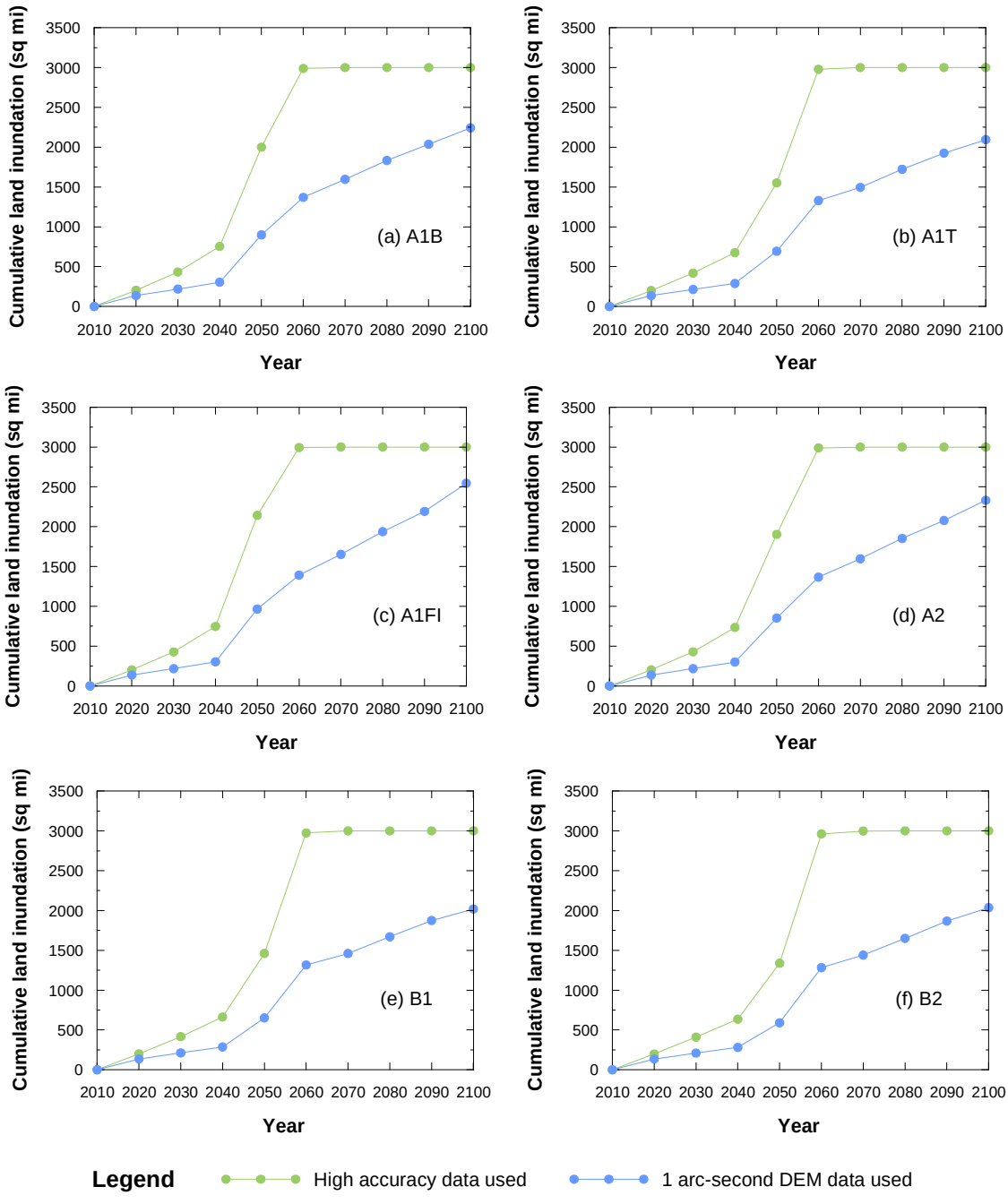

Figure 5.12 Influence of elevation data's accuracy on the inundation assessment result for Florida under scenario: (a) A1B; (b) A1T; (c) A1FI; (d) A2; (e) B1; (f) B2.

5.6 Conclusions

Inundation impact assessment is conducted for future sea levels projected in Chapter 4 of this study. Significant differences exist between the projected land inundation situations of the three target regions, namely Florida, Georgia and New Jersey, which reflect the variations among their land topography. Under all the six SRES scenarios, Florida will experience the most severe land inundation, with the total area of inundation from 2010 to 2100 calculated to be about 3,000 square miles. The area of inundation from 2010 to 2100 for Georgia ranges from 201 to 376 square miles, while that range for the state of New Jersey is from 142 to 202 square miles. These projected inundation areas correspond to about 5.4%, 0.3% - 0.6%, and 1.9% - 2.7% of the total current land area for Florida, Georgia, and New Jersey.

Because of the characteristics in the target regions topography, non-linear patterns are observed in the time series of calculated land inundation areas for Florida and Georgia. The rate of inundation starts to accelerate from 2040 and decelerate after 2060 for Florida. For the study region of Georgia, the acceleration becomes noticeable from 2080, especially under the scenarios A1FI and A2. Close examination of topographic features revealed the characteristic regions that contributed to the non-linear pattern. These regions are correspondingly facing the most significant threat of land inundation. For Florida, the Everglades and the Fort Lauderdale area are identified as the most vulnerable to land inundation; while the most vulnerable region for New Jersey is its southeast coastal region. For the case of Georgia, the inundation threat appears to be relatively uniform in space.

In the inundation mapping process, the importance of referencing land elevation and sea level to the same datum was demonstrated using the example of Florida. Results showed

that using NAVD88 as the datum for sea level lead to significant errors in the inundation mapping result. For future inundation assessment studies, the elevation datum issue must be carefully examined for their specific study regions before related assumptions are made. Also for the case of Florida, using land elevation data with lower accuracy significantly underestimated the magnitude of inundation, which also changed the temporal pattern of the inundation process. In light of the data accuracy issue, efforts should be devoted to the creation and compilation of high accuracy elevation data, such as the Light Detection and Ranging (LiDAR) data.

CHAPTER 6

CONCLUSIONS AND FUTURE WORK

6.1 Conclusions

Sea level rise is one of the most damaging consequences of climate change. As more than 20 percent of the world's population live within 100 km from the coast and less than 100 m above sea level (Nicholls et al., 2007), even relatively small magnitude of sea level rise can pose significant threats to the human society. Facing the severe impacts of sea level rise the scientific community has devoted significant efforts to building mathematical models to simulate and project the climate change based sea level rise (SLR). It is reported in the literature that SLR is not spatially uniform, thus the development of modeling techniques to predict future regional sea levels becomes critical. As the physical, empirical, and stochastic models up to date are still in a fairly preliminary stage, this study attempts to develop a comprehensive framework to identify the spatial patterns of sea level in the historical records, project regional mean sea levels in the future, and assess the corresponding impacts on the coastal communities.

6.1.1 Spatial pattern recognition and data reconstruction

A pattern recognition technique based on clustering algorithms was first developed for characterizing patterns in historical spatial sea level records. This technique is capable of clustering sea level data with changing magnitude of spatial variations over time into different characteristic regions. It can also be utilized assess the relative strengths of different climate phenomena's sea level footprints. Under this technique, the optimal number of characteristic regions is identified by the cluster validity metric Silhouette

Index, which removes the limitations of arbitrary region number assignment. When applied to a spatial sea level dataset for the period of 1950 to 2001, the pattern recognition technique developed was able to identify spatial patterns in the data that are potentially associated with climate phenomena such as El Nino-Southern Oscillation (ENSO), Pacific Decadal Oscillation (PDO), and North Atlantic Oscillation (NAO). ENSO was identified as the strongest spatial signal in the data, which supports related findings of previous studies.

The issue of short time span of regional average sea level time series is commonly faced by modeling studies on SLR. A neural network approach is proposed in this study to resolve this issue by reconstructing regional average sea levels from time series of global mean sea level. Since the general temporal trend of sea level is constrained by the time series of global mean sea level, the essential task of this neural network is to accurately characterize the spatial variations of sea level among the target regions. The proposed neural network approach accomplishes this task by utilizing the correlative relationship between sea level and sea surface temperature (SST). Taking regional average SST's and global average sea level as input variables, the neural network is configured to generate corresponding regional average sea levels as outputs. The network was demonstrated to reproduce observational records well at the training stage and has good generalization performance at the validation stage. It was then applied to reconstruct the average sea levels for regions identified by the spatial recognition technique, as well as those for regions defined based on major ocean basins. Combined with the spatial pattern recognition technique, the neural network approach provides a viable tool for future research on spatial variations of sea level.

6.1.2 DSM model for spatial sea level rise analysis

The reconstructed spatial sea level data and spatial SST data from other sources were utilized to calibrate the spatial dynamic system model (DSM) developed in the following part of this study. This spatial DSM is an extension of the DSM by Aral et al. (2012) on global mean sea level and SST simulation. It assumes that most of the physical mechanisms of sea level change are directly or indirectly connected with the sea level and the SST of the oceans. By characterizing the relationship between the state variables (sea levels and SST's) in the historical records through a dynamic system approach, the spatial DSM model aims to capture the complex system behaviors that are embedded in the records. The spatial DSM model was calibrated for two different configurations: (i) external forcing function embedded in the system matrix (without explicit form of external forcing function); and, (ii) external forcing function treated explicitly. The calibrated dynamic system coefficient matrices suggest that SST is a negative feedback system, which indicates that the system response is controllable when external anthropogenic controls are implemented.

With dynamic system coefficient matrices calibrated, future sea levels and SST's can be projected. With the first configuration (without an explicit form of external forcing function), the spatial DSM model predicted that both sea levels and SST's will rise significantly in the 21st century in all the three major ocean basins, but their magnitudes differ. The magnitude of sea level rise in the Indian Ocean is significantly lower than those in the Pacific and the Atlantic Ocean, while that of SST rise is the lowest in the Pacific Ocean. Calculated from the model projections, the global average of sea level rise from 2001 to 2100 is 48 cm (45-51 cm as the 90% confidence interval). For the spatial DSM model configured to have the explicit form of external forcing function, sea levels and SST's for the three major ocean basins in the 21st century were projected using the

predicted global mean CO_2 concentrations under six IPCC SRES scenarios. According to the model projection results, under all six scenarios sea levels and SST's of the Indian Ocean at 2100 will be significantly lower than those of the Pacific and the Atlantic Ocean. Sea levels of the Pacific Ocean at 2100 will be slightly higher than those of the Atlantic Ocean under every scenario. The highest and the lowest projected SST's occur under scenarios A1FI and B1, respectively, responding to the highest and the lowest predicted global mean CO_2 concentrations. The highest sea levels are predicted under the scenario A1FI, ranging from 71 cm to 86 cm (relative to 1990 global mean sea level); the lowest predicted sea levels are under the scenario B1, ranging from 51 to 64 cm. Calculate global mean sea level rise from 2001 to 2100 varies from 56 to 78 cm. Sea levels projected by the spatial DSM models are generally lower than those by previous semi-empirical sea level models. This difference is likely associated with the incorporation of feedback mechanisms into the spatial DSM model, which illustrates the importance of feedback mechanisms to the dynamic system of sea level and SST.

Corresponding analyses were conducted for the spatial DSM model with a different region division scheme. This region division scheme is obtained through the spatial pattern recognition technique, thus the temporal patterns of regional average sea levels are potentially associated with certain climate phenomena. However, the large model calibration and validation errors suggest that the spatial DSM model is not well suited to capture the temporal oscillatory signals in the sea level records for this application. The result is most likely caused by the spatial DSM's limitation of only targeting long-term trends of sea levels and SST's. Future research may further improve the model formulation for this type of applications, so that it can utilize the information contained in the oscillatory signals. In addition, the projected sea levels by the spatial DSM model, which can be viewed as an improved semi-empirical model, are still noticeably higher than those indicated by the IPCC. Research efforts are still needed on both the process-

based and the semi-empirical models to improve our understanding of related physical mechanisms and to further develop model formulations to better characterize these mechanisms.

6.1.3 Case study on inundation impacts

Inundation impacts of the spatial DSM model's projected sea levels were quantitatively assessed for three representative states along the east coast of the United States, namely Florida, Georgia and New Jersey. Remarkably different magnitudes of land inundation were projected for these three study regions, which reflect the variations among their land topography. The projected total area of land inundation from 2010 to 2100 is about 3,000 square miles for Florida under all six IPCC SRES scenarios, making it the most severely affected region among the three. The corresponding value for Georgia ranges from 201 to 376 square miles, while that range for the state of New Jersey is from 142 to 202 square miles. These projections correspond to about 5.4%, 0.3% - 0.6%, and 1.9% - 2.7% of the current total land area of Florida, Georgia, and New Jersey.

Non-linear patterns were observed in the time series of projected land inundation for Florida and Georgia, which are associated with their topographic characteristics. The rate of inundation in Florida will accelerate from 2040 and decelerate after 2060; the acceleration in Georgia becomes noticeable starting from 2080, especially under the scenarios A1FI and A2. These non-linear patterns are mainly contributed by the areas facing the most urgent threat of land inundation. Subsequent examination of the inundation mapping result was conducted to locate these areas. The Everglades and the Fort Lauderdale area were identified as the most vulnerable to land inundation in Florida; while the most vulnerable region for New Jersey is its southeast coastal region. For the case of Georgia, the inundation threat appears to be relatively uniform in space. The

consistent datum referencing for land elevation data and sea level data is critical for accurate land inundation mapping. Through the example of Florida, it is shown that using NAVD88 as the datum for sea level lead to significant errors in the inundation assessment result. Also for the case of Florida, the magnitude of inundation was significantly underestimated when lower accuracy land elevation data were adopted, which also changed the temporal pattern of the inundation process.

6.2 Recommendations for future research

Although this study demonstrates a successful attempt on modeling the spatial variations of sea level, further research is still needed on several aspects of spatial SLR models. The first potential area for future research is an improved representation of the relationship between different state variables of the dynamic system. As the first step in the direction of spatial DSM model, this study configures this relationship to be linear. The linear relationship has been tested to be adequate for modeling global mean sea level, and it is shown to capture the major trends of regional sea levels in this study. However, other forms of correlative relationship may further improve the model's ability to characterize "irregular" temporal and spatial signals of sea level. For example, the relationship between regional sea levels can be configured in a new way, so that it will implement an upper limit constrain on the difference between two neighboring regions' sea levels. This modification considers the gravitational constrain on the regional sea levels' elevation difference, so it characterizes the physical system better. Research in this direction, as noted by recent studies (Gasson et al., 2012; Orlic and Pasaric, 2013), might need a non-trivial amount of work.

One critical configuration of the spatial DSM model in this study is that its dynamic system coefficient matrices are constant. This configuration enables the model to

simulate the historical records well, but it might limit the model's flexibility to simulate the behaviors of sea levels under sudden extreme climate changes. Future research may look into approaches to obtain the dynamic system coefficient matrices when they are not constrained to be constant. For instance, changing matrices can be applied under a changing ocean circulation scheme. Studies following this direction need to devote more efforts on linking the dynamic system matrices to physical mechanisms so that the task of model calibration is achievable and the subsequent model projections are robust. Improvement in this aspect might also make the model better suited to simulate the oscillatory sea level signals, such as those shown in the application based on characteristic regions identified by the pattern recognition technique.

Future research is also needed to separate regional SLR contributions that are associated with climate change from those that are not. The method of spatial averaging within regions of large areas helps to reduce the influence of regional and local non-climate-change-related effects in this study. Nonetheless, regional average sea levels and SST's might be affected to a certain extent by sources that are not associated with climate change. To address this issue, significant efforts are needed to collect spatial data on related activities such as dam building and groundwater depletion, so that spatial sea level and temperature can be corrected for the contributions not caused by climate change.

Another potential direction for future research is the feasibility of adding other state variables to the dynamic system of sea level and temperature. As discussed in this study, certain contributing factors of SLR, such as ice sheet melting, interact with sea level and temperature in a complex manner. Adding them as a separate term or even as a new state variable can potentially improve the DSM model's skills at characterizing the sophisticated behaviors of sea level. Research progress in this area can also help to improve specific configurations of the current process-based models, thus it can serve as

a knowledge bridge between process-based models and semi-empirical models on SLR. One example in this area would be the case of mountain glaciers. In the current formulation of semi-empirical models, including the DSM model, the impacts of mountain glaciers on sea level are assumed to be reflected by temperature change. Although this assumption has been shown to be acceptable on a global scale, it introduces additional uncertainties to spatial models. If formulated as a new state variable in the dynamic system, mountain glacier's impacts on the spatial variations of sea level can be potentially better captured. Note that this potential area of research also relies heavily on the availability of spatial data on related contributing factors of SLR. So progress in remote sensing technology and systematic compilation and processing of related data will benefit research on SLR modeling much.

For future inundation assessment studies, the potential change of land topography during the inundation process can be considered to better capture the spatial and temporal characteristics, especially at the local scale. The elevation differences caused by datum change must be carefully examined to assess the necessity of referencing related elevation data to a specific datum. In addition, in light of the data accuracy issue, efforts should be devoted to the creation and compilation of high accuracy elevation data, such as the Light Detection and Ranging (LiDAR) data.

REFERENCES

Alley, R. B., and Joughin, I. (2012). “Modeling ice-sheet flow.” *Science*, 336(6081), 551-552.

Alley, R. B., Clark, P. U., Huybrechts, P., and Joughin, I. (2005). “Ice-sheet and sea-level changes.” *Science*, 310(5747), 456-460.

Allison, I., et al. (2009). *The Copenhagen diagnosis: updating the world on the latest climate science*. Climate Change Research Centre (CCRC), The University of New South Wales, Sydney, Australia.

Aral, M.M., Guan, J., and Chang, B. (2012). “A dynamic system model to predict global sea-level rise and temperature change.” *J. Hydrol. Eng.*, 17(2), 237-242.

Baarshch, J. And Celebi, M. (2012). “Investigation of internal validity measures for K-means clustering.” In: Proceedings of the International MultiConference of Engineers and Computer Scientists, IMECS, Hong Kong.

Babuska, R., van der Veen, P, and Kaymak, U. (2002). “Improved covariance estimation for Gustafson-Kessel clustering.” In: Proceedings of the 2002 IEEE International Conference on Fuzzy Systems, IEEE, Honolulu, HI, USA (pp. 1081-1085).

Bader, D. C. , et al. (2008). *Climate models: an assessment of strengths and limitations*. A report by the US Climate Change Science Program and the Subcommittee on Global Change Research, Office of Biological and Environmental Research, Department of Energy, Washington, DC, USA.

Bahr, D. B., Meier, M. F., and Peckham, S. D. (1997). “The physical basis of glacier volume-area scaling.” *J. Geophys. Res.-Solid Earth*, 102(B9), 20355-20362.

Becker, M., Meyssignac, B., Letetrel, C., Llovel, W., Cazenave, A., and Delcroix, T. (2012). “Sea level variations at tropical Pacific islands since 1950.” *Glob. Planet. Change*, 80-81, 85-98.

Bezdek, J. C., Ehrlich, R., Full, W. (1984). “FCM: the fuzzy c-means clustering algorithm.” *Comput. Geosci.*, 10(2-3), 191-203.

Bindoff, N. L., et al. (2007). “Observations: oceanic climate change and sea level.” Chapter 5, *Climate Change 2007: The Physical Science Basis. Contribution of Working Group I to the Fourth Assessment Report of the Intergovernmental Panel on Climate Change*, S. Solomon, D. Qin, M. Manning, Z. Chen, M. Marquis, K. B. Averyt, M. Tignor and H. L. Miller, eds., Cambridge University Press, Cambridge, United Kingdom and New York, NY, USA.

Braithwaite, R. J., and Zhang, Y. (1999). “Modelling changes in glacier mass balance that may occur as a result of climate changes.” *Geografiska Annaler. Series A, Physical Geography*, 81(4), 489-496.

Bursa, M., Kouba, J., Muller, A., Radej, K., True, S. A., Vatrt, V., and Vojtfskova, M. (1999). “Differences between mean sea levels for the Pacific, Atlantic and Indian Oceans from TOPEX/POSEIDON altimetry.” *Stud. Geophys. Geod.*, 43(1), 1-6.

Cabanes, C., Huck, T., and Verdiere A. (2006). “Contribution of wind forcing and surface heating to interannual sea level variations in the Atlantic Ocean.” *J. Phys. Oceanogr.*, 36(9), 1739-1750.

Cabanes, C., Huck, T., Verdiere, A. (2006). “Contribution of wind forcing and surface heating to interannual sea level variations in the Atlantic Ocean.” *J. Phys. Oceanogr.*, 36(9), 1739-1750.

Cazenave, A., and Llovel, W. (2010). “Contemporary sea level rise.” *Annu. Rev. Mar. Sci.*, 2(1), 145-173.

Cazenave, A., Dominh, K., Guinehut, S., Berthier, E., Llovel, W., Ramillien, G., Ablain, M., and Larnicol, G. (2008). “Sea level budget over 2003-2008: A reevaluation from GRACE space gravimetry, satellite altimetry and Argo.” *Glob. Planet. Change*, 65(1-2), 83-88.

Chambers, D. P., Merrifield, M. A., Nerem, R. S. (2012). “Is there a 60-year oscillation in global mean sea level?” *Geophys. Res. Lett.*, 39, L18607.

Chuang, K., Tzeng, H., Chen, S., Wu, J., Chen, T. (2006). “Fuzzy c-means clustering with spatial information for image segmentation.” *Comput. Med. Imag. Grap.*, 30, 9-15.

Church, J. A. And White, N. J. (2011). “Sea-level rise from the late 19th to the early 21st century.” *Surv. Geophys.*, 32, 585-602.

Church, J. A., and White, N. J. (2006). “A 20th century acceleration in global sea-level rise.” *Geophys. Res. Lett.*, 33(1), L01602.

Church, J. A., et al. (2001). “Changes in sea level.” Chapter 11, *Climate Change 2001: The Scientific Basis. Contribution of Working Group I to the Third Assessment Report of the Intergovernmental Panel on Climate Change*. J. T. Houghton, Y. Ding, D. J. Griggs, M. Noguer, P. J. van der Linden, X. Dai, K. Maskell, and C. A. Johnson, eds., Cambridge University Press, Cambridge, United Kingdom and New York, NY, USA.

Church, J. A., Gregory, J. M., White, N. J., Platten, S. M., and Mitrovica, J. X. (2011). “Understanding and projecting sea level change.” *Oceanography*, 24(2), 130-143.

Church, J. A., White, N. J., Coleman, R., Lambeck, K., and Mitrovica, J. X. (2004). “Estimates of the regional distribution of sea level rise over the 1950-2000 period.” *J. Clim.*, 17(13), 2609-2625.

Cooper, H. M., Chen, Q., Fletcher, C. H., and Barbee, M. M. (2013). “Assessing vulnerability due to sea-level rise in Maui, Hawaii using LiDAR remote sensing and GIS.” *Clim. Change*, 116(3-4), 547-563.

Cooper, M. J. P., Beevers, M. D., and Oppenheimer, M. (2008). “The potential impacts of sea level rise on the coastal region of New Jersey, USA.” *Clim. Change*, 90, 475-492.

Cowpertwait, P. S. P. and Metcalfe, A. V. (2009). *Introductory time series with R*. Springer, New York, NY, USA.

Curry, J. A., and Webster, P. J. (2011). “Climate science and the uncertainty monster.” *B. Am. Meteorol. Soc.*, 92(12), 1667-1682.

Dasgupta, S., Laplante, B., Meisner, C., Wheeler, D., and Yan, J. (2009). “The impact of sea level rise on developing countries: A comparative analysis.” *Clim. Change*, 93, 379-388.

Davies, D. and Bouldin, D. (1979). “A cluster separation measure.” *IEEE Trans. Pattern Anal. Mach. Intell.*, 1(2), 224-227.

Dembele, D. And Kastner, P. (2003). “Fuzzy C-means method for clustering microarray data.” *Bioinformatics*, 19(8), 973-980.

Di Martino, F., and Sessa, S. (2009). “Implementation of the extended fuzzy C-means algorithm in geographic information systems.” *J. Uncertain Syst.*, 3(4), 298-306.

Dunn, J. C. (1974). “Well-separated clusters and optimal fuzzy partitions.” *J. Cybern.*, 4(1): 95-104.

Equihua, M. (1990). “Fuzzy clustering of ecological data.” *J. Ecol.*, 78(2), 519-534.

Etkins, R., and Epstein, E. S. (1982). “The rise of global mean sea-level as an indication of climate change.” *Science*, 215(4530), 287-289.

Gasson, E., Siddall, M., Lunt, D. J., Rackham, O. J. L., Lear, C. H., and Pollard, D. (2012). “Exploring uncertainties in the relationship between temperature, ice volume, and sea level over the past 50 million years.” *Rev. Geophys.*, 50, RG1005.

Gornitz, V., Couch, S., and Hartig, E. K. (2002). “Impacts of sea level rise in the New York City metropolitan area.” *Global Planet. Change*, 32, 61-88.

Gornitz, V., Lebedeff, S., and Hansen, J. (1982). “Global sea-level trend in the past century.” *Science*, 215(4540), 1611-1614.

Gregory, J. M., and Huybrechts, P. (2006). “Ice-sheet contributions to future sea-level change.” *Philos. Trans. R. Soc. A-Math. Phys. Eng. Sci.*, 364(1844), 1709-1731.

Gregory, J. M., Church, J. A., Boer, G. J., Dixon, K. W., Flato, G. M., Jackett, D. R., Lowe, J. A., O'Farrell, S. P., Roeckner, E., Russell, G. L., Stouffer, R. J., and Winton, M. (2001). “Comparison of results from several AOGCMs for global and regional sea-level change 1900-2100.” *Clim. Dyn.*, 18(3-4), 225-240.

Gregory, J. M., Lowe, J. A., and Tett, S. F. B. (2006). “Simulated global-mean sea level changes over the last half-millennium.” *J. Clim.*, 19(18), 4576-4591.

Gregory, J. M., White, N. J., Church, J. A., et al. (2012). “Twentieth-century global-mean sea-level rise: is the whole greater than the sum of the parts?” *J. Clim.*, in press.

Grinsted, A., Moore, J. C., and Jevrejeva, S. (2010). “Reconstructing sea level from paleo and projected temperatures 200 to 2100 ad.” *Clim. Dyn.*, 34(4), 461-472.

Guan, J., Chang, B. and Aral, M. M. (2013). “A dynamic control system model for global temperature change and sea-level rise with CO2 emissions impact.” *Submitted*.

Gustafson, D. And Kessel, W. (1978). “Fuzzy Clustering with a fuzzy covariance matrix.” In: IEEE Conference on Decision and Control (pp. 761-766).

Hagan, M. T., Demuth, H. B., and Beale, M. H. (1996). *Neural Network Design*, PWS Publishing, Boston, MA, USA.

Hamerly, G. and Elkan, C. (2002). “Alternatives to the k-means algorithm that find better clusterings.” In: Proceedings of the Eleventh International Conference on Information and Knowledge Management, ACM, New York, NY, USA.

Hamlington, B. D., Leben, R. R., and Kim, K. Y. (2012). “Improving sea level reconstructions using non-sea level measurements.” *J. Geophys. Res.*, 117, C10025.

Hansen, J. E. (2007). “Scientific reticence and sea level rise.” *Environ. Res. Lett.*, 2, 1-6.

Haque, M., and Kim, J. (2013). “An analysis of content-based classification of audio signals using a fuzzy C-means algorithm.” *Multimed. Tools Appl.*, 63(1), 77-92.

Haylock, M. R., Cawley, G. C., Harpham, C., Wilby, R. L., and Goodess, C. M. (2006). “Downscaling heavy precipitation over the United Kingdom: A comparison of dynamical and statistical methods and their future scenarios.” *Int. J. Climatol.*, 26(10), 1397-1415.

Hegerl, G., Stott, P., Solomon, S., and Zwiers, F. (2011). “Comment on ‘Climate science and the uncertainty monster’ J. A. Curry and P. J. Webster.” *B. Am. Meteorol. Soc.*, 92(12), 1683-1685.

Hennecke, W. G., Greve, C. A., Cowell, P. J., and Thom, B. G. (2004). “GIS-based coastal behavior modeling and simulation of potential land and property loss: Implications of sea-level rise at Collaroy/Narrabeen Beach, Sydney (Australia).” *Coast. Manag.*, 32: 449-470.

Holgate, S., Jevrejeva, S., Woodworth, P., and Brewer, S. (2007). “Comment on ‘A semi-empirical approach to projecting future sea-level rise’.” *Science*, 317(5846), 1866b.

Horton, R., Herweijer, C., Rosenzweig, C., Liu, J. P., Gornitz, V., and Ruane, A. C. (2008). “Sea level rise projections for current generation CGCMs based on the semi-empirical method.” *Geophys. Res. Lett.*, 35(2), L02715.

Huss, M. And Farinotti, D. (2012). “Distributed ice thickness and volume of all glaciers around the globe.” *J. Geophys. Res.*, 117, F04010.

IPCC. (2012). *Carbon dioxide: projected emissions and concentrations*. <http://www.ipcc-data.org/ddc_co2.html> (September 15, 2012)

Jain, A. K., Kheshgi, H. S., Wuebbles, D. J. (1994). *Integrated science model for assessment of climate change*. Lawrence Livermore National Laboratory, UCRL-JC-116526.

Jevrejeva, S., Grinsted, A., and Moore, J. C. (2009). “Anthropogenic forcing dominates sea level rise since 1850.” *Geophys. Res. Lett.*, 36(20), L20706.

Jevrejeva, S., Moore, J. C., and Grinsted, A. (2010). “How will sea level respond to changes in natural and anthropogenic forcings by 2100?” *Geophys. Res. Lett.*, 37(7), L07703.

Jevrejeva, S., Moore, J. C., and Grinsted, A. (2012). “Sea level projections to AD2500 with a new generation of climate change scenarios.” *Glob. Planet. Change*, 80-81, 14-20.

Jones, E. G., Desmond, G. B., Henkle, C., and Glover, R. (2012). “An approach to regional wetland digital elevation model development using a differential positioning system and a custom-built helicopter-based surveying system.” *Int. J. Remote Sens.*, 33(2), 450-465.

Kaplan, A., Kushnir, Y., and Cane, M. (2000). “Reduced space optimal interpolation of historical marine sea level pressure: 1854-1992.” *J. Clim.*, 13, 2987-3002.

Kim, Y., Kim, D, Lee, D, Lee, K. (2004). “A cluster validation index for GK cluster analysis based on relative degree of sharing.” *Inform. Sciences*, 168, 225-242.

King, M. A., Bingham, R. J., Moore, P., Whitehouse, P. L., Bentley, M. J., and Milne, G. A. (2012). “Lower satellite-gravimetry estimates of Antarctic sea-level contribution.” *Nature*., 491(7425), 586-589.

Larour, E., Seroussi, H., Morlighem, M., and Rignot, E. (2012). “Continental scale, high order, high spatial resolution, ice sheet modeling using the Ice Sheet System Model (ISSM).” *J. Geophys. Res.*, 117(F1), F01022.

Ledoux, H. and Gold, C. (2005). “An efficient natural neighbour interpolation algorithm for geoscientific modeling.” In: Developments in Spatial Data Handling: 11th International Symposium on Spatial Data Handling, Edited by: Fisher, P.F. Springer, Berlin, Germany, 97–108.

Leuliette, E. W., and Miller, L. (2009). “Closing the sea level rise budget with altimetry, Argo, and GRACE.” *Geophys. Res. Lett.*, 36(4), L04608.

Leuliette, E. W., and Willis, J. K. (2011). “Balancing the sea level budget.” *Oceanography*, 24(2), 122-129.

Levitus, S., Antonov, J. And Boyer, T. (2005). “Warming of the world ocean, 1955-2003.” *Geophys. Res. Lett.*, 32, L02604.

Levitus, S., Antonov, J., Boyer, T., Locarnini, R., and Garcia, H. (2009). “Global ocean heat content 1955-2008 in light of recently revealed instrumentation problems.” *Geophys. Res. Lett.*, 36, L07608.

Li, X., Rowley, R. J., Kostelnick, J. C., Braaten, D., Meisel, J., and Hulbutta, K. (2009). “GIS analysis of global impacts from sea level rise.” *Photogramm. Eng. Remote Sens.*, 75, 807-818.

Liao, T. W. (2005). “Clustering of time series – a survey.” *Pattern Recognit.*, 38, 1857-1864.

Lichter, M. and Felsenstein, D. (2012). “Assessing the costs of sea-level rise and extreme flooding at the local level: A GIS-based approach.” *Ocean Coast. Manag.*, 59, 47-62.

Llovel, W., Cazenave, A., Rogel, P., Lombard, A., Nguyen, M. B. (2009). “Two-dimensional reconstruction of past sea level (1950-2003) from tide gauge data and an Ocean General Circulation Model.” *Clim. Past*, 5, 217-227.

Lombard, A., Cazenave, A., MoMinh, K., Cabanes, C., Nerem, R. S. (2005). “Thermosteric sea level rise for the past 50 years; comparison with tide gauges and inference on water mass contribution.” *Global Planet. Change*, 48, 303-312.

Meehl, G.A., et al. (2007). “Global climate projections.” Chapter 10, *Climate Change 2007: The Physical Science Basis. Contribution of Working Group I to the Fourth Assessment Report of the Intergoverment Panel on Climate Change*. S. Solomon, D. Qin, M. Manning, Z. Chen, M. Marquis, K. B. Averyt, M. Tignor and H. L. Miller, eds., Cambridge University Press, Cambridge, United Kingdom and New York, NY, USA.

Menemenlis, D., Fukumori, I., and Lee, T. (2007). “Atlantic to Mediterranean sea level difference driven by winds near Gibraltar Strait.” *J. Phys. Oceanogr.*, 37, 359-376.

Merrifield, M., Tompson, P., and Lander, M. (2012). “Multidecadal sea level anomalies and trends in the western tropical Pacific.” *Geophys. Res. Lett.*, 39, L13602.

Meyssignac, B., Salas y Melia, D., Becker, M., Llovel, W., and Cazenave, A. (2012). “Tropical Pacific spatial trend patterns in observed sea level: internal variability and/or anthropogenic signature?” *Clim. Past*, 8, 787-802.

Miller, L., and Douglas, B. C. (2004). “Mass and volume contributions to twentieth-century global sea level rise.” *Nature*, 428(6981), 406-409.

Milne, G. A., Gehrels, W. R., Hughes, C. W., and Tamisiea, M. E. (2009). “Identifying the causes of sea-level change.” *Nat. Geosci.*, 2(7), 471-478.

Mitrovica, J. X., Gomez, N., and Clark, P. U. (2009). “The sea-level fingerprint of west antarctic collapse.” *Science*, 323(5915), 753-753.

Mitrovica, J. X., Tamisiea, M. E., Davis, J. L., and Milne, G. A. (2001). “Recent mass balance of polar ice sheets inferred from patterns of global sea-level change.” *Nature*, 409(6823), 1026-1029.

Mitrovica, J. X., Wahr, J., Matsuyama, I., Paulson, A., and Tamisiea, M. E. (2006). “Reanalysis of ancient eclipse, astronomic and geodetic data: A possible route to resolving the enigma of global sea-level rise.” *Earth Planet. Sci. Lett.*, 243(3-4), 390-399.

Mitrovica, J.X., M.E. Tamisiea, J.L. Davis, G.A. Milne. 2001. “Recent mass balance of polar ice sheets inferred from patterns of global sea-level change.” *Nature*, 409(6823): 1026-1029.

Mitrovica, J.X., N. Gomez, P.U. Clark. 2009. “The sea-level fingerprint of West Antarctic collapse.” *Science*, 323(5915): 753-753.

Moore, J. C., Jevrejeva, S., and Grinsted, A. (2010). “Efficacy of geoengineering to limit 21st century sea-level rise.” *Proc. Natl. Acad. Sci. U. S. A.*, 107(36), 15699-15703.

Munk, W. (2002). “Twentieth century sea level: an enigma.” *Proc. Natl. Acad. Sci. U. S. A.*, 99(10), 6550-6555.

Nakicenovic, N., et al. (2000). *IPCC Special Report on Emissions Scenarios*. Cambridge University Press, UK.

NASA. *Forcings in GISS climate model: well-mixed anthropogenic greenhouse gases*. <http://data.giss.nasa.gov/modelforce/ghgases> (September 15, 2012)

National Research Council. (1990). *Sea-level change*. National Academies Press, Washington, D.C., USA.

National Snow and Ice Data Center. (2012). *World Glacier Inventory*. <https://nsidc.org/data/g01130.html> (Dec. 6, 2012)

Nicholls, R. J., et al. (2007). “Coastal systems and low-lying areas.” Chapter 6, *Climate Change 2007: Impacts, Adaptation and Vulnerability. Contribution of Working Group II to the Fourth Assessment Report of the Intergovernmental Panel on Climate Change*, M.L. Parry, O.F. Canziani, J.P. Palutikof, P.J. van der Linden and C.E. Hanson, eds., Cambridge University Press, Cambridge, United Kingdom and New York, NY, USA.

NOAA Coastal Services Center. (2010). *Mapping Inundation Uncertainty*, 10 pp.

NOAA. (2011). *Coastal and Marine Spatial Planning Data Registry*. <http://egisws02.nos.noaa.gov/cmspgisdataregistry/> (December 9, 2011)

Orlic, M. And Pasaric, Z. (2013). “Semi-empirical versus process-based sea-level projections for the twenty-first century.” *Nature Clim. Change.*, in press.

Pardaens, A. K., Lowe, J. A., Brown, S., Nicholls, R. J., and de Gusmao, D. (2011). "Sea-level rise and impacts projections under a future scenario with large greenhouse gas emission reductions." *Geophys. Res. Lett.*, 38(2), L12604.

Parkinson, R. W. and McCue, T. (2011). "Assessing municipal vulnerability to predicted sea level rise: City of Satellite Beach, Florida." *Clim. Change*, 107, 203-223.

Pfeffer, W. T., Harper, J. T., and O'Neel, S. (2008). "Kinematic constraints on glacier contributions to 21st century sea-level rise." *Science*, 321(5894), 1340-1343.

Pham, D. (2001). "Spatial models for fuzzy clustering." *Comput. Vision Image Understanding*, 84, 285-297.

Phillips, W., Velthuizen, R., Phuphanich, S., Hall, L., Clarke, L, and Silbiger, M. (1995). "Application of fuzzy C-means segmentation technique for tissue differentiation in MR images of a hermorrhagic glioblastoma multiforme." *Magn. Reson. Imaging*, 13(2), 277-290.

Powers, D. and Xie, Y. (2008). *Statistical methods for categorical data analysis* (2nd Ed.). Emerald Group Publishing Limited, UK.

Rahmstorf, S. (2007). "A semi-empirical approach to projecting future sea-level rise." *Science*, 315(5810), 368-370.

Rahmstorf, S. (2010). "A new view on sea level rise." *Nature Rep. Clim. Change*, 4, 44-45.

Rahmstorf, S. (2012). "Modeling sea level rise." *Nat. Educ. Knowl.*, 3(10), 4.

Rahmstorf, S., Cazenave, A., Church, J. A., Hansen, J. E., Keeling, R. F., Parker, D. E., and Somerville, R. C. J. (2007). "Recent climate observations compared to projections." *Science*, 316(5825), 709-709.

Rahmstorf, S., Foster, G., and Cazenave, A. (2012a). "Comparing climate projections to observations up to 2011." Environ. Res. Lett., 7(4), 044035.

Rahmstorf, S., Perrette, M., and Vermeer, M. (2012b). "Testing the robustness of semi-empirical sea level projections." *Clim. Dyn.*, 39(3-4), 861-875.

Randall, D.A., et al. (2007). “Cilmate models and their evaluation.” Chapter 8, *Climate Change 2007: The Physical Science Basis. Contribution of Working Group I to the Fourth Assessment Report of the Intergoverment Panel on Climate Change*. S. Solomon, D. Qin, M. Manning, Z. Chen, M. Marquis, K. B. Averyt, M. Tignor and H. L. Miller, eds., Cambridge University Press, Cambridge, United Kingdom and New York, NY, USA.

Rawashdeh, M. and Ralescu, A. (2012). “Crisp and fuzzy cluster validity: generalized intra-inter silhouette index.” In: Proceedings of the 2012 NAFIPS Annual Meeting, Berkeley, CA.

Ridley, J. K., Huybrechts, P., Gregory, J. M., and Lowe, J. A. (2005). “Elimination of the greenland ice sheet in a high CO2 climate.” J. Clim., 18(17), 3409-3427.

Rignot, E., and Kanagaratnam, P. (2006). “Changes in the velocity structure of the greenland ice sheet.” *Science*, 311(5763), 986-990.

Rignot, E., Velicogna, I., van den Broeke, M. R., Monaghan, A., and Lenaerts, J. (2011). “Acceleration of the contribution of the Greenland and Antarctic ice sheets to sea level rise.” *Geophys. Res. Lett.*, 38(5), L05503.

Rippeth, T. P., Scourse, J. D., Uehara, K., and McKeown, S. (2008). “Impact of sea-level rise over the last deglacial transition on the strength of the continental shelf CO2 pump.” *Geophys. Res. Lett.*, 35(24), L24604.

Rousseeuw, P. (1987). “Silhouettes: a graphical aid to the interpretation and validation of cluster analysis.” *J. Comput. Appl. Math.*, 20, 53-65.

Schmith, T., Johansen, S., and Thejll, P. (2007). “Comment on ‘A semi-empirical approach to projecting future sea-level rise’.” *Science*, 317(5846), 1866c.

Schmith, T., Johansen, S., and Thejll, P. (2012). “Statistical analysis of global surface temperature and sea level using cointegration methods.” *J. Clim.*, 25(22), 7822-7833.

Schoof, J. T. and Pryor, S. C. (2001). “Downscaling temperature and precipitation: a comparison of regression-based methods and artificial neural networks.” *Int. J. Climatol.*, 21, 773-790.

Selim, S. And Ismail, M. (1984). “K-means-type algorithms: a generalized convergence theorem and characterization of local optimality.” *IEEE Trans. Pattern Anal. Mach. Intell.*, PAMI-6(1), 81-87.

Smith, T. M. (2000). “Tropical Pacific sea level variations (1948-98).” *J. Clim.*, 13, 2757-2769.

Smith, T. M., Reynolds, R. W., Livezey, R. E., and Stokes, D. C. (1996). “Reconstruction of historical sea surface temperatures using empirical orthogonal functions.” *J. Clim.*, 9, 1403-1420.

Smith, T. M., Reynolds, R. W., Peterson, T. C., Lawrimore, J. (2008). “Improvements to NOAA's historical merged land-ocean surface temperature analysis (1880-2006).” *J. Clim.*, 21, 2283-2296.

SOFIA. (2012). *Elevation Data*. <http://sofia.usgs.gov/exchange/desmond/desmondelev.html> (January 22, 2012)

Taboada, F. G., and Anadon, R. (2010). “Critique of the methods used to project global sea-level rise from global temperature.” *Proc. Natl. Acad. Sci. U. S. A.*, 107(29), E116-E117.

U.S. Census Bureau. (2012). *Statistical Abstract of the United States: 2012*. U.S. Government Printing Office, Washington, D.C.

U.S. Census Bureau. (2013). *TIGER/Line® Shapefiles and TIGER/Line® Files*. <http://www.census.gov/geo/maps-data/data/tiger-line.html> (March 15, 2013).

USGS. 2012. *Vertical Accuracy of the National Elevation Dataset*, 11 pp.

van de Wal, R. S. W., and Wild, M. (2001). “Modelling the response of glaciers to climate change by applying volume-area scaling in combination with a high resolution GCM.” *Clim. Dyn.*, 18(3-4), 359-366.

van Lipzig, N. P. M., van Meijgaard, E., and Oerlemans, J. (2002). “Temperature sensitivity of the antarctic surface mass balance in a regional atmospheric climate model.” *J. Clim.*, 15(19), 2758-2774.

VDatum. (2012). *Vertical Datum Transformation*. <http://vdatum.noaa.gov> (January 20, 2012).

Velicogna, I., and Wahr, J. (2006). "Measurements of time-variable gravity show mass loss in antarctica." *Science*, 311(5768), 1754-1756.

Vermeer, M. and Rahmstorf, S. (2009). "Global sea level linked to global temperature." *Proc. Natl. Acad. Sci. U.S.A.*, 106(51), 21527-21532.

von Storch, H., Zorita, E., Gonzalez-Rouco, J. F. (2008). "Relationship between global mean sea-level and global mean temperature in a climate simulation of the past millennium." *Ocean Dyn.*, 58(3-4), 227-236.

Wenzel, M. And Schroter, J. (2010). "Reconstruction of regional mean sea level anomalies from tide gauges using neural networks." *J. Geophys. Res.*, 115, C08013.

Wilby, R. L., Wigley, T. M. L., Conway, D., Jones, P. D., Hewitson, B. C., Main, J., and Wilks, D. S. (1998). "Statistical downscaling of general circulation model output: a comparison of methods." *Water Resour. Res.*, 34(11), 2995-3008.

Wild, M., Calanca, P., Scherrer, S. C., and Ohmura, A. (2003). "Effects of polar ice sheets on global sea level in high-resolution greenhouse scenarios." *J. Geophys. Res.*, 108(D5), 4165.

Winkelmann, R., and Levermann, A. (2013). "Linear response functions to project contributions to future sea level." *Clim. Dyn.*, 40(11-12), 2579-2588.

Winkelmann, R., Martin, M. A., Haseloff, M., Albrecht, T., Bueler, E., Khroulev, C., and Levermann, A. (2011). "The Potsdam parallel ice sheet model (PISM-PIK) – Part 1: Model description." *Cryosphere*, 5(3), 715-726.

Wunsch, C., Ponte, R. M., and Heimbach, P. (2007). "Decadal trends in sea level patterns: 1993-2004." *J. Clim.*, 20(24), 5889-5911.

Xie, X. and Beni, G. (1991). "A validity measure for fuzzy clustering." *IEEE Trans. Pattern Anal. Mach. Intell.*, 13(8), 841-847.

Xue, Y., Smith, T. M., Reynolds, R. W. (2003). “Interdecadal changes of 30-yr SST normals during 1871-2000.” *J. Clim.*, 16(10), 1601-1612.

Yin, J. Yin, Z., Wang, J., and Xu, S. (2012). “National assessment of coastal vulnerability to sea-level rise for the Chinese coast.” *J. Coast. Conservat.*, 16, 123-133.

Zecca, A., and Chiari, L. (2012). “Lower bounds to future sea-level rise.” *Glob. Planet. Change*, 98–99(0), 1-5.

Zhang, K. (2011). “Analysis of non-linear inundation from sea-level rise using LIDAR data: a case study for South Florida.” *Clim. Change*, 106, 537-565.

Zhang, K., Dittmar, J., Ross, M., and Bergh, C. (2011). “Assessment of sea level rise impacts on human population and real property in the Florida Keys.” *Clim. Change*, 107, 129-146.

Zuo, Z., and Oerlemans, J. (1997). “Contribution of glacier melt to sea-level rise since AD 1865: a regionally differentiated calculation.” *Clim. Dyn.*, 13(12), 835-845.